

Post Finishing Techniques to Improve the Functionality of 3D Printed Parts

by

Gabriel Beltrao Pontes Salata

A thesis submitted in partial fulfillment of the requirements for the degree of

Master of Science

Department of Mechanical Engineering

University of Alberta

© Gabriel Beltrao Pontes Salata, 2019

# Abstract

Generating functional parts using additive manufacturing (AM) has many challenges. These can be material- and/or process-based. This is especially true when the produced part is required to withstand or be sealed for pressure due to the potential air gaps inherent to AM processes that generate weak points within the geometry. Also, due to the manufacturing process, 3D printed parts have an anisotropic behavior, therefore having weaker mechanical properties when compared to regular materials, such as metals. This study aims to investigate and understand how to make 3D printed parts more functional when it comes to sealing applications and whenever better mechanical properties are required.

The sealing performance will be investigated by understanding the effect of coating on a 3D printed acrylonitrile butadiene styrene (ABS) cylinder and compare its capacity to withstand pressure among three different samples: non-coated (raw), epoxy coated; and spray painted 3D printed ABS cylinders. A unique test procedure has been developed to monitor pressure within the cylinder over an extended period. Preliminary tests were undertaken by using a custom-built pressure vessel designed to fit the cylinder samples while minimizing all the loads other than the prescribed internal pressure. Pressure withstanding capacities of the samples were compared. The results showed that the samples coated with epoxy had improved sealing performance, followed by the spray painted ones. The raw 3D printed ABS samples had the least sealing performance.

The idea of improving the mechanical properties of a 3D printed part was done by applying the concept of post tensioning technique to samples printed in different orientations, where a metal rod would be added as a reinforcement to the part. To better understand the effect of the reinforcement to the 3D printed parts, tensile and 3-point bending tests were done. There were

three different types of reinforced samples for the tensile tests, including 1, 3, and 5 turn, while only two reinforced samples were tested on the 3-point bending, the 3, and 5 turn samples. The different reinforced samples indicated the different amount of compressive load applied into the 3D printed sample. The results, for the tensile test, showed an improvement on both elastic modulus and tensile strength. The elastic modulus had an improvement of 58%, and 48% for the longitudinal, and  $z$ -direction samples, respectively, when comparing the raw to the 5 turn samples. The tensile strength had an improvement of 70%, and 97%, for the longitudinal, and  $z$ -direction samples, respectively, when comparing the same group of samples. The bending tests showed that when adding reinforcement to the neutral axis, it does not effect on the flexural modulus of the part. However, an improvement of 14%, and 12% could be seen on the flexural strength, for the longitudinal and  $z$ -direction samples, when comparing the raw to the 5 turn samples.

# Preface

This thesis is original work by Gabriel Salata. Part of Chapter 3 of this thesis have been published as Salata, G., Ayranci, C., Nobes, D. (2018) “*Effect of coating on the sealing performance of a 3D printed ABS cylinder*” at the Canadian Materials Science Conference.

# Acknowledgements

I would like to sincerely thank both my supervisors, Dr. David S. Nobes and Dr Cagri Ayranci, for their continuous support throughout my studies, especially Dr Nobes. I think without his encouragement and motivation, I would not be able to finish this masters. I am very thankful to have had him as my advisor. I could not imagine having other supervisors and I will be forever grateful for both of them.

I would like to dedicate this thesis to my family and friends. It is not easy to go study abroad leaving everything behind, however their support, and encouragement, made me come to this end. Thanks to my father, Denylson Salata, to my mother, Lilian Beltrao Pontes Salata, and to my sister, Luisa Beltrao Pontes Salata.

I could not forget to thank all my lab mates and friends for all their support, friendship, and help. Friends that I will, for sure, have forever in my heart, especially Beatriz Bravo, David Serrano, Hermes Gordon, Lisa Kinsale, Shadi Ansari, Yishak Yusuf.

Gabriel Salata

June, 2019

# Table of Contents

Abstract.....	ii
Preface .....	iv
Acknowledgements.....	v
Table of Contents.....	vi
List of Tables .....	x
List of Figures.....	xi
List of Symbols and Acronyms.....	xviii
Chapter 1. Literature Review.....	1
1.1 Introduction.....	1
1.2 3D printing as an additive manufacturing process.....	1
1.3 Fused Filament Fabrication.....	4
1.4 Materials used on FFF 3D printing technology .....	5
1.5 Pre-manufacturing stage of FFF 3D printing technology .....	7
1.6 Post-manufacturing stage of FFF 3D printing technology.....	10
1.6.1 Sanding .....	11
1.6.2 Priming and Painting.....	11

1.6.3	Dipping .....	12
1.6.4	Acetone vapor smoothing .....	13
1.6.5	Epoxy coating .....	14
1.7	Mechanical properties of FFF 3D printed parts .....	15
1.8	Stirling engines .....	19
1.9	Challenges of designing a Stirling engine using FFF 3D printing technology as the main manufacturing process .....	20
1.9.1	Sealing and temperature related issues .....	21
1.9.2	Mechanical properties related issues .....	21
1.10	Study of the sealing performance of an 3D printed part using FFF 3D printing technology .....	22
1.11	Study of the post tensioning technique applied to 3D printed parts .....	24
1.12	Objective and motivation .....	27
1.13	Thesis Outline .....	28
Chapter 2.	Experimental Setup .....	30
2.1	Introduction .....	30
2.2	Effect of coating on the pressure withstanding capacity of 3D printed ABS cylinder .....	30
2.2.1	Samples for the experiment .....	31
2.2.2	Pressure Vessel .....	36

2.2.3	Experiment procedure .....	40
2.2.4	Data collection .....	41
2.3	Effect of reinforcing 3D printed ABS parts .....	42
2.3.1	The process of making the samples for both tensile and bending test .....	43
2.3.2	Components used for the reinforced samples .....	48
2.3.3	Experiment procedure .....	52
2.4	Uncertainty analysis .....	57
Chapter 3.	Effect of Coating on the Pressure Withstanding Capacity of 3D Printed ABS Cylinder.....	60
3.1	Results .....	61
3.1.1	Cylinders with wall thickness of 1/8" .....	61
3.1.2	Cylinders with wall thickness of 1/16" .....	66
3.2	Conclusion .....	70
3.2.1	1/8" samples .....	70
3.2.2	1/16" samples .....	71
Chapter 4.	Effect of Reinforcing 3D Printed ABS Parts .....	72
4.1	Tensile tests .....	72
4.1.1	Metal rods .....	72
4.1.2	Longitudinal samples .....	74

4.1.3	Z-direction samples.....	85
4.1.4	Comparison between longitudinal and z-direction samples .....	93
4.2	Bending tests .....	98
4.2.1	Longitudinal samples .....	98
4.2.2	Z-direction samples.....	105
4.2.3	Comparison between longitudinal and z-direction samples .....	111
4.3	Conclusion .....	116
4.3.1	Tensile tests.....	116
4.3.2	Bending tests.....	117
Chapter 5.	Conclusion and Future Work.....	119
5.1	Future work .....	120
References	.....	121
Appendix A:	3D printing parameters.....	135
Appendix B:	Properties of the TC-1614 A/B epoxy.....	138
Appendix C:	Drawing package.....	141
Appendix D:	Codes written for processing data .....	151

# List of Tables

Table 1: Comparison between PLA and ABS when using the FFF 3D printing technology. ....	6
Table 2: The dimensions of the two configurations of the cylinder. ....	32
Table 3: Main parameters used on the slicing software for printing the specimens for both tensile and bending samples. ....	43
Table 4: Average weight and number of samples used for each experiment. ....	48
Table 5: Error sources, error types, and their standard uncertainty. ....	59
Table 6: Overall comparison amongst the elastic modulus for the longitudinal samples. ....	78
Table 7: Overall comparison amongst the tensile strength for the longitudinal samples. ....	79
Table 8: Overall comparison amongst the elastic modulus for the <i>z</i> -direction samples. ....	89
Table 9: Overall comparison amongst the tensile strength for the <i>z</i> -direction samples. ....	89
Table 10: Overall comparison amongst the flexural modulus for the longitudinal samples. ....	101
Table 11: Overall comparison amongst the flexural strength for the longitudinal samples. ....	101
Table 12: Overall comparison amongst the flexural modulus for the <i>z</i> -direction samples. ....	108
Table 13: Overall comparison amongst the flexural strength for the <i>z</i> -direction samples. ....	108

# List of Figures

Figure 1: All the different stages of the 3D printing manufacturing process, from the 3D CAD model to the 3D printed prototype.....	2
Figure 2: The FFF 3D printing technology with (a) its main components of the machine and the (b) coordinate axis taken into consideration for the studies. ....	5
Figure 3: The acetone vapor smoothing technique applied to 3D printed parts. Figure (a) shows the prototype after the vapor smoothing technique, while (b) shows the failure of the same part after exposed to temperatures of 92 °C. This shows that the presence of acetone on a 3D printed part can affect their glass transition temperature [105].....	24
Figure 4: The different samples used for the experiment, in which for each wall thickness there was tested three different samples: raw, spray painted, and epoxy coated. ....	31
Figure 5: Description of the main parameters of the dimension of the cylinder. ....	32
Figure 6: Inside view of the Ultimaker 2+ illustrating the printing direction of the cylinders in which in the figure it is printing a z-direction sample. ....	33
Figure 7: Utensils used on the post processing of the epoxy sample.....	36
Figure 8: Pressure vessel designed for the pressure test experiment: (a) front and top view of assembly with main dimensions, (b) components of the assembly in an aligned section view, including a detailed view showing the inside gaps of the geometry. ....	38
Figure 9: A digital image showing a mix of water and soap to check if leakage was present during the experiment through the body of the cylinder.....	41

Figure 10: The setup of the experiment with a (a) a picture of the actual setup taken in the laboratory, and (b) a schematic of the complete setup from the air compressor to the data processing..... 42

Figure 11: Overall dimensions for the samples used for the tensile tests, including: (a) raw, (b) with hole only and (c) reinforced samples. The samples used for the bending test including: (d) raw, (e) with hole only and (f) reinforced samples..... 45

Figure 12: Resume of all the samples used for each experiment. There were tested five samples of each type for both tensile and bending tests..... 46

Figure 13: The process of threading the metal rods using a (a) thread rolling machine. (b) A closer look of the roll dies used for the thread creation..... 49

Figure 14: The setup for testing the metal rods in the laboratory. The (a) overall view of assembly, and (b) a closer image showing the main components of the assembly..... 52

Figure 15: The setup of the MTS 810 for the (a) tensile, and (b) 3-point bending tests ..... 53

Figure 16: The assembly used for the tensile test of the metal rods on the MTS 810. The grips of the machine were attached to the black ABS 3D printed part..... 54

Figure 17: Setup of the MTS 810 for the 3-point bending tests. .... 56

Figure 18: The three different cylinder samples with a wall thickness of 1/8” used on the pressure measurement..... 60

Figure 19: The change in pressure with respect to time for the raw sample with a wall thickness of 1/8”..... 61

Figure 20: The change in pressure with respect to time for the spray painted sample with a wall thickness of 1/8” ..... 62

Figure 21: The change in pressure with respect to time for the epoxy coated sample with a wall thickness of 1/8” ..... 63

Figure 22: Comparison amongst the three different samples with a wall thickness of 1/8”, showing the effect of the coatings in the sealing performance with respect to time. .... 64

Figure 23: Comparison of the pressure drop for the (a) raw, (b) spray painted, and (c) epoxy coated samples with a wall thickness of 1/8”, showing the effect of the coatings in the sealing performance with respect to time. .... 65

Figure 24: Comparison of the change in pressure with respect to time amongst the samples with a wall thickness of 1/8” for each pressure setting. .... 66

Figure 25: The change in pressure with respect to time for the raw sample with a wall thickness of 1/16” ..... 67

Figure 26: The change in pressure with respect to time for the spray painted sample with a wall thickness of 1/16” ..... 68

Figure 27: The change in pressure with respect to time for the epoxy coated sample with a wall thickness of 1/16” ..... 68

Figure 28: Comparison of the change in pressure with respect to time amongst the samples with a wall thickness of 1/16” for each pressure setting. .... 69

Figure 29: The change in pressure with respect to time for the 110% infill raw sample with a wall thickness of 1/16” ..... 70

Figure 30: The stress-strain curve showing the results of the tensile tests done on five different samples of the metal rod.....	73
Figure 31: The stress-strain curve of the metal rod samples illustrating the position that each turn of the nut would represent in the curve. ....	74
Figure 32: The stress-strain curve showing the results of the tensile tests for the (a) raw, and (b) hole longitudinal samples.....	75
Figure 33: The stress-strain curve showing the results of the tensile tests for the (a) 1 turn, (b) 3 turn, and (c) 5 turn longitudinal samples.....	77
Figure 34: Overall comparison of the elastic modulus for the longitudinal samples where the error bars are the standard deviation of the mean .....	78
Figure 35: Overall comparison of the tensile strength for the longitudinal samples where the error bars are the standard deviation of the mean. ....	79
Figure 36: The stress-strain curve comparing the results of the tensile tests between the raw, and the hole longitudinal samples.....	82
Figure 37: The stress-strain curve comparing the results of the tensile tests between the raw, and the 5 turn longitudinal samples.....	83
Figure 38: The stress-strain curve comparing the results of the tensile tests between the (a) 1 turn and 3 turn, and the (b) 3 turn and 5 turn longitudinal samples.....	84
Figure 39: The stress-strain curve comparing the results of the tensile tests amongst the raw, 1 turn, and the 5 turn longitudinal samples.....	85

Figure 40: The stress-strain curve showing the results of the tensile tests for the (a) raw, and (b) hole <i>z</i> -direction samples. ....	86
Figure 41: Stress-strain curve showing the results of the tensile tests for the (a) 1 turn, (b) 3 turn, and (c) 5 turn <i>z</i> -direction samples. ....	88
Figure 42: Overall comparison amongst the elastic modulus for the <i>z</i> -direction samples where the error bars are the standard deviation of the mean.....	89
Figure 43: Overall comparison amongst the tensile strength for the <i>z</i> -direction samples where the error bars are the standard deviation of the mean.....	90
Figure 44: The stress-strain curve comparing the results of the tensile tests between the raw, and the hole <i>z</i> -direction samples. ....	90
Figure 45: The stress-strain curve comparing the results of the tensile tests between the raw, and the 5 turn <i>z</i> -direction samples.....	91
Figure 46: The stress-strain curve comparing the results of the tensile tests between the (a) 1 turn and 3 turn, and the (b) 3 turn and 5 turn <i>z</i> -direction samples.....	92
Figure 47: The stress-strain curve comparing the results of the tensile tests amongst the raw, 3 turn, and the 5 turn <i>z</i> -direction samples. ....	93
Figure 48: The stress-strain curve comparing the results of the tensile tests between the (a) raw, and the (b) hole samples for the longitudinal and <i>z</i> -direction. ....	94
Figure 49: The stress-strain curve comparing the results of the tensile tests amongst the (a) 1 turn, (b) 3 turn, and (c) 5 turn samples for the longitudinal and <i>z</i> -direction.....	95

Figure 50: The stress-strain curve comparing the results of the tensile tests between the raw, and the 5 turn longitudinal and z-direction samples, where the samples with higher tensile strength are the 5 turn, and the ones with lower tensile strength are the raw samples..... 96

Figure 51: The comparison of results from the tensile tests for both longitudinal and z-direction samples. It compares the (a) elastic modulus, and (b) tensile strength amongst all samples for both printing orientations..... 97

Figure 52: The axial load-stroke curve showing the results of the 3 point bending tests for the (a) raw, and (b) hole longitudinal samples..... 99

Figure 53: The axial load-stroke curve showing the results of the 3 point bending tests for the (a) 3 turn, and (b) 5 turn longitudinal samples..... 100

Figure 54: Comparison of the (a) flexural modulus, and (b) flexural strength amongst all the longitudinal samples. The error bars represent the standard deviation of the mean. .... 103

Figure 55: The axial load-stroke curve comparing the results of the 3 point bending tests for the (a) raw and hole samples, and for the (b) 3 turn and 5 turn longitudinal samples. .... 104

Figure 56: The axial load-stroke curve comparing the results of the 3 point bending tests for the raw, and 3 turn longitudinal samples..... 105

Figure 57: The axial load-stroke curve showing the results of the 3 point bending tests for the (a) raw, and (b) hole z-direction samples..... 106

Figure 58: The axial load-stroke curve showing the results of the 3 point bending tests for the (a) 3 turn, and (b) 5 turn z-direction samples..... 108

Figure 59: Comparison of the (a) flexural modulus, and (b) flexural strength amongst all the z-direction samples. The error bars represent the standard deviation of the mean ..... 109

Figure 60: The axial load-stroke curve comparing the results of the 3 point bending tests for the (a) raw and hole samples, and for the (b) 3 turn and 5 turn for the  $z$ -direction samples... 110

Figure 61: The axial load-stroke curve comparing the results of the 3 point bending tests for the raw, and 3 turn  $z$ -direction samples..... 111

Figure 62: The axial load-stroke curve comparing the results of the 3 point bending tests between the (a) raw, and the (b) hole samples for the longitudinal and  $z$ -direction..... 112

Figure 63: The axial load-stroke curve comparing the results of the 3 point bending tests between the (a) 3 turn, and (b) 5 turn samples for the longitudinal and  $z$ -direction..... 113

Figure 64: The comparison of results from the 3-point bending tests for both longitudinal and  $z$ -direction samples. It compares the (a) flexural modulus, and (b) flexural strength amongst all samples for both printing orientations..... 115

Figure 65: The stress distribution showing the effects of the compressive loads applied on the reinforced samples and how it improved their flexural strength, assuming the rod has negligible effect on it. Figure (a) demonstrates the uniform distribution of the compressive loads applied from the washers through the tightening of the nuts; (b) stress distribution of the hole sample during the bending test at its failure point; (c) shows the effect of the compressive loads on the normal stress distribution of the hole sample; (d) the final stress distribution of the combined stresses applied to the reinforced samples. .... 116

# List of Symbols and Acronyms

Symbol/Acronyms	Description	Unit
CAD	Computer Aided Drawing	-
STL	Standard Tessellation Language	-
AM	Additive Manufacturing	-
FFF	Fused Filament Fabrication	-
ABS	Acrylonitrile Butadiene Styrene	-
PLA	Polylactic Acid	-
DOE	Design of Experiments	-
PEEK	Polyether Ether Ketone	-
ASTM	American Society for Testing and Materials	-
ASM	American Society for Metals	-
DAQ	Data Acquisition	-
$\emptyset_{outer}$	Outer Diameter	mm
$\emptyset_{inner}$	Inner Diameter	mm
$L$	Length of Cylinder	mm
SLA	Stereolithography	-
NPT	National Pipe Thread Taper	-
NPTF	National Pipe Taper Fuel	-
ISO	International Organization for Standardization	-
MTS	Material Test System	-
$N$	Number of Samples	-
$s_X$	Standard Deviation	-
$s_{\bar{X}}$	Uncertainty	-
$K$	Number of Random Error Sources	-
$s_{\bar{X}_k}$	Random Uncertainty of $k^{th}$ Source	-
$b_{\bar{X}}$	Bias Uncertainty	-
$b_{\bar{X}_k}$	Bias Uncertainty of $k^{th}$ Source	-

$u_{\bar{x}}$	Combined Standard Uncertainty	-
$\varepsilon_{cm}$	Strain of the Composite Material	mm/mm
$\varepsilon_f$	Strain of the Fiber	mm/mm
$\varepsilon_m$	Strain of the Matrix	mm/mm
$P_{cm}$	Load Carried by the Composite Material	N
$P_f$	Load Carried by the Fiber	N
$P_m$	Load Carried by the Matrix	N
$\sigma_{cm}$	Tensile Strength of Composite Material	Pa
$\sigma_f$	Tensile Strength of Fiber	Pa
$\sigma_m$	Tensile Strength of Matrix	Pa
$A_{cm}$	Cross Sectional Area of Composite Material	mm <sup>2</sup>
$A_f$	Cross Sectional Area of Fiber	mm <sup>2</sup>
$A_m$	Cross Sectional Area of Matrix	mm <sup>2</sup>
$E_{cm}$	Elastic Modulus of Composite	Pa
$E_f$	Elastic Modulus of Fiber	Pa
$E_m$	Elastic Modulus of Matrix	Pa
$V_f$	Volume Fraction of Fiber	-
$V_m$	Volume Fraction of Matrix	-
$E_{fms}$	Flexural Modulus of Sample	Pa
$L_s$	Length of Support Spam	mm
$F$	Load Applied onto the Center of the Sample	N
$w$	Width of Sample	mm
$h$	Height of Sample	mm
$d$	Deflection of Sample due to $F$	mm
$\sigma_{fs}$	Flexural Strength of Sample	Pa
$I$	Second Moment of Area	mm <sup>4</sup>
$I_r$	Second Moment of Area of a Rectangle	mm <sup>4</sup>
$I_c$	Second Moment of Area of a Circle	mm <sup>4</sup>
$y$	Distance from the Neutral Axis	mm
$M$	Bending Moment	N.mm

$r$	Radius of Circle	mm
$\sigma_c$	Compressive Stress	Pa
$\sigma_t$	Tensile Stress	Pa

# **Chapter 1.Literature Review**

## **1.1 Introduction**

In the field of manufacturing, there has been many developments of new methods for producing/creating different prototypes. This study investigates the use of 3D printing manufacturing techniques to fabricate low temperature Stirling engines, considering the limitations of standard manufacturing processes. This chapter includes a brief introduction on the 3D printing technology and its applications, while later, being more specific on how to make these parts more functional when it comes to designing/manufacturing an engine using this technology.

## **1.2 3D printing as an additive manufacturing process**

3D printing is an additive manufacturing process that can generate physical objects from a Computer Aided Drawing (CAD) design [1]. There are several different 3D printing technologies and a broad range of materials available currently [2]–[5]. However, even though there are many options, they are all based on the same concept, where a CAD model is turned into a physical object in a layer by layer process [6]. Its applications cover a broad range of industries and professions. The automotive industries have been using 3D printing for prototyping and for custom car parts used in professional racing cars [7]. The medical and prosthetics industries have been customizing hearing aids which can be produced with lower costs and faster [8]. Also, dentists are 3D scanning jaws and teeth and digitally designing custom braces and dental aids [9]. The

prosthetics field has been working on making some people's lives easier by creating prosthetic hands, arms and legs and therefore helping disabled people [10]. The aircraft industries have designed 3D printed fuel nozzles for jet engines which facilitates the changing and replacement of complex parts, and also makes the aircraft lighter [11]. Aerospace companies are manufacturing engine chamber out of 3D printed parts on spacecraft, using Inconel, which is a high-performance super alloy, as the material [12]. The entertainment industries have been using 3D printed props on some of the movies, since 3D printing has become more accessible currently [13]. The architects have been creating 3D printed scale models out of existing CAD files. Scale models can also be 3D printed in multiple materials and colors, making these models almost identical to reality [14]. Shoe manufactures started using 3D printing technology to produce midsoles as part of some shoes [15].

Every 3D printed object comes from a CAD model [16]. All the different stages of the 3D printing manufacturing process are shown in Figure 1. These digital designs are saved as a Standard Tessellation Language (STL) file format and then send to a slicing software who will slice the 3D CAD model into thin layers [17]. Thus, the digital model is ready to be send to the 3D printer. At this point, the printing process and the outcome result will vary depending on the type of 3D printing technology and material used. The 3D printing technology could be very useful in some aspects, however, just like any other manufacturing process has its pros and cons [6].

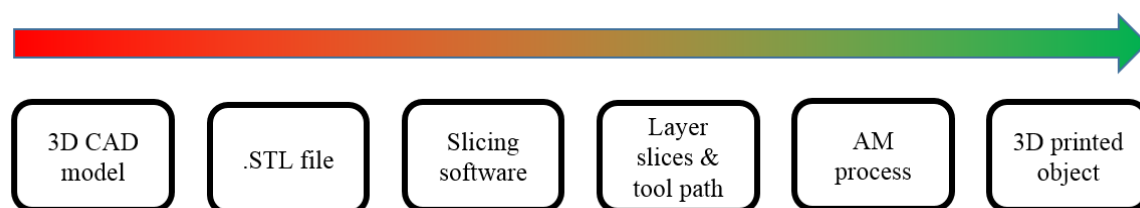


Figure 1: All the different stages of the 3D printing manufacturing process, from the 3D CAD model to the 3D printed prototype.

There are many advantages in this manufacturing process and one of them is the ability of creating complex geometries, and customized items while having a lower fixed cost and less waste of material [18]–[20]. The layer by layer process allows 3D printers to generate complex geometries of which cannot be produced by conventional manufacturing processes [19]. 3D printed parts can also be customized according to its application, unlike the parts coming from conventional manufacturing process where most of the time it comes in standards sizes and geometries [21]. The lower fixed cost is another plus for this technology, especially when its compared to injection molding or metal casting, for example, for small-scale production [22]. The injection molding and metal casting require a new mold each time a different part is to be produced, while 3D printers do not require any mold [22]. Similarly, since, 3D printing is a layer by layer process, when manufacturing an object, it only requires as much material as needed, unlike the conventional manufacturing processes where most of the time parts comes from blocks that are cut and machined until the intended object is achieved, wasting a lot of material [19]. However, just like any other technology, 3D printing has its downsides as well. The choices of materials are still inferior when compared to what conventional manufacturing process could utilize [23]. Also, conventional manufacturing processes are still a better choice when it comes to large production runs, including injection molding and metal casting [22]. Another issue is the limited mechanical stiffness and strength of 3D printed parts. Since 3D printed parts are produced in a layer by layer process, it makes the parts' properties non-uniform and leading to an anisotropic behavior [24], [25]. Their elastic and mechanical properties are also different when the same part is printed in different machines where the repeatability could be another issue [26].

Despite the advantages and issues related to the 3D printing, this technology has grown fast, and different printing methods started to take place. The different methods are divided mainly in

six groups of additive manufacturing techniques: material extrusion [2], vat photopolymerization [27], material jetting [4], binder jetting [2], powder bed fusion [2], and sheet lamination [2]. One of the most common is the material extrusion technique called Fused Filament Fabrication (FFF) due to its price, accessibility, and broad range of materials such as plastics, metals and composites [28], [29].

### **1.3 Fused Filament Fabrication**

The FFF 3D printing technology uses a string of solid material (filament) as the material [1]. Figure 2 shows the FFF 3D printing process including its main components. The filament coil is loaded into the printer and guided through a heated nozzle where the filament is extruded [30]. The extrusion starts whenever the nozzle reaches a certain temperature which is dependent on the type of material being used, for example the nozzle temperature for ABS ranges from 225 °C to 260 °C [31], while for PLA it goes from 185 °C to 205 °C [32]. Once the nozzle reached the expected temperature and started melting the filament, the extrusion head starts moving around depositing the melted filament, which cools down and solidifies, creating the first layer of the desired 3D printed object [1], [33]. The second layer starts by moving down the building platform, and then repeating the process done on the first layer [1]. This process repeats until the part is completely built [1].

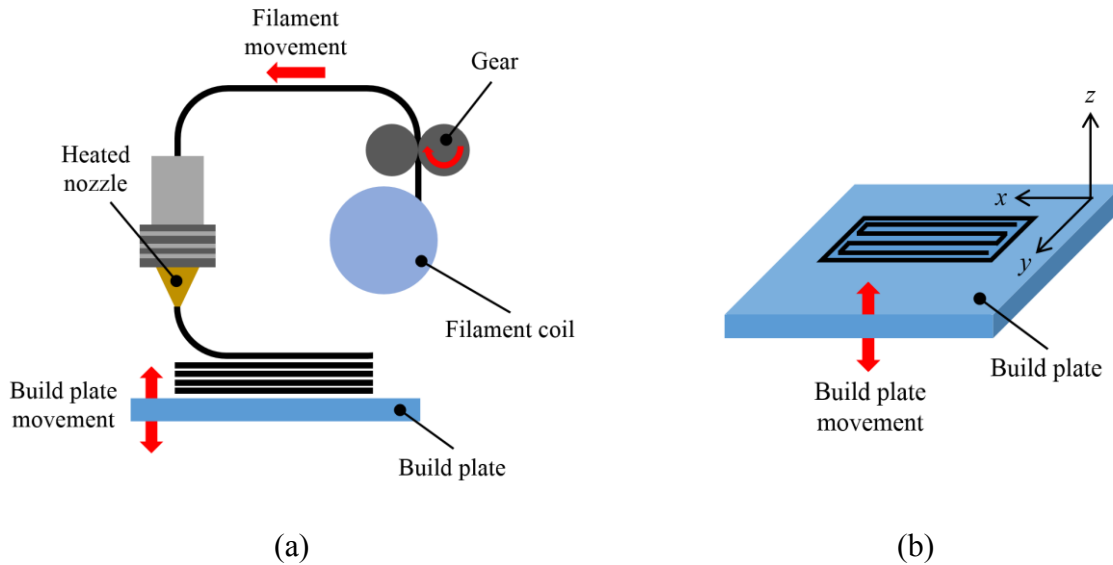


Figure 2: The FFF 3D printing technology with (a) its main components of the machine and the (b) coordinate axis taken into consideration for the studies.

The properties and parameters of a 3D printed prototype, such as printing resolution, or mechanical strength, is directly related to the chosen parameters during the pre-manufacturing stage [34]. The size of the nozzle and the layer height set on the slicing software, for example, could either increase or decrease the printing resolution of the prototype [34]. Also, the printing orientation could help on creating a 3D printed part more functional for its intent [25]. Parameters like those are crucial on the result of the prototype printed, and therefore should be chosen carefully. Next section will explain in detail each of the parameters that could be proper set during the pre-manufacturing stage.

#### 1.4 Materials used on FFF 3D printing technology

The FFF 3D printing technology can use a very broad range of materials that could go from plastics to metal [30]. Currently, the most common materials used are thermoplastic polymers, including, acrylonitrile butadiene styrene (ABS) [35], polycarbonate (PC) [36], polylactic acid (PLA) [37], polyether ether ketone (PEEK) [38]–[40], and others, where most of those polymers

are fabricated in a filament form. However, as mentioned, not only polymers can be extruded when using the FFF 3D printing technology. Composite materials are also very commonly utilized by using a polymeric matrix and short advanced fibers [41]–[44], as well as, ceramics [45], and metals [46].

Out of all the thermoplastic polymers used on the FFF 3D printing technology, ABS and PLA are the most common ones where one tends to be stronger and more flexible at higher temperatures while the other is easier to use [47]. PLA works for a wide variety of 3D printing applications because it is easier to print with while it is not as sensitive to temperature changes as ABS, therefore, it does not need a heated build plate or full enclosure, for example [47]. However, ABS is very sensible to temperature changes, requiring a full enclosure and a heated build plate to obtain a higher success on the final printed prototype [48]. When printing with ABS, the printing object cools down slowly, otherwise it could crack other layer lines or warp during the printing process [47]. Another downside of printing with ABS is the requirement of ventilation due to the fumes during the melting process, which is more toxic than the one from the PLA [49]. However, overall, ABS can withstand more heat, pressure, and stress when compared to PLA at higher temperatures due to its higher glass transition temperature [50], [51]. Table 1 shows a comparison between ABS and PLA filaments of the main parameters taken into consideration when using the FFF 3D printing technology.

Table 1: Comparison between PLA and ABS when using the FFF 3D printing technology.

	PLA	ABS
Printing temperature	180-230 °C	210-250 °C
Glass transition temperature	60-65 °C	~105 °C
Warping	No	Yes
Full enclosure	Optional	Recommended
Heated bed required	No	Yes
Fumes	No	Yes

PLA and ABS have both their advantages and disadvantages depending on the application and the intent of the prototype that needs to be printed. Overall, PLA seems to be a better option. However, it has a limitation with high temperature applications due to its low glass transition temperature. Therefore, if a higher temperature resistance is required, ABS is the better option.

## **1.5 Pre-manufacturing stage of FFF 3D printing technology**

The pre manufacturing stage plays one of the main roles on the result of the printing process. The 3D printer machine and the parameters on the slicing software should be appropriately set in order to have a 3D printed prototype satisfying its intent. There are several things on the 3D printer machine that needs to be checked, such as, the size of the nozzle that will better fit what is needed, the build plate should be clean and leveled. Those are two of the parameters that could directly interfere on the result of the 3D printed part. The slicing software is also important because all the printing parameters are set on it, and therefore, for example, the printing speed, the layer height, the infill percentage, can be optimized according the specific prototype. The main parameters that effects the results of the 3D printed prototype parts will be explained in this section, such as building volume of the printer, print resolution, warping, layer adhesion, build orientation, layer thickness, and more.

The objects printed using the FFF technology have their sizes restricted to the building volume of the 3D printer [52]. Usually, the dimensions for a desktop printer are around  $200 \times 200 \times 200$  mm, while industrial printers could go up to  $1000 \times 1000 \times 1000$  mm or even more [1]. When parts are bigger than the building volume of the 3D printer, the best solution would be split into two different parts and later post process them to put both components together [1]. The printing resolution of those parts are basically defined by two parameters: nozzle diameter

and layer height. The smaller the nozzle diameter and the layer height the higher the resolution and the surface smoothness [53], [54]. However, to achieve higher accuracy parameters such as, building speed, extrusions speed, and nozzle temperature control and consistency of extrusion should be properly set [1].

The layer thickness or layer height is the measure of the height of the material that is deposited during the layer by layer process or the vertical resolution obtained on the z-direction [54]. This parameter is affected by the diameter of the nozzle and the rule of thumb is that the layer height is half of the diameter of the nozzle [55]. The layer thickness has direct effect on the surface finish and how smooth it will be [55]. The smaller the layer thickness the smoother the surface of the 3D printed parts and the rougher it will be as the diameter of the nozzle increases [1].

A problem faced sometimes when using the FFF technology is that parts tend to warp during the printing process due to the differential cooling rate of each layer [56]. As the filament is deposited onto the build platform and cools down, it shrinks and creates internal stresses [57]. Therefore, whenever a filament is deposited on top of another one and shrinks, it tends to pull the surrounding areas, thus leading to warping the distortion [57]. The most recommended ways of reducing these problems are using a heated bed, having a good bed adhesion, and having a uniform temperature inside the 3D printing machine [1].

The layer adhesion is another parameter that plays an important role in FFF technology. The layer adhesion is responsible for bonding the layers together [58]. As the filament is extruded from the nozzle and is pressed onto the previous layer that had already been deposited, re-melting the previous layer due to the higher temperature that when solidified creates a cohesive part [58]. As the filament is pressed onto the previous layers, the shape of the filament deposited becomes oval,

instead of a circle [30]. This oval geometry can lead to stress concentration spots, generating an anisotropic behavior and rougher surface finish of the 3D printed part [1].

To overcome this anisotropic behavior the building orientation of the 3D printed part should be properly set according to its intent [59]. The building orientation is the direction that the filament is going to be deposited on the 3D printed parts [25]. The building orientation can affect the mechanical properties of the part making it weaker or stronger depending on the orientation and what would be the applicability of it [25]. If the application requires to withstand a load on the  $z$ -direction for example, and the parts were 3D printed on the  $x$ -direction, this would make it weaker. In this case, by just printing it on the  $z$ -direction would make your part stronger and more applicable for that situation [25]. The build orientation also contributes for the anisotropic properties of 3D printed parts where the mechanical properties are different for different directions [1], [25].

Another parameter that works together with the building orientation is the raster and contour width. The raster and contour width are measured by the width of the material deposited on the 3D printed part [60]. These parameters can also be modified by changing the diameter of the nozzle, the smaller the diameter the thinner the width [54]. The contour width also contributes for the wall thickness parameter, where the more contour lines on the wall the thicker it will be, since the wall thickness is composed the contour lines [1]. Another factor that is also associated to the raster width is the raster angle. The raster angle is related to the path taken by the nozzle during the infill printing and it can vary from  $0^\circ$  to  $90^\circ$  [61]. It is used to overcome mechanical strength limitations where depending on the application of the part, changing the raster angle could be beneficial [61]. Such as, if a load is applied onto the part, it is important to have the raster angle parallel to that

load, improving its strength for that specific application [25]. While, having it perpendicular to the load could make the part weaker [25], [1].

To save on material and time, FFF parts are not usually printed solid. The internal structure of the part has low density which is known as infill [62]. The infill percentage varies based on the application required for that specific part. When it is required high strength, parts are usually printed with >80% infill and for low strength requirements, infill can be as low as 10% [1]. The infill geometry can vary from triangular, rectangular, honeycomb and others [1].

There are some downsides related to the FFF technology, and one of them is the requirement of support structures depending on the geometry of the part intended to be printed, in order to print successfully [63]. The supports are required whenever there are overhanging features narrower than 45 degrees relative to the build platform [1]. Another downside is the air gaps that could be created during the printing process. The air gap is how much overlap the 3D printed parts will have between layers/raster. This parameter is created during the filament deposition process. The best way to overcome it is by increasing the overlap on your printing and it should be done on the slicing software [1].

## **1.6 Post-manufacturing stage of FFF 3D printing technology**

FFF parts are known for their cost effectiveness in prototypes. However, most of the time these prototypes require some post processing, for example, if a smoother surface is essential, since the printed layers can be sanded on the surface of the printed object. In addition to the smoothness of the surface, some post processing methods can also contribute to the sealing performance by filling the air gaps, by improving the strength of the part, or even helping on moderating the anisotropic performance of these objects. This section will explain in detail some of the post-processing

techniques that could be done in order to achieve the intent of the part, such as sanding, priming and painting, dipping, acetone vapor smoothing, and epoxy coating.

### **1.6.1 Sanding**

Once the support material is removed, sometimes it can leave imperfections and extra material on the surface, also due to the layer by layer process. Therefore, if a smooth/controlled surface is required, sanding the surface of the 3D printed parts can be helpful on keeping the geometry and dimensions more accurate. The process of sanding can be done by using sandpapers in a range from 80 to 2000 grit. It is important to start with the coarse grit and proceed up to a finer one, always sanding in small circular motions [64]. However, depending on the applicability of the 3D printed part and the smoothness needed, sometimes going up to 800 grit should be enough, whereas sometimes its needed to go up to 5000 grit. It is recommended to start with dry sanding for the coarser grids and finish with wet sanding, to provide a better result [64]. The advantages of this technique are the extremely smooth surface finish and helps if additional post-processing is required, such as spray painting. However, sanding is usually not recommended when prints have 2 or less wall lines, also it is difficult to apply this technique for complex geometries where it could be hard to reach all the surface equally. Also, if sanding is done too aggressively and too much material is removed from the part, it could impact on the overall dimension accuracy [65].

### **1.6.2 Priming and Painting**

The process of priming and painting is probably the best approach when a more professional and a better visual appearance of the final product is required. This technique can provide a very smooth surface and a wide range of final product including colors, which are independent of the material it was printed in. Before priming, the 3D printed part should be sanded up to 600-800 grit

sandpapers to get rid of imperfections on the surface [65]. After sanding, the priming should be done in two coats, or more if necessary, using an aerosol primer. Once the primer is dry, the surface could be sanded again to obtain a uniform and smooth surface [64]. Therefore, the painting process can be done by either using regular inks or aerosol can, however aerosol painting cans provide a better result, by filling in the gaps better. There should be applied from 2-4 thin coats of aerosol paint, letting it dry between coats [64].

### **1.6.3 Dipping**

The dipping process is done by submerging a 3D printed parts in container filled with a specific solvent for an specific time to enhance the surface finishing, as mentioned by Galantucci et al. [66]. This process is very similar to the vapor smoothing, however, in this technique the part is completely dipped in the solvent, unlike the vapor smoothing technique where the vapor coming from the evaporation of the solvent interact with the part [67]. It is required an eye hook or similar attached to any type of wire for dipping the part in the solvent. The 3D printed part should be quickly submerged in the solvent for just couple seconds, depending on the material. Schmid et al. [68] , for example, used acetone dipping as a post processing where parts were dipped in acetone bath for about 5 min to reach the desired surface finish . After removing the part from the solvent, it should be hanged to let the solvent evaporate completely. The main advantages of this technique when compared to vapor smoothing technique is that it is much quicker, however since it is a more aggressive approach, it could impact on the overall geometry and tolerances of the part. Also, if the part is left for too long submerged, it might completely damage the part [66].

Galantucci et al. [69] studied the effect of acetone dipping on the flexural and tensile strengths. The results showed an improvement of the flexural strength, however, it slightly reduced

the tensile strength [69]. Percoco et al. [70] also found an improvement on the weight, ductility, flexural and compressive strength after dipping samples in acetone, however, 1% of those samples shrank and had to be discarded [70]. Rao et al. [71] studied the effect that each parameter such as solution concentration, time, initial roughness, and temperature of chemicals would have on the 3D printed part using DOE and ANOVA. It was found that concentration with regards to concentration-temperature and concentration-time interaction have the highest influence on the surface roughness [71]

#### **1.6.4 Acetone vapor smoothing**

The acetone vapor smoothing process allows the vapor of the acetone contained within the confined space to break the secondary bonds of the ABS creating this smoother and softer superficial layer. Therefore, 3D parts end up with a better surface finish. This whole post processing technique of ABS 3D printed parts happens inside a container. To start off the vapor smoothing process, acetone is poured onto paper towel/paper tissue and covering the inside of the container with this wet paper. Afterwards, to have most of the surface of the 3D printed parts exposed to the vapor, two small pieces of aluminum foil can be twisted and placed on the bottom of the container, working as a base support to the 3D printed part to be exposed. To finish the process, the container should be closed with a lid on top, letting the 3D printed part exposed to the acetone vapor for about 30 min. The acetone vapor smoothing post-processing technique should be done in a fume hood to avoid exposure to the odor coming from the acetone.

Kuo and Mao [72] studied the effect of heated acetone vapor on the surfaced finishing of 3D printed FFF parts. The experiment was done in a closed chamber where a fan, placed inside the chamber, was responsible for forcing the vapor circulation into the specimen. It was found that for

the higher rpm of the fan the better surfaced finished obtained, however, longer exposure was required for enhance the surface finishing of 3D printed parts with larger surface areas [72]. . Garg et al. [73] used cold vapor treatment of acetone of FFF specimens in a closed container to enhance the surface finish and investigate the dimensional accuracy. The results showed that the surface finish of components was greatly improved with minimum variation on the dimensions, however, if specimens were exposed for too long (90 min) corners and sharp edges would get rounded off [73]. Priedeman and Smith [74] developed a technique to understand the effect of exposure to vapor, evolved by heating of chemical in a controlled environment on the surface finishing of FFF specimens [74]. Espalin et al. [75] also studied the effect of vapor smoothing on FFF 3D printed ABS samples. In this study, parts were first allowed to cool down for few minutes in drying chamber and then placed in a smoothing chamber for about 10-30 s [75]. In this study, the solvent is heated in the smoothing chamber, and the vapors are, therefore, deposited onto the ABS samples which was hanged inside the chamber [75]. The vapors coming from the solvent penetrate through the surface of the sample due to surface tension, smoothing the surface finish [76].

Post-processing FFF parts using acetone could be very fast, cheap, and effective to improve surface finishing. However, the amount of exposure should be controlled in order to reduce damages to small features, as well as, dimensioning changes. In order to improve accuracy, methods such as acetone vapor smoothing could be automated and mechanized [77].

### **1.6.5 Epoxy coating**

The epoxy coating technique is done by using a two-part epoxy. This technique can provide a sealed part due to the shell created by the epoxy [78]. To start the post processing, the two parts of the epoxy need to be mixed according to the mix ratio given by the manufacturer. Improper

ratios could change the result, for example if not enough hardener is mixed, the epoxy might take longer to cure, also, the part might be tacky once cured. Once mixed, the epoxy should be applied onto the surface of the 3D printed part using a foam brush, for example [78]. One layer of epoxy should be enough, however, if more layers are needed, the dimensional accuracy might be altered [79]. After the epoxy is completely cured, again curing time is estimated by the manufacturer, the 3D printed part is ready to use.

## **1.7 Mechanical properties of FFF 3D printed parts**

The mechanical properties of an FFF 3D printed part is directly related to the printing parameters used, such as printing temperature, raster angle, etc [63]. Studies have been done to understand how changing parameters like those could affect on the mechanical property of a FFF 3D printed parts. Those studies will be described in the next paragraphs. Parameters that could affect on the mechanical properties can be split into two groups: manufacturing, and structural parameters. The manufacturing parameters include some of the settings selected during the pre-manufacturing, such as, printing speed and temperature, layer height, build plate temperature, etc. While, the group related to the structural parameters can include raster angle and width, building orientation, infill percentage, etc.

The FFF 3D printing technology, as mentioned earlier, produces parts that most of the time has an anisotropic behavior, and depending on the printing orientation they could be assume orthotropic. To understand more of these behaviors and how they affect the mechanical property of an FFF 3D printed part, many studies were done using tensile, compression, bending, and other types of tests. Ahn et al. and Rodriguez et al.[25], [80], studied the influence of both manufacturing and structural parameters, including printing temperature, raster angle, and air gaps. Ahn et al.

studied the effects of those parameters on the strength of the 3D printed part by testing samples printed in different raster angle and air gaps [25], while Rodriguez et al. studied the elastic properties of specimens printed in ABS prototypes where the results showed a reduction of 11% to 37% in the elastic modulus for fused deposition ABS materials when compared to the monofilament itself. The reductions happened when the samples were fabricated with positive air gaps (air gaps between each layer deposited) [80]. Another important factor that affects on the tensile strength of a 3D printed part are the bonding between layers, building orientation, also imperfections on the samples due to the layer by layer process [81].

Tymrak et al. studied the effects of the layer thickness for ABS and PLA on the tensile strength and elastic modulus for different raster angles of 0/90° and 45/-45° [82]. Uddin et al. also studied the effect of the layer thickness on 100% infilled ABS samples, where the highest values for tensile strength and elastic modulus were found with the thinnest layers [48]. However, the infill percentage showed to have a higher effect on the mechanical properties than the layer thickness [83]. This happens because the empty spots weaken the 3D printed part, contributing to an inferior mechanical property when compared to parts printed with 100% infill [84].

The printing orientation is another parameter that could affect on the tensile strength and elastic modulus of an FFF 3D printed part. However, Cantrell et al. showed that for 100% filled ABS specimens, different printing orientations did not have much effect on the elastic modulus [85]. The tensile strength of samples printed with different printing orientations seemed to be greatly affected by the bonding between layers [85]. Onwubolu and Rayegani [86] found that by reducing parameters such as layer thickness, raster width and air gaps the tensile strength increased [86]. They used design of experiments (DOE) approach to understand and identify parameters that would lead to a higher mechanical strength [86]. Deng et al. [40] also used the DOE approach to

find optimal parameters for a better tensile strength of specimens printed with PEEK. The higher tensile strength was found when parts were printed using a printing speed of 60 mm/s, layer thickness of 0.2 mm, nozzle temperature of 370 C and infill density of 40% [40].

The tensile strength and elastic modulus of a FFF 3D printed part also is affected by the number of wall lines/contour rasters when the filaments are deposited aligned to the loading direction [84], [87]. Samples for tensile testing printed with the wall lines along the *y*-direction usually have their mechanical properties misinterpreted due to the contribution of rasters printed in the *x*-direction [30]. Laureto and Pearce [88] studied the effect of two different types of specimens from the standard ASTM D638 on the tensile strength of 3D printed PLA. The type I and IV were used for the comparison and results showed the results may overestimated the ultimate tensile strength when comparing sample IV to I, respectively [88]. Following the same idea, Torrado and Roberson [89] studied the different ASTM D638 specimen types more in depth. The study showed that type V had a lower elongation up to breakage of 0.6-0.9 % when compared to the other types of standard specimens. The conclusion was that the variability in the raster had major effect on it [89].

The reductions of 11-37 % in the elastic modulus and 22-37 % in the tensile strength of FFF parts when comparing different air gaps found by Rodriguez et al. [83] were due to the difference in the presence of voids in each specimen [83]. Hossain et al. [63], [90], studied the effect of reducing the presence of air gaps by changing printing parameters looking for an improvement on the ultimate tensile strength. It was found that by increasing the raster width and reducing the air gaps led to 10-30 % improvement in the ultimate tensile strength, when compared to parts printed using default parameters [63], [90]. The voids within FFF parts can be controlled by modifying the infill percentage, also, by changing the overlapping between each deposited layer [62].

Studies were also done where 3D printed parts were reinforced with fillers like montmorillonite [91], with discontinuous [43], [44], and continuous fibers [92]–[95], in order to fill in the voids and improve the mechanical properties of the samples. Also, researches have been done on post-processing technique to improve surface quality, strength and tightness [96], [97].

Researches have been done to characterize the behavior of 3D printed parts under flexural loads. Sood et al. [98] studied the importance of parameters such as layer thickness, print orientation, raster angle, raster width and air gap, on the flexural properties of FFF 3D printed samples using the three-point bending test procedure. It was found that the printing with a raster angle of  $0^\circ$ , layer thickness of 0.25 mm, zero air gaps, and raster width of 0.5 mm provided the maximum flexural strength [98]. Wu et al. [99] found that the bending strength increased in 15% by having a raster angle of  $0^\circ$  for parts printed in PEEK when compared to parts printed in ABS [99].

Three-point bending tests were done on 100% infilled ABS samples with different printing angles and orientations to understand the behavior of the flexural strength [81]. Durgun and Ertan [81] also reported that surface roughness has an important effect on the flexural strength [81]. Lužanin et al. [100] studied the effects of different infill percentage, layer thickness, raster angle and width, on the flexural properties of PLA specimens. It was found that samples printed with a raster angle of  $0^\circ$  (filaments oriented parallelly with the length of the sample) and infill of 30% had the highest flexural strength [100]. That happens because the rasters that run axially with the sample withstand most of the load applied [101]. Somireddy et al. [102] studied the effect of different raster angles on the flexural modulus of ABS specimens. The maximum variation on the flexural modulus was found to be only 169 MPa amongst all the different samples which was expected since all the samples were printed with 100% infill [102]. Wagari Gebisa and Lemu [103]

used a full factorial DOE taking into consideration air gap, raster width and angle, contour number and width, as the variables, in order to characterize the flexural strength and modulus of FFF 3D printed specimens [103]. They found that the raster width and angle had the most influence on the flexural properties. Based on the DOE study, the optimal parameters were found to be zero air gap, raster thickness of 0.7814 mm, raster angle of  $0^\circ$  and five contours. The specimens printed with those parameters had a flexural strength of 127 MPa, flexural modulus of 2.4GPa, and ultimate flexural strain of 0.081 [103].

Chacon et al. [37] studied the flexural modulus of PLA samples with a zero air gap using the classic beam theory, while ignoring the effects of shear in the transverse deflection. It was found that printing speed had the most influence on the flexural modulus. Also, by having an air gap close to zero, the maximum flexural modulus variation amongst all the different combinations of printing orientation, layer thickness and printing speed was found to be 33% [37]. Cuan-Urquizo and Bhaskar [101] studied the effect of air gaps greater than zero, and different printing orientations on PLA specimens [101]. Kuznetsov et al. [47] did a different research where the ultimate fracture strength was studied on a tubular FFF 3D printed sample with 0% infill under three-point bending tests [47].

## **1.8 Stirling engines**

Stirling engine is a heat engine that is functioned by a closed-cycle with compression and expansion of a gas at different temperatures [104]. The temperature difference is composed by the hot and cold side, where each side correspond to either the compression or expansion section of the engine [105]. Therefore, any provided heat, creating a differential in temperature would be able to run the engine, such as solar, geothermal, etc. However, usually Stirling engine operates at

higher temperature difference in order to maximize power which is harder to obtain from natural resources such as solar and geothermal sources [106].

According to studies, the state of Alberta, in Canada, has a large geothermal potential for providing temperatures below to 150 °C [107]. Therefore, in order to understand the behavior of these engines under a low temperature difference, a Stirling engine was custom-built using different manufacturing processes. Due to the non-standard size and parameters used for the engine, some parts had to be 3D printed using the FFF technology. Since, the compression and expansion happen in a closed-cycle, the performance of the engine is very dependent on the sealing performance and mechanical strength of the whole mechanism. That is where the motivation for this work came from.

## **1.9 Challenges of designing a Stirling engine using FFF 3D printing technology as the main manufacturing process**

3D printed parts can be very helpful especially when it comes to complex and non-standard geometries. However, it also comes with some issues that need to be addressed. Stirling engines require a good sealing of their components, especially for the parts involved on the compression and expansion cycle, and 3D printed parts don't provide a good sealing performance. Also, due to its anisotropic behavior, 3D printed parts cannot withstand a lot of mechanical loads. Another issue is that even if the engine was designed for lower temperature difference, some of the plastics used on the FFF technology still have their glass transition temperature over it, meaning that it is required a material that would have a higher glass transition temperature when compared to the running temperatures used on the engine. The next two sections will describe those main issues faced while designing the engine, the sealing and temperatures, and mechanical properties issues.

### **1.9.1 Sealing and temperature related issues**

The sealing problems of 3D printed parts come from the layer-by-layer process where air gaps are created due to the retraction of the filament. These air gaps also lead to a non-uniform load distribution throughout the part, making some spots weaker. Therefore, to overcome the sealing limitation, this study aims to understand the effect of coatings on the sealing performance of 3D printed parts, therefore, getting the engine to run more efficiently.

The Stirling engine designed worked with temperatures up to 92 °C, therefore, as mentioned earlier, depending on the material used it might get damaged due to temperature related issues. The material chosen should have a glass transition temperature higher than the temperatures used to operate the engine. The glass transition temperature is the temperature where a material starts changing from a hard/brittle to a rubbery stage. By taking into consideration two of the most common materials used on FFF processes which are PLA and ABS, their glass transition temperature ranges from 60-65 °C and 105 °C for PLA and ABS, respectively [50], [51]. Therefore, ABS was the material chosen to help overcoming this limitation.

### **1.9.2 Mechanical properties related issues**

The other major problem face while building the engine was the failure of some 3D printed parts. The first approach trying to overcome this issue was to over dimension the part and therefore make it stronger. However, the bigger the dimensions, the more material is wasted as well as printing time. Another concern was that since the engine was very compact, the parts could be too much bigger than what it was designed at first. This study aims to understand the effect of the post tensioning technique applied to 3D printed parts in order to improve their mechanical properties and solve the issues faced while build the low temperature Stirling engine.

## **1.10 Study of the sealing performance of an 3D printed part using FFF 3D printing technology**

Studies have been done trying to understand the sealing performance of a 3D printed part. Mireles et al. [79] studied the applicability of 3D printed parts as sealants on fluid pressure applications by reducing the porosity of specimens with chemical treatment. There were eleven sealants, including epoxies, with different chemical properties that were applied to the specimens through vacuum infiltration and brushing. The results showed that the sealing method using the BJB TC-1614 epoxy (TC-1614 A/B, BJB Enterprises), had the best performance, where the brushed specimens could withstand to ~40 psi, and up to ~20 psi when using the vacuum infiltration approach. However, even though the mechanically brushed parts seemed to withstand higher pressure loads, they had a higher change in dimension while the parts treated through the vacuum infiltration system did not seemed to have change on their dimensions [79].

McCullough and Yadavalli [108] studied the sealing performance and surface finish of 3D printed ABS parts using acetone dipping. They designed and 3D printed a micro fluidic channel where water would be the fluid used for their experiment. However, it was leaking through the air gaps, therefore they used the acetone dipping approach, trying to dissolve the ABS enough to be capable to hold water without leaking. The acetone dipping proved to help on make 3D printed parts impervious to water. Optimum conditions were found to be 1-8h of exposure with 60 per cent aqueous solution which resulted in a surface finish up to nanoscale while preserving part features [108].

The acetone vapor smoothing was the first approach done trying to get the low temperature Stirling engines to be properly sealed. After applying the vapor smoothing technique, the parts

seemed to seal well, however, after some time with the machine running, the 3D printed parts would start to fail as shown in Figure 3 [105]. Therefore, an investigation was done trying to understand what the actual effects of acetone on an ABS 3D printed part are. Zhang and Shin studied the effect of the acetone vapor smoothing on the mechanical properties of ABS parts manufactured using the FFF technology. They observed temperature-dependent storage modulus, and coefficient of thermal expansion for parts exposed to a different concentration of acetone during the vapor smoothing process by using dynamic mechanical analysis and dilatometer. It could be seen a decrease in the glass transition temperature for parts chemically treated with acetone vapor smoothing, where parts not treated had a glass transition temperature of about 114 °C, while parts treated had values around 70 °C. Therefore, they could conclude that acetone vapor smoothing weakens the thermal stability of the 3D printed part. According to this study, the reason for the parts in the engine to be failing after some time, is the temperature of the machine being higher than the new glass transition temperature of the 3D printed part [109]. However, further study needs to be done when it comes to the time given for the acetone to evaporate before testing it, since it was not very clear in the study by Zhang and Shin.



(a)

(b)

Figure 3: The acetone vapor smoothing technique applied to 3D printed parts. Figure (a) shows the prototype after the vapor smoothing technique, while (b) shows the failure of the same part after exposed to temperatures of 92 °C. This shows that the presence of acetone on a 3D printed part can affect their glass transition temperature [105].

Bélanger and Marquet [67] used a 3D printed prototype for digital holographic microscopy in the field of microfluids. The prototype was a perfusion chamber that had to be able to handle a rapid laminar flow without leaking. Initially, the 3D printed perfusion chamber was leaking through the internal porosities coming from the printing process. Therefore, in order to seal the closed chamber, they used the acetone vapor smoothing technique. They found that using this approach was helpful to successfully seal the mechanism and proceed with their experiments.

### 1.11 Study of the post tensioning technique applied to 3D printed parts

Concrete is the main material when it comes to construction of bridges, buildings, etc. However, for those bridges, for example, to withstand the mechanical loads applied to it while in service, the concrete is required to be reinforced, and this reinforcement is done by using a technique called pre/post tensioning. This technique consists in compressing the concrete using reinforcement material called tendons, that could be wires, rebars, etc. There are two different

ways of prestressing the concrete, by pre-tensioning the tendons or by post-tensioning them. The pre-tensioning technique consists in having the tendons tensioned prior to the concrete being cast, while the post-tensioning technique have the concrete casted first, and by using ducts through the concrete, the tendons are added and then tensioned afterwards. The concrete should be compressed because their tensile strength is only about 10% of its compressive strength, therefore, plain concrete parts are likely to crack/fail when loaded in tension. This technique strengthens the concrete due to the compressive load that now would have to be canceled by the tensile load before it starts cracking the concrete [110].

Studies have shown that 3D printed parts when printed in the  $z$ -direction have a higher compressive than tensile strength [24], [25]. Sung Hoon et al. found the compressive strength of 3D printed parts in the  $z$ -direction to be about 170% higher than the tensile strength [25]. Constance Ziemian et al. also found the compressive strength to be higher than the tensile strength by 140% for samples printed in the  $z$ -direction [24]. The American Society for Metals (ASM International) mentioned that the tensile strength of bulk ABS ranges from 32-45 MPa while the compressive strength goes from 65-90 MPa [111]. Therefore, having a compressive strength about 180% higher than the tensile strength, when considering the lowest value of the tensile strength and maximum value of compressive strength. According to these studies provided, 3D printed parts also seem to be a good fit for the post-tensioning technique, since their compressive strength is higher than the tensile strength. Also, parts coming from the FFF technique cannot use the pre-tensioning approach because it would have to be manufactured on top of a tensioned reinforcement in which would be a difficult task to accomplish, specially to get the tendons to have a good bonding with the 3D printed part.

There are not many studies related to the post-tensioning on 3D printed parts. The only one found in the literature was done by Hinchcliffe and Srubar III that studied the effect of the post-tensioning technique using natural-fibers as reinforcement on beam printed with PLA. The PLA specimens were tested for both tensile and flexural properties using different types of natural-fibers, as well as different levels of stresses applied to the reinforcement for different compressive loads purposes. The results indicated an increase of 116% and 62% for tensile strength and elastic modulus, and 14% and 10% for flexural strength, and flexural modulus, respectively [112]. According to this study, 3D printed parts seemed to have a good response when applying the post tensioning technique to it. Therefore, in order to better understand the effects of reinforcements on 3D printed parts, this study aims to quantify the improvements that can be obtained by using the post tensioning technique to the field of additive manufacturing.

## **1.12 Objective and motivation**

The objective of this thesis is to understand how to make 3D printed parts coming from the fused filament fabrication technique more functional when it comes to applications where good sealing performance and better mechanical properties are required.

The motivation of this research came from challenges faced while building a low temperature Stirling engine using fused filament fabrication 3D printed parts as the main manufacturing process for the parts of the engine. A variety of challenges were faced, and the main ones were leakage and failure/breakage of 3D printed parts. Therefore, ideas on how to overcome those issues started to be studied, such as the application of different coatings, and the post tensioning technique applied to 3D printed parts.

## 1.13 Thesis Outline

The structure of this thesis will be as described below:

In Chapter 1, the idea behind this thesis and what has been already done by other researchers is introduced. It will start by explaining basic concepts of additive manufacturing and 3D printing, including technologies available in this field, as well as applications related to this area. The fused filament fabrication technique will be explained more in details since this is the technique studied in this research. The materials commonly used on the FFF technique will be described while introducing to the most used ones, ABS and PLA. The main difference between these two polymers will be explained. The basic parameters of the 3D printing process will be introduced, such as building orientation, layer thickness, and others, while explaining how much influence those parameters could have on the result of the printed prototype. Post processing techniques will also be introduced, including acetone vapor smoothing, spray painting, and epoxy coating, which are the ones used on part of this study. Also, studies related to the mechanical properties of 3D printed parts will be described. This chapter will also, introduce Stirling engines, and the challenges that were faced while building an engine of this type using 3D printed parts. The main issues were related to sealing, and mechanical properties, therefore, studies related to those topics will also be introduced, such as coating applications and post tensioning technique.

Detailed information regarding the experimental procedures, equipment, design, data acquisition devices (DAQ), data processing techniques, and the uncertainty analysis are given in Chapter 2.

Chapter 3 will provide experimental results related to the pressure test experiment. These results helped understanding the effects of coatings on the sealing performance of an FFF 3D printed part.

Chapter 4 will showcase the results of tensile and three point bending tests using the post tensioning technique. The effect of adding reinforcement to 3D printed parts is better understood, as well as, how much it influences on the mechanical properties of a 3D printed part.

Chapter 5 will provide conclusion that could be taken from this study, also suggesting ideas for future work related to the area of functionality of 3D printed parts when it comes to sealing performance and mechanical properties improvement.

# **Chapter 2. Experimental Setup**

## **2.1 Introduction**

This chapter contains the detailed configuration of the experimental setup and describes the method used to process acquired data. In this section, all the equipment, software, and tools needed for this experimental study are listed and described. The steps needed for the evaluation of the sealing performance of a 3D printed parts are demonstrated. In addition, the method for adding reinforcement to 3D printed parts is described in detail. An additive manufacturing process using a 3D printer (Ultimaker 2+, Ultimaker B.V.) was used to manufacture all the samples for both experiments. This 3D printer uses the FFF technology to create prototypes. All the samples were printed using ABS as a material. The uncertainty calculations for the experiments were also considered.

## **2.2 Effect of coating on the pressure withstanding capacity of 3D printed**

### **ABS cylinder**

The effect of coating on the pressure withstanding capacity of a 3D printed ABS cylinder aims to understand how much adding a coating to a 3D printed part would improve its sealing performance. To achieve that, a custom-built pressure vessel was designed in order to perform pressure test to evaluate the sealing performance. The samples used as the main body of the pressure vessel were 3D printed ABS cylinders. The pressure inside the cylinders would be

monitored by a pressure transducer, and therefore, if any leakage happened through the cylinder, it would be recorded.

### 2.2.1 Samples for the experiment

The sealing performance experiment was done with six different 3D printed ABS cylinders. The samples can be categorized into two groups of three, based on their wall thickness, illustrated in Figure 4. Needing to understand the effect of coating on the sealing performance of a 3D printed ABS part, two different post processing techniques of spray painting and epoxy coating were used.

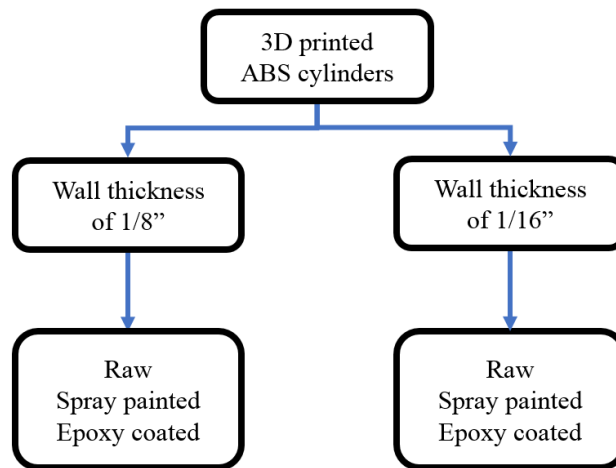


Figure 4: The different samples used for the experiment, in which for each wall thickness there was tested three different samples: raw, spray painted, and epoxy coated.

The two configurations of the cylinder were designed using the commercial software (SolidWorks, Dassault Systèmes SolidWorks Corp). The main dimensions of the cylinders can be found in the Table 2 and Figure 5. After the solid model was created, the file was saved as a .STL file which is the type of file is used for rapid prototyping, 3D printing and CAD manufacturing. The .STL file would then be opened on a slicing software (Ultimaker Cura, Ultimaker B.V.), where the parameters such as printing orientation, layer height, and printing speed can be adjusted. The setup parameters and their values used in the manufacturing procedure can be found in the

Appendix A. The printing speed was set to be 45 mm/s for all the sample thickness. According to the slicing software, the 1/8" and 1/16" samples had a printing time of 6 h and 40 secs, and 4 h and 14 secs, respectively. The difference in the printing time was due to the total weight of the printed material which were 132 g of material, and 67 g for the 1/8" and 1/16" samples respectively.

Table 2: The dimensions of the two configurations of the cylinder.

Parameters	Cylinders	
	1/8"	1/16"
Outer diameter, $\phi_{outer}$ (mm)	83.32 (3 1/4")	83.32 (3 1/4")
Inner diameter, $\phi_{inner}$ (mm)	76.97 (3")	80.15 (3 3/16")
Length, $L$ (mm)	152.4 (6")	152.4 (6")

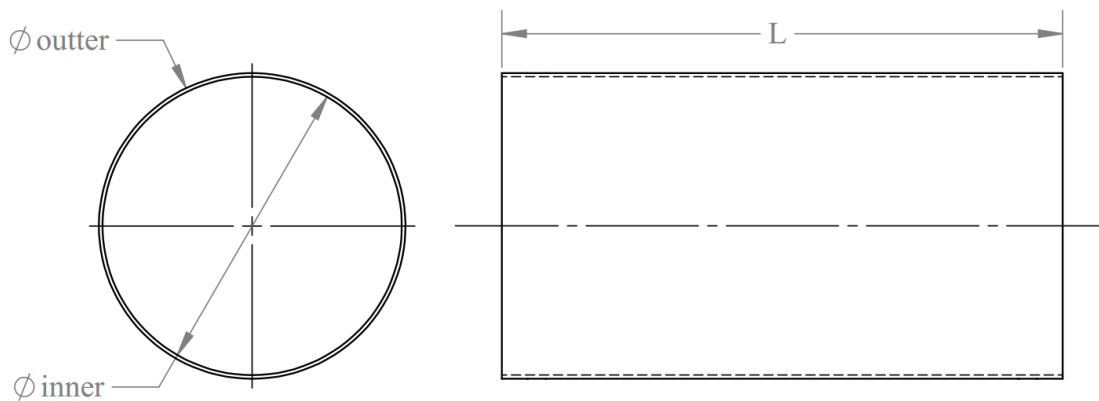


Figure 5: Description of the main parameters of the dimension of the cylinder.

The cylinders were 3D printed using a commercial FFF machine (Ultimaker 2+, Ultimaker B.V.). The 3D printer manufactures the desired features using fused filament fabrication (FFF) printing technology. The printer had a physical dimension of  $342 \times 357 \times 388$  mm (width  $\times$  length  $\times$  height) and build volume of  $223 \times 223 \times 205$  mm. Acrylonitrile butadiene styrene (ABS) was used as the printing material due to its higher glass transition temperature of  $\sim 105$  °C when compared to Polylactide (PLA), which is  $\sim 60$ - $65$  °C. This thermal resistance of the

printing material was selected as the representative since the Stirling engines operate with temperatures around 90-95 °C, which is higher than glass transition temperature of the PLA.

The filament used was the Ultimaker ABS+ black filament with 2.85mm diameter from Ultimaker B.V. The cylinders were printed in the z-direction, as defined in Figure 6, with a 0.8 mm nozzle. They were printed one at a time to avoid any issues due to retraction. As recommended by the manufacturer of the filament, the temperature of the build plate and the nozzle were selected to be 100 °C and 240 °C, respectively. The surface build plate was covered using a BuildTak sheet to improve printing adhesion. The manufactured cylinders were removed from the build plate using a scraper.

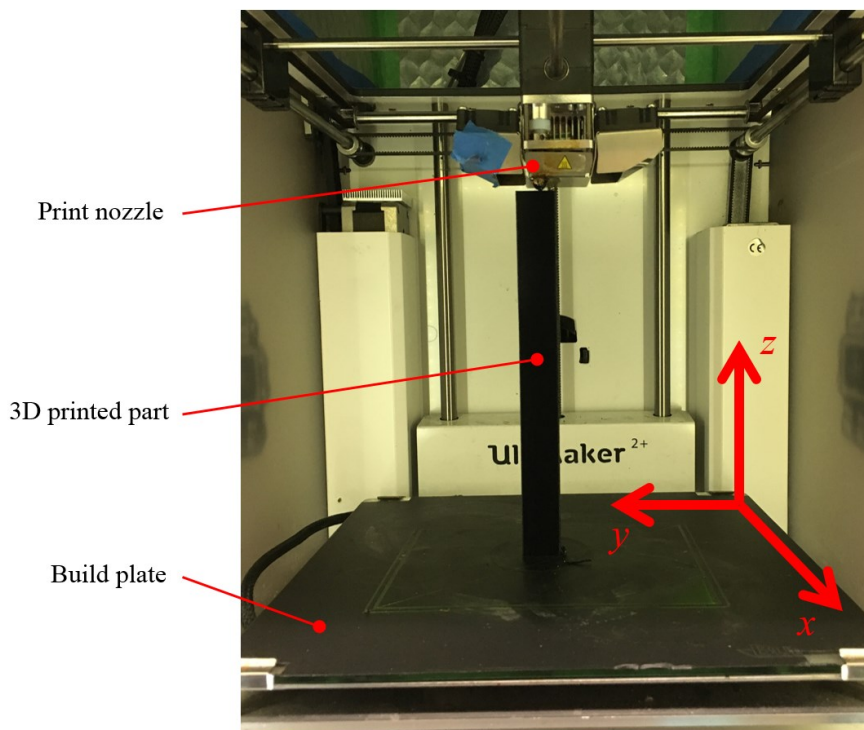


Figure 6: Inside view of the Ultimaker 2+ illustrating the printing direction of the cylinders in which in the figure it is printing a z-direction sample.

The 3D printed parts can have imperfections, gaps and bumps between the layers of the manufactured surface due to the layer-by-layer fabrication process. These gaps may ultimately

lead to potential leaking spots and that could also be abrasive when in contact with O-rings later during the experiment. Sanding and smoothing the surface will help to minimize the leaking potentials in such condition. Therefore, the next step of the manufacturing procedure was to sand the outer surface of cylinder at 20 mm from each end. The sanding was done to smooth only the surfaces that would be in contact with the O-rings in the experiments. The outside edges from both top/bottom surfaces were also sanded to provide a rounded surface which improves the assembly of the cylinder with the pressure vessel.

The sanding process was done starting with a coarse grit and finishing with a finer one. The first sanding was done with 120 grit sandpaper, followed by 200, 400, 800 and 1500. The first three sanding were dry sanded while the last two, 800 and 1500, were wet sanded. The raw samples used in the experiments are ready to pass through the pressure test after this step. For the spray painted and epoxy samples, however, more post processing steps are required. These steps are described in detail in the following sections.

### **Preparing a spray painted sample**

To improve the sealing of the 3D printed material, a filler primer (Filler Primer Spray, Rust-Oleum) was used to fill in the grooves and air gaps existent on the surface of the 3D printed cylinder. In this step, a gray filler primer (Filler Primer Spray, Rust-Oleum) was applied after sanding the raw material. To insure the proper sealing, three layers of filler primer was applied onto the outer surface with an interval of 10 min between layers. Also, to have a homogeneous spray material on the surface, the sealing material was shaken for one minute before spraying each layer. The last step of the preparation of the spray painted sample was done by applying three layers of black spray painting (2x Ultra Cover Paint+Primer, Rust-Oleum) for plastic adhesion. The same spraying procedure was used in this stage.

## **Manufacturing steps for Epoxy coated sample**

In order to prepare the epoxy coated samples, the initial stage was to sand the samples as described in the raw sample pre-processing steps. After sanding, a layer of epoxy was applied onto the outer surface of the cylinder. The epoxy mixture was a two parts epoxy (TC-1614 A/B, BJB Enterprises), as recommended by the manufacturer, to seal 3D printed parts. The epoxy will penetrate and seal porous surfaces due to its low viscosity (600 cps at 25 °C) and high adhesion properties. The sealing will remain consistent for the operating temperatures up to 177 °C. The properties of the epoxy are described in more detailed in Appendix B.

To have a homogeneous epoxy mixture, the viscosity of the mixing components needs to be reduced first. In this step, both parts were collected from their respective containers using two different 10 ml pipettes (one for each part of the epoxy) and poured into two different regular plastic cups. The plastic cups were placed in an oven and exposed to a temperature of 35 °C for 20 min. After taking the part out of the oven, part A and B were then poured into the same plastic cup and a wooden stick was used to mix it together. The ratio of the parts was 100/23 by volume (part A and B, respectively) as recommended by the manufacturing company. All the utensils used for this sample can be seen in Figure 7. The mixture of epoxy has its highest sealing performance up to 2 hours after the mixing time. Therefore, the mixture was applied to the sample just after mixing it. A foam brush was used to apply one layer of the epoxy onto the outside surface of the cylinder. The applied layer was cured by letting it stand inside of a fume hood for 24 hours before using it for the experiment.

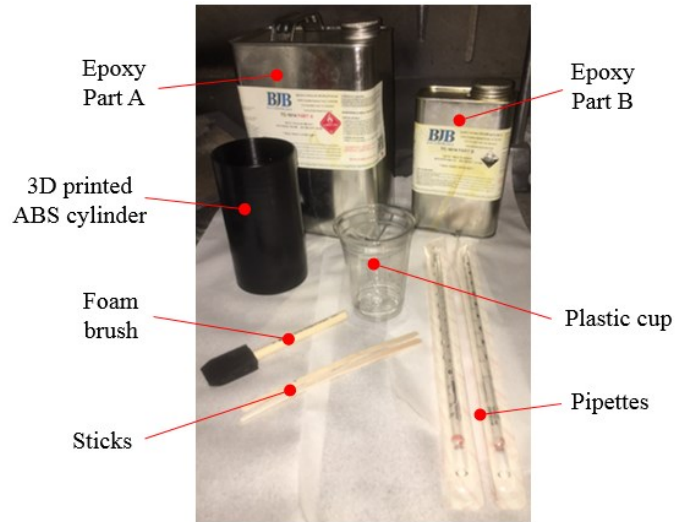


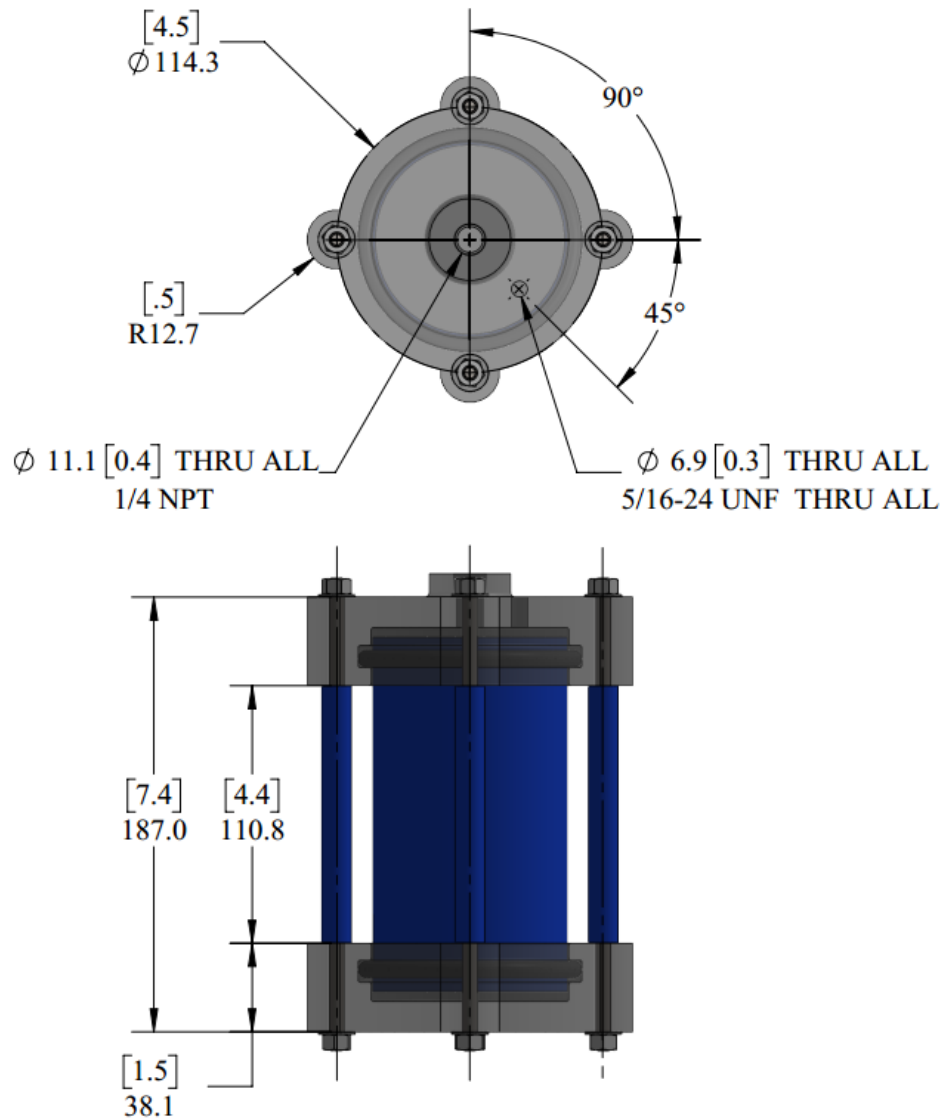
Figure 7: Utensils used on the post processing of the epoxy sample.

### 2.2.2 Pressure Vessel

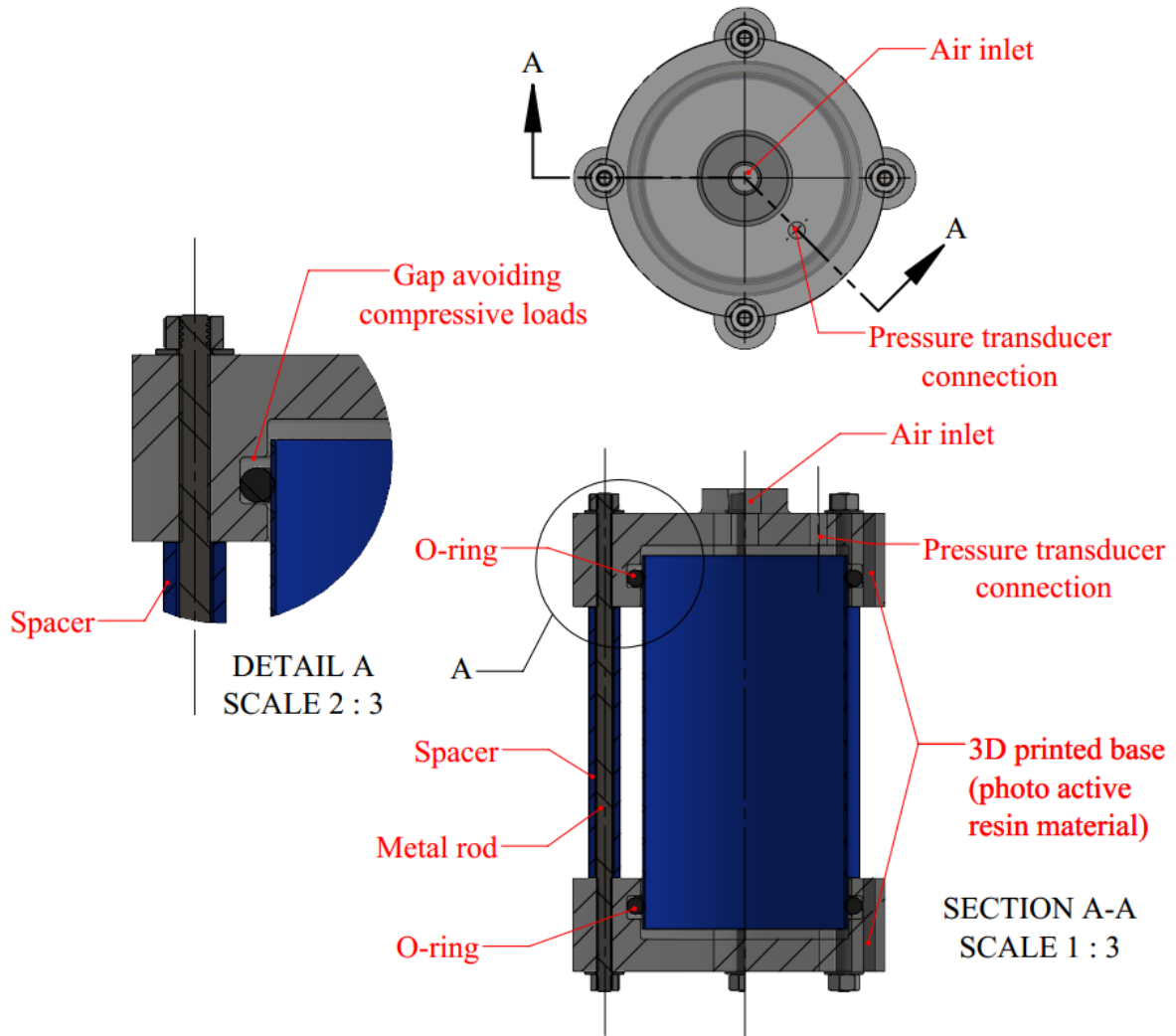
A pressure vessel was designed in order to perform the pressure test on the 3D printed ABS cylinders. The design intent of the pressure vessel was to fit the cylinder, sealing the whole assembly by using two O-rings, one for each support base. The top support base would have a hole used for the air inlet. The solid model of the pressure vessel assembly is shown in Figure 8. The assembly consists of two base supports, two O-rings, four spacers, four metal rods, nuts, and washers.

The bases were printed using a 3D printer (Form 2, Formlabs Inc.) in which uses the stereolithography (SLA) technology. The SLA technology uses photopolymerization to create models, prototypes and parts, in a layer-by-layer process. The support bases were printed using a clear photopolymer resin (RS-F2-GPCL-04, Formlabs Inc.). An issue of the stereolithography technology is the requirement of support material to every print, which creates a non-flat surface after the support material is taken off. The support material is also required whenever there is overhanging areas, therefore, it was required to apply support material to the O-rings grooves. Those support materials were all sanded off using the same procedure used for the cylinders. It

was important to sand those areas in order to avoid abrasive damages to the O-rings. The top base has two holes, one for the inlet air pressure and the other one for fitting the pressure transducer which reads the pressure inside the cylinder. The hole for the pressure transducer was tapped for 5/16"-24 thread while the inlet air pressure was tapped for 1/4" NPT threads. The presence of the O-rings in the top and the bottom of the main pressure vessel enhances the sealing of the cylinder within the two support bases. The two O-rings had a width of 1/4" and the material was Buna-N rubber.



(a)



(b)

Figure 8: Pressure vessel designed for the pressure test experiment: (a) front and top view of assembly with main dimensions, (b) components of the assembly in an aligned section view, including a detailed view showing the inside gaps of the geometry.

The spacers in the pressure vessel were designed to set a limit to the movement of the support bases to avoid compressive loads to be applied onto the cylinder. Therefore, the presence of the spacers in the pressure vessel will only enable loads due to pressure to act onto the cylinder. The four spacers were 3D printed on an FFF printer (Ultimaker 2+, Ultimaker B.V.), out of ABS material. The same printing procedure and settings as of the cylinders were used to print these parts. The alignment of the lead and the pressure vessel was achieved using four 1/4"-20 threaded metal rods combined with eight 1/4" washers and eight 1/4"-20 nuts.

## **Procedure for assembly of the pressure vessel**

Prior to placing the cylinder within the pressure vessel, the assembly started by applying a layer of high-performance synthetic grease onto the O-rings as well as onto the top/bottom outside surface of the cylinder. The synthetic grease enhances the sealing performance of the O-rings and helps on the fitting of the cylinder within the top/bottom support bases. It also helps by avoiding that abrasion happens due to the decrease in the friction between the cylinder and the O-ring. After applying the grease, the O-rings were placed on the internal grooves located inside of both support bases.

The next step was to place the cylinders inside both support bases until it passes by the O-rings and gets in contact with the internal side of the base. After the bases and cylinder are placed together, it is necessary to align the four holes of the top base to the four from the bottom. The alignment is done by spinning the support bases until the holes are approximately aligned. After the alignment, the spacers were placed between the support bases and the metal rods were introduced, passing through the top base, spacer, and bottom base. To complete the assembly of the pressure vessel, eight nuts and eight washers were put on both ends of each of the four metal rods.

Air at a controlled pressure was proved to the test cylinder assembly using a commercial air compressor (C2004-WK - Porter Cable, Stanley Black & Decker, Inc.). The compressor has a built-in pressure regulator to help on applying the desired pressure to the cylinder. The hose of the air compressor was attached to a needle valve (1/4" NPTF pipe size female) through a high-pressure brass nipple threaded on both ends for pipe sizes of 1/4" NPT. The needle valve was used to lock and control the pressure inside the cylinder. Both sides of the needle valve were directly connected to two of the nipples at each end. One side connected to the hose coming from the air

compressor and the other one was directly connected to another hose that would be connected to the cylinder. The hose and the cylinder were connected using a nipple that were threaded onto the ¼” NPT hole of the top base of the pressure vessel to the hose coming from the air compressor. To improve the sealing of the connections Teflon tape was used for all the threaded fittings existent in the overall assembly. The other hole on the top support base was threaded with 3/16”-24 for the pressure tap.

### **2.2.3 Experiment procedure**

Once the system was assembled together, a brief load of 10 psi was applied in order to proper seal the system. Ultimately, the pressure inside the cylinder was reduced to 5 psi, to evaluate the sealing performance of the system. To check for any possible leakage, a mixture of water and neutral detergent was used to coat the outer surface of the system. This mixture was applied throughout the entire systems, especially at fittings connections such as nipples, valve, hose connections, and between cylinder and O-rings. In case of presence of a leakage, bubbles would be produced in the system. After retreating the leakage of the system and ensuring the proper sealing, the system is ready to be used for the experiments.

The experiment was carried out by applying pressure inside the cylinder starting at 10 psi to maximum pressure of 100 psi to evaluate the pressure drop with respect to time. In each set of experiment, the increase in pressure was achieved by steps of 10 psi with 5 min intervals. For each pressure tested, the needle valve was remained open at the start and then it was closed after the desired pressure was reached. During the 5 mins of the test in each set pressure, leakage would be indicated as a pressure change on the live pressure measurement plot data. For safety purposes,

the cylinder test assembly was placed in a metal confined spaced and safety glasses were used in case of blown out during the experiment.

Once all the experiments were done and the data was collected, the pressure inside the cylinder was reduced to atmospheric pressure. The cylinder sample was removed from the metal container for a secondary leakage test. In this step, a pressure of 20 psi was applied to the sample in order to identify where the air was leaking through. The only accepted leakages spot was through the main body of the cylinder as shown in Figure 9. After this step, the same experimental procedure was used to evaluate the sealing performance of different cylinder samples. This experiment was repeated 6 times to insure the repeatability of the experiments



Figure 9: A digital image showing a mix of water and soap to check if leakage was present during the experiment through the body of the cylinder.

#### 2.2.4 Data collection

The pressure was measured using a pressure transducer that was directly connected to the cylinder. The voltage signal emitted from the pressure transducer was measured by a data acquisition system (DAQ) system. The recording and monitoring of data were achieved by using a custom-built software in an integrated development environment (LabWindows CVI, National Instruments). The inhouse code collected the data from the pressure transducer every 0.5 sec. The

pressure transducer used in this experiment had an uncertainty of 0.5 % of the measured pressure. The setup of the experiment plus the data acquisition system can be seen in Figure 10.

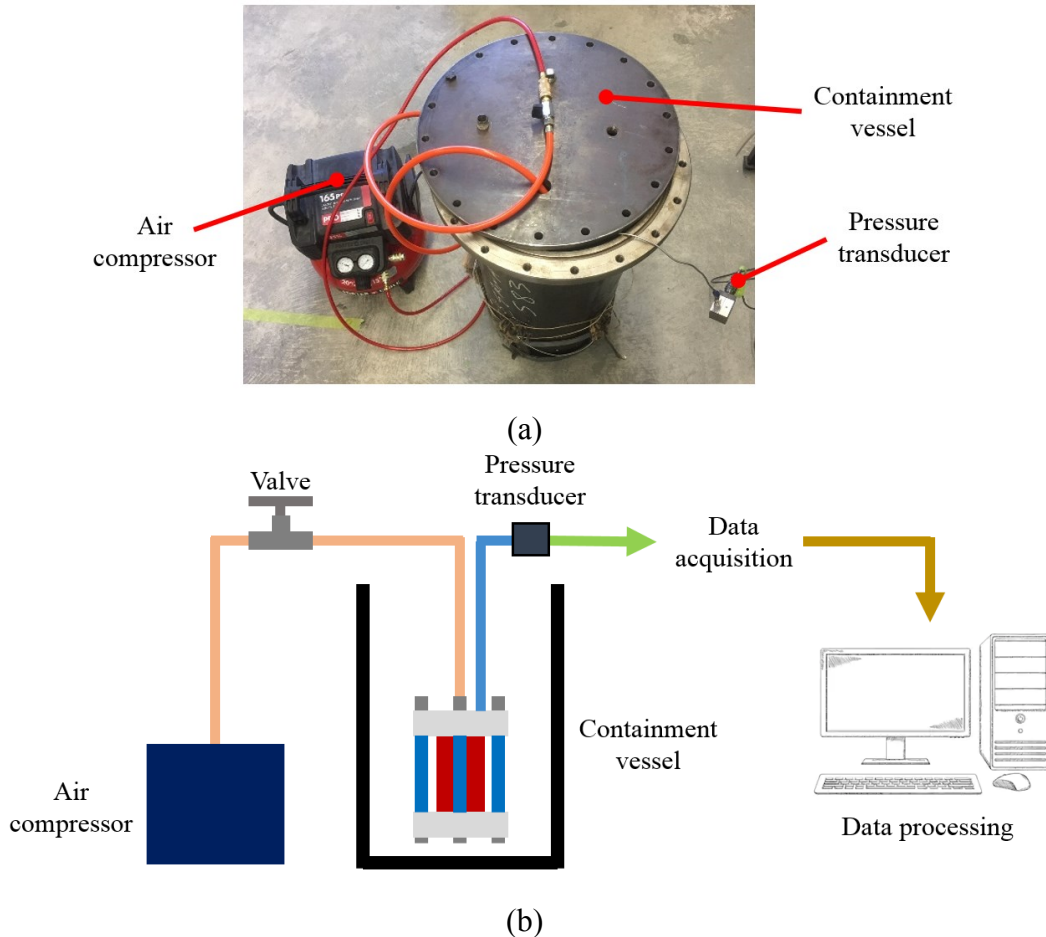


Figure 10: The setup of the experiment with a (a) a picture of the actual setup taken in the laboratory, and (b) a schematic of the complete setup from the air compressor to the data processing.

### 2.3 Effect of reinforcing 3D printed ABS parts

This section will discuss the steps of the experimental setup for the reinforcement study. It will include the preparation of the metal rods, and the process of 3D printing the two different types of specimens, which are longitudinal and z-direction, for both tensile and bending tests. The procedure of adding the metal rods into the 3D printed ABS samples is also explained in detail. The data acquisition method is also described.

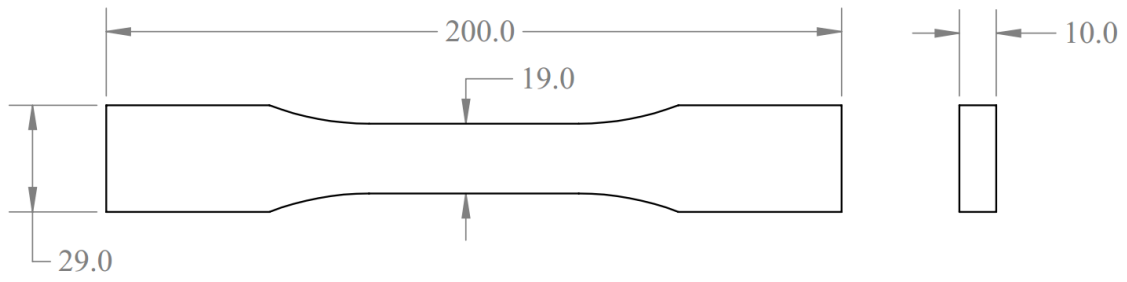
### 2.3.1 The process of making the samples for both tensile and bending test

The tensile samples (dog bones) were tested following the standards for tensile properties and bending tests. The ASTM D638 - Type III [113], was the standard procedure followed for the tensile tests. This standard specifically used for tensile properties of plastic. The bending tests were based on the ISO 178 [114] standards. The ISO 178 is used to determine the flexural properties of plastics which is like the ASTM D790 [115], in case of following the ASTM for the bending test as well. However, there is a difference between them. The ISO 178 standard test continues until the sample breaks while the ASTM D790 does not.

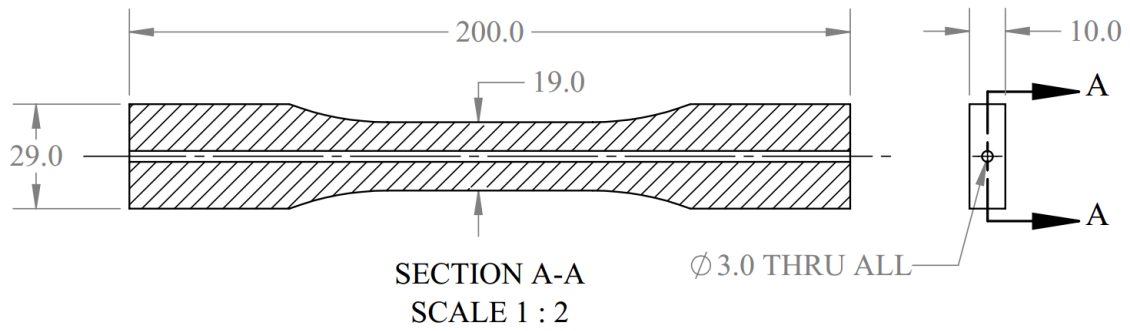
Both configurations of specimens used in these experiments were designed using a commercially available software (SolidWorks, Dassault Systèmes SolidWorks Corp), and the main dimensions for both tensile and bending samples are shown in Figure 11. The detailed drawing is provided on Appendix C. The finalized sample designs were saved as a STL file, that corresponds to stereolithography, in order to be prepared for the slicing software. The Ultimaker Cura (Ultimaker Cura, Ultimaker B.V.) was used as the slicing software. All the printing parameters such as printing orientation, infill percentage, and layer height were set to their optimal conditions in this software as shown in the Table 3. The complete set of parameters used in the slicing software are shown in Appendix A.

Table 3: Main parameters used on the slicing software for printing the specimens for both tensile and bending samples.

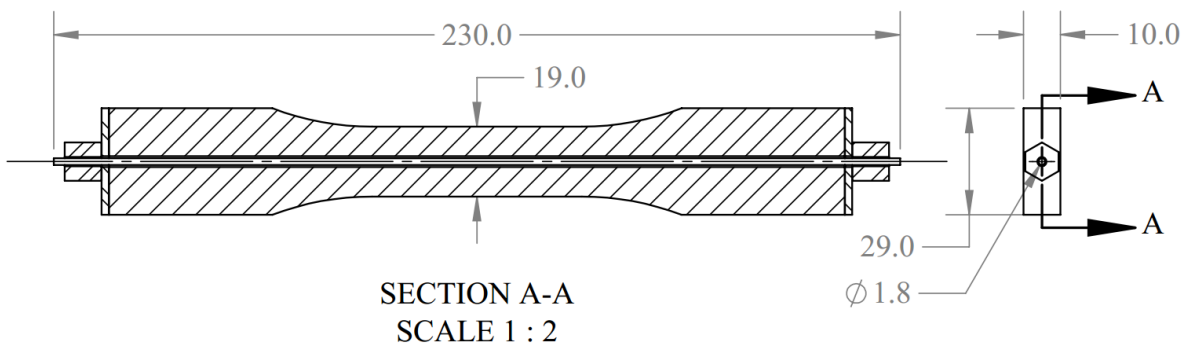
Parameters	Samples	
	Bending	Tensile
Layer Height (mm)	0.2	0.2
Line Width (mm)	0.7	0.7
Wall Thickness (mm)	2.1	2.1
Infill	100 %	100 %
Print Speed (mm/s)	45	45



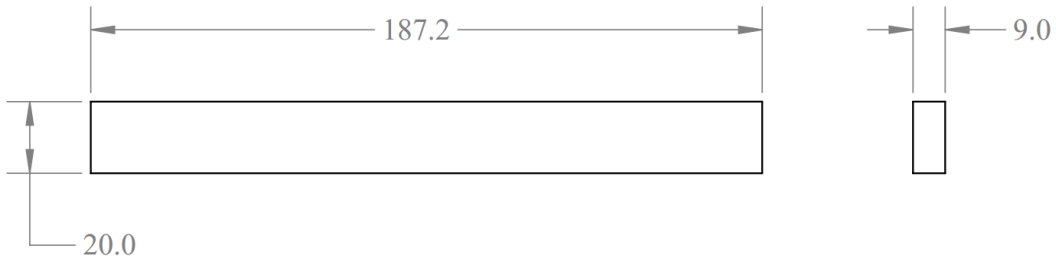
(a)



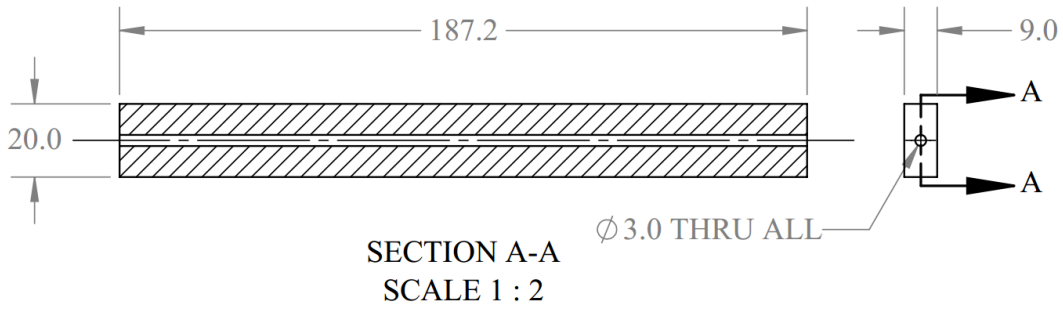
(b)



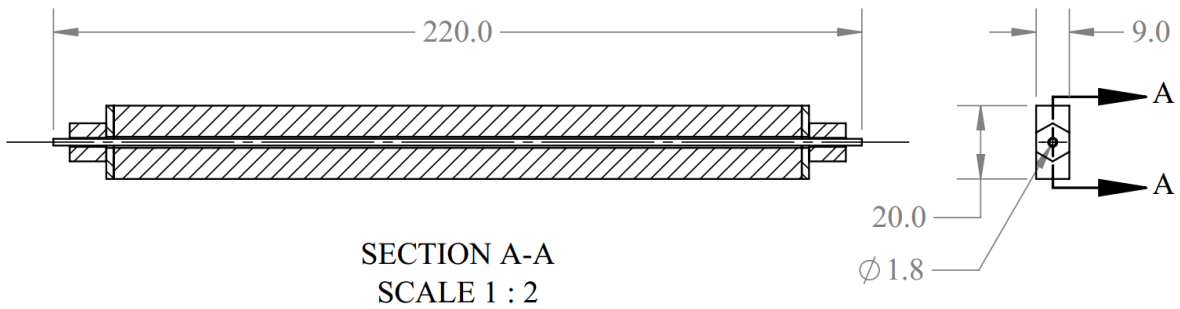
(c)



(d)



(e)



(f)

Figure 11: Overall dimensions for the samples used for the tensile tests, including: (a) raw, (b) with hole only and (c) reinforced samples. The samples used for the bending test including: (d) raw, (e) with hole only and (f) reinforced samples.

For both tensile and bending tests, there were two different types of specimens where the difference was related to the printing orientation. The two different printing orientations were the longitudinal ( $y$ -direction) and  $z$ -axis orientation. The coordinate system used is the same as the schematic shown earlier in Figure 6. The idea behind the two selected orientations was to understand the effect that having two complete opposite filament deposition orientations would have on the mechanical properties of a 3D printed part. It is expected, for example, that the longitudinal ( $y$ -direction) samples will be mechanically stronger than the  $z$ -direction samples for both tensile and bending experiments. There were printed and tested five samples of each group category. Figure 12 shows all the different types of specimens used for both tensile and bending tests. The tensile test was composed by the raw, hole and 1, 3 and 5 turn samples referring to the integer number of turns of the tension nut. The groups of samples of the bending test had the raw, hole, 3 and 5 turn samples.

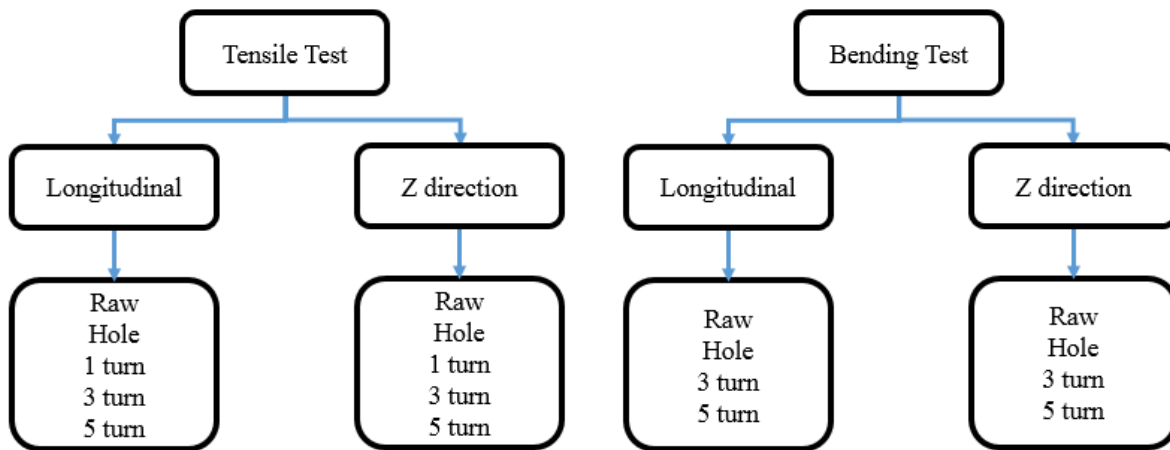


Figure 12: Resume of all the samples used for each experiment. There were tested five samples of each type for both tensile and bending tests.

The 3D printer used to manufacture the specimens was an FFF printer (Ultimaker 2+, Ultimaker B.V.). The size of the nozzle was chosen to be 0.8 mm of diameter and its printing temperature was set at 240 °C. The build plate had a temperature of 100 °C and to improve the

material adhesion it was covered with a BuildTak (Ideal Jacobs Corporation) The material used for the specimens was a black ABS 2.85 mm filament (Filaments.ca 3D Printer Filaments Canada) All the printing parameters were chosen based on the filament's manufacturer recommendations.

The raw sample is a solid prototype, as it is shown in Figure 11, while the hole sample had a hole of 3 mm in diameter going through the entire length of the part and located at the neutral axis. The samples used for the reinforcement test were basically the same hole samples but with a metal rod that would be added just before the experiment. The samples reinforced with the metal rods will be explained in more details later in this chapter. Every sampled used for the experiments had a printing infill of 100%. The printing time of the longitudinal, and  $z$ -direction raw specimens used on the tensile test were 2 h 21 min, and 4 h 18 min, respectively. The total weight of the raw samples after manufacturing, for example, were  $39.8 \pm 1.3$  g, and  $40.5 \pm 0.3$  g for longitudinal, and  $z$ -direction, respectively. The weight and number of samples printed for each experiment can be seen in the Table 4. The samples were printed one at a time in order to reduce the effect of the retraction, that could cause under extrusion of the filament, possibly generating stress concentration spots, and air gaps on the sample. The stress concentration spots and air gaps would reduce the materials strength and as well as interfere on the results of the experiments. Therefore, the samples were weighed and labeled for consistency and to keep track of the results, in case any inconsistency during the tests was found. The samples were also stored and separated into different sealed bags to avoid moisture.

Table 4: Average weight and number of samples used for each experiment.

	Bending samples				Tensile samples			
	Longitudinal		z-direction		Longitudinal		z-direction	
	Qty	Average weight (g)	Qty	Average weight (g)	Qty	Average weight (g)	Qty	Average weight (g)
Raw	5	28.6±1.2	5	33.5±0.2	5	39.8±1.3	5	45.9±0.3
Hole	5	27.5±0.8	5	31.7±0.3	5	39.9±0.9	5	44.9±0.5
1 turn	N/A	N/A	N/A	N/A	5	39.1±1.1	5	44.3±0.8
3 turns	5	28.1±1.0	5	30.6±0.1	5	39.3±0.8	5	44.7±0.6
5 turns	5	27.5±0.7	5	31.9±0.1	5	40.0±1.5	5	44.7±0.5

### 2.3.2 Components used for the reinforced samples

Detailed information regarding the manufacturing procedure of the reinforced samples is provided in this section. It will include the manufacturing processes used to fabricate each of the components of the reinforced samples' assembly. The assembly of each reinforcement specimen was composed by the 3D printed part, metal rod, two nuts, and two washers. The specification of each component is also described in this section.

#### **Metal rod**

The metal rods used were 0.071" (1.80 mm) in diameter and had a tensile strength of 261,000 psi (1800 MPa), according to the manufacturer (9666K42, McMaster-Carr Supply Company). The size of the wires was chosen carefully in order to have the approximate strength when compared to the 3D printed ABS samples used for the experiments. This comparison was done by calculating the tensile strength of each material, according to the equivalent area that each material would have on the total cross sectional area. The size of wire was also chosen specifically to match the

thread rolling machine (C-700 – Spoke Thread Chaser, HOZAN TOOL IND.CO., LTD.) used to create threads on both ends of the wire. It was an iron made thread rolling mechanism that could generate #2-56 threads for 14 and 15 wire gauge. The depth of the pitch depends on how tight together the three roll dies are. Figure 13 shows the thread rolling machine and its components, also how the metal rods were positioned to be threaded.

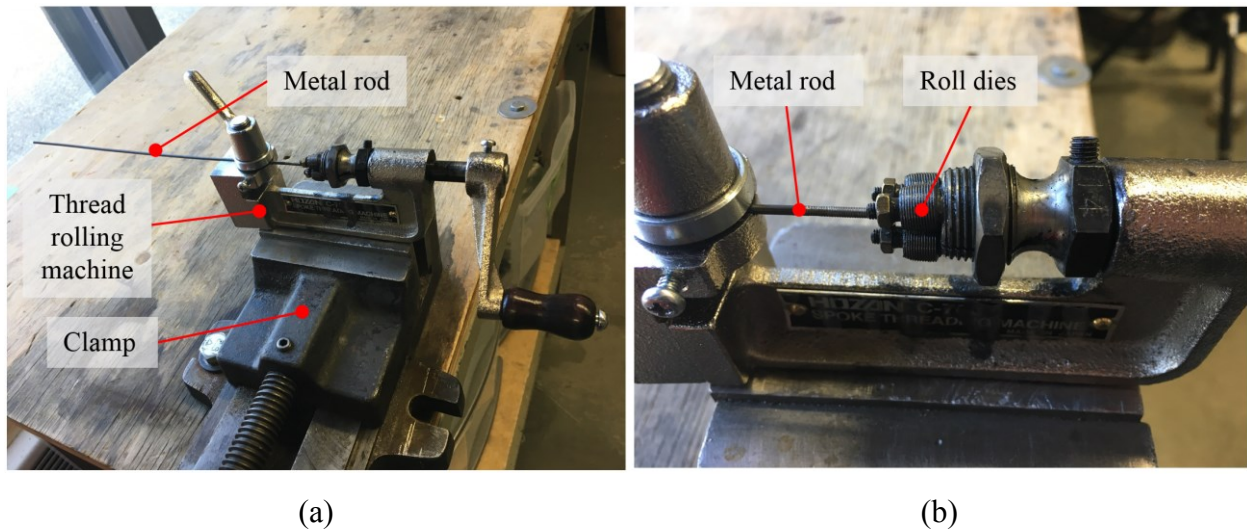


Figure 13: The process of threading the metal rods using a (a) thread rolling machine. (b) A closer look of the roll dies used for the thread creation.

The first step of preparing metal rods ready for the experiment was to cut it to a specific length, where it would be long enough to go through both sides of the samples, leaving ~15 mm extending from each end. Since the bending and tensile samples had different length, 187.2 mm, and 200.0 mm, respectively, two different size of wires were cut, one for each type sample. The wires for the bending samples were ~217 mm long, while the ones for the tensile samples were ~230 mm.

The wire used was purchased in a 0.5 kg coil. Therefore, it was clamped using a regular clamping mechanism and cut using a hacksaw to the respective length needed. After cutting the wire, it was necessary to file them on both ends into a cone shape. That was important in order to

get rid of imperfections and creating a cone shape would facilitate the beginning of the deformation on the wire later, when creating the threads by using a thread rolling machine.

The threads were made in two steps, the first one with the roll dies at a loose setting in order to create just the shape and path of the threads, and the second with the roll dies tighter together to finalize and increase the depth of the threads. Three passes were done for each step, looking for creating a clean, smooth and more uniform thread. Before starting the thread deformation, the mechanism was lubricated (WD-40, WD-40 Company), to ease and smooth out the thread's creation.

### **Nuts and washers**

The nuts and washers were both custom built according to some necessities that the experiment required, and that will be discussed in this section. The parts purchased were a hexagonal steel bar (Low-Carbon Steel Hex Bar - 5/16" Wide, 6512K141, McMaster-Carr Supply Company) for the nuts and one metal sheet (Low-Carbon Steel Sheet - 3" × 3" × 1/16", 1388K142, McMaster-Carr Supply Company) for the washer. The nuts were manufactured at the machine shop located in Mechanical Engineering building at the University of Alberta, while the washers were manufactured in the laboratory 5-25 on the 5<sup>th</sup> floor of the same building. The nuts were made of the hexagonal steel bar that was cut 10 mm long to increase the contact area between the rod and nuts. The nuts were manufactured this way since standard sizes of #2-56 nuts would not provide enough contact area by being very thin and small. After cut, it was faced for alignment purposes, and the last manufacturing step would be tapping a #2-56 thread in it. The washers were cut using a hacksaw and its dimensions were chosen to cover the entire area of both ends of the samples, therefore whenever a force is applied it would be distributed equally onto the surface of

the sample. The washers were  $29.0 \times 10.0$  mm for the tensile samples and  $20.0 \times 9.0$  mm for the bending samples. The same nuts were used for both tensile and bending samples.

### **Testing the rods**

The metal rods had at first their strength tested in the laboratory, and then it would be tested later in the machine shop using a tensile machine MTS 810 (Material Test System 810, MTS Systems Corporation), and the results compared. Hole samples were 3D printed to help on the study where the rods would be tested simulating the actual experiment to understand how much compression/tension the dog bone/rod could withstand. The study was done with hole 3D printed samples, metal rods threaded on both ends, washers and nuts.

The components were assembled and clamped, only on the 3D printed part, with a mechanical clamp present in the laboratory, showed in Figure 14. The nuts were then tightened until the metal rod broke/failed while compressing the hole sample. The compression applied onto the 3D printed part was counted by the number of complete full rotations of the nut, which corresponds to the pitch of the 2-56# thread 2.265 mm. After testing 10 different metal rods it was found that the average breaking point was around 7 complete full rotations, corresponding to ~13.6 mm of displacement of the nut. Based on the value found, in order to not exceed the yield strength point, the maximum value used during the actual experiment was 5 turns. Later, as mentioned, the metal rod was also tested using a tensile machine and an extensometer.

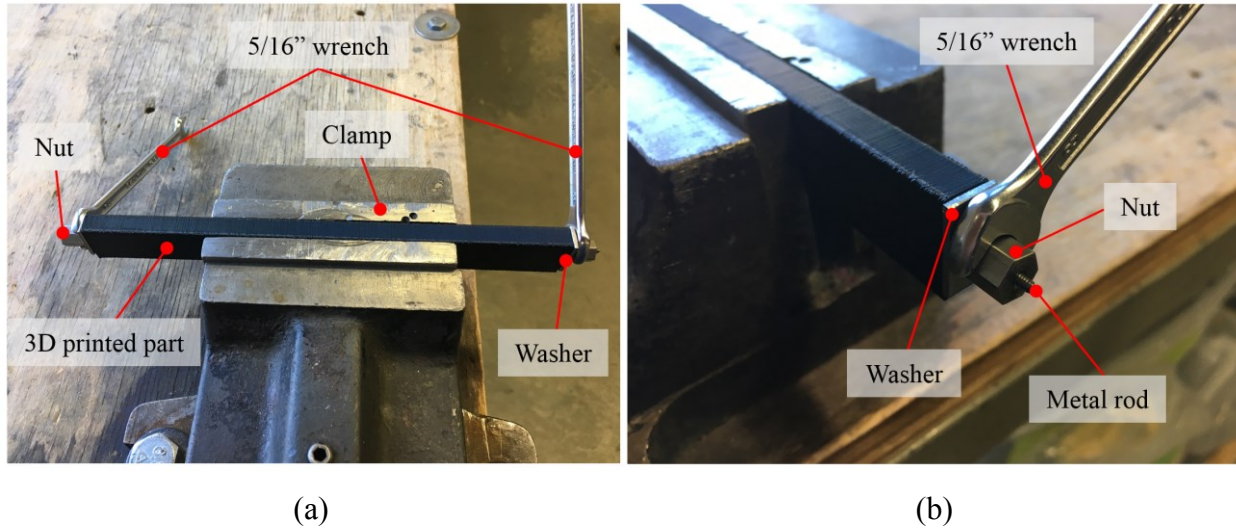
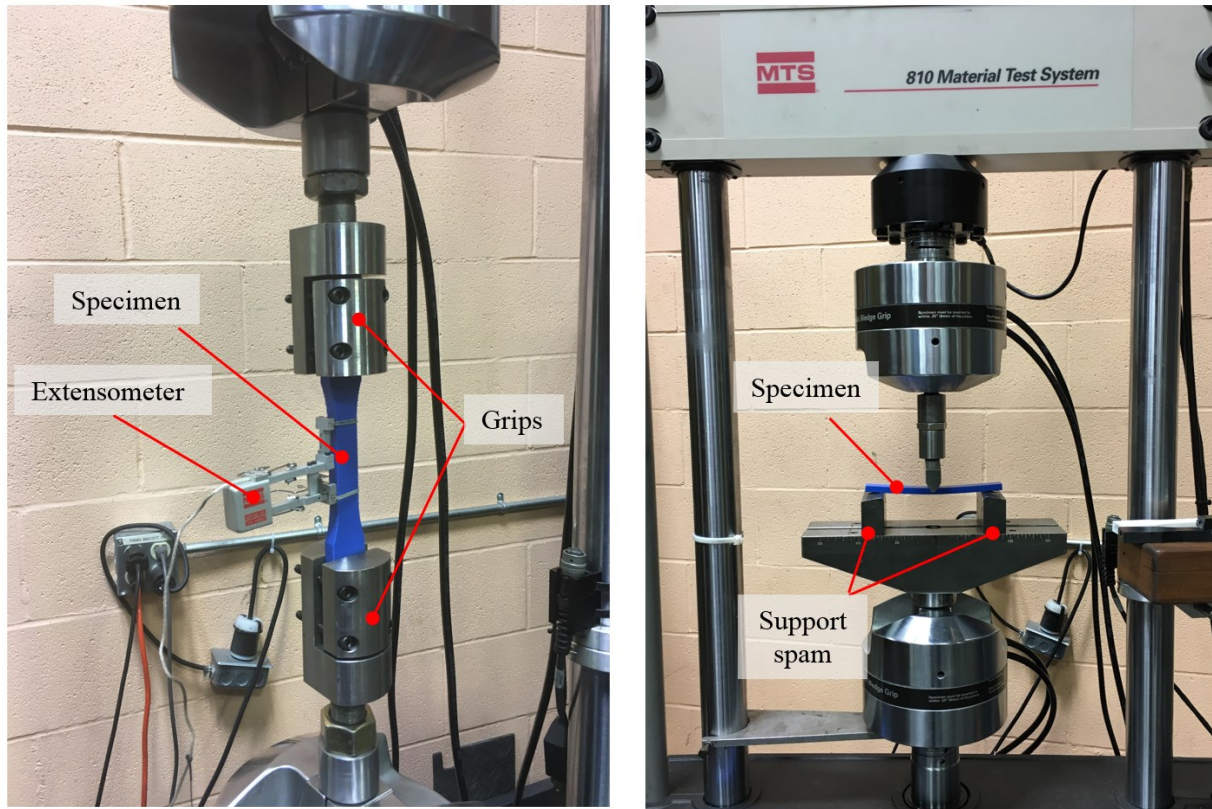


Figure 14: The setup for testing the metal rods in the laboratory. The (a) overall view of assembly, and (b) a closer image showing the main components of the assembly.

### 2.3.3 Experiment procedure

This section discusses about the experimental procedure used for the different tests in this study. Tensile and 3-point bending tests were the two tests used to achieve the goal of this study. The two tests are described in this subsection, and both used the MTS 810 (Material Test System 810, MTS Systems Corporation) machine for the experiments. There were only few differences between the setup used for the tensile and for the bending test. The tensile and the bending were done using a different set of grips. Figure 15 shows the difference on the setup of the machine, as well as the different grips used for the two tests. For the tensile tests, it was also required the use an extensometer (Material Test System 634.12E-24, MTS Systems Corporation) with an extension able to cover about 3 inches of the length to calculate the strain of the specimen being tested. In this setup, the extensometer was gripped onto the specimens by using an elastic band on both top and bottom grips of the extensometer to insure the stability of the system throughout the entire experiment.



(a) (b)  
 Figure 15: The setup of the MTS 810 for the (a) tensile, and (b) 3-point bending tests

### Tensile tests (metal rod)

The metal rods were tested by using two squared 3D printed parts. These parts were manufactured due to limited options of grips to use for this experiment. These squared parts were used for each grip to adapt the existing grip of the tensile machine. They were also used to simulate the actual experiment that would be done using a dog bone Figure 16 shows the complete assembly used for the experiment. The adaptors had a central hole which was located on the neutral axis of the cross section and all the way through the entire part. As shown in Figure 16, the parts were assembled by aligning the metal with both holes and placing a washer and a nut to lock the rod in place in each end. After the assembly was done, each adaptor was attached to the top and bottom

grips of the machine and tightened by four bolts from both grips of the machine. The same extensometer was also connected to the metal rod using elastic band to prevent undesired movements of the extensometer. After ensuring the stability of the system, the experiments were started.

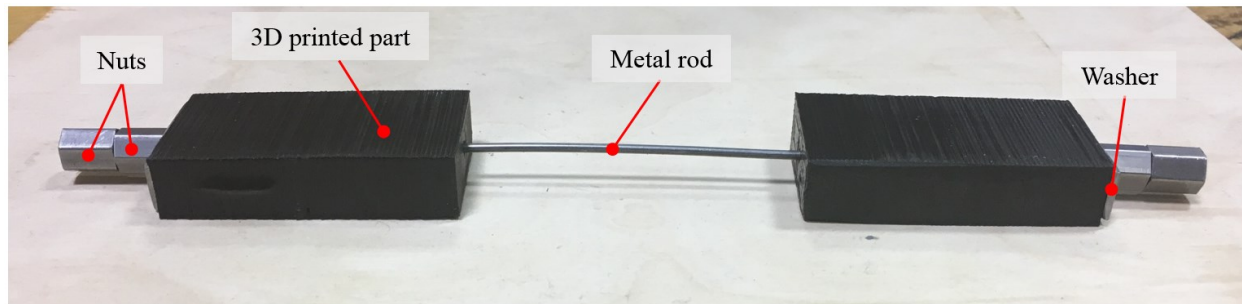


Figure 16: The assembly used for the tensile test of the metal rods on the MTS 810. The grips of the machine were attached to the black ABS 3D printed part.

The speed of the machine during the test was set at 1 mm/min with a data acquisition frequency of 20 Hz. A total of five samples were tested in this study and the tests were continued until the metal rod broke. The data acquired in each test provided the stroke (mm), axial load (N), strain (mm/mm), and time (s). The results collected from the experiments contained some offsets due to the very precise measurements collected from the extensometer. The small offsets of the results were corrected in a way that all the data plotted would start from the plot origin, providing a smoother and more consistent graph. There was also some inconsistency on the data at the end of each experiment. This inconsistency was due to the data collected after the breakage of the rod that would overextend the extensometer, and therefore those measurements would be completely off the real data. An in-house code was used to generate the plots of the corrected results for each condition.

### **Tensile tests (3D printed samples)**

There was a total of 25 dog bones samples tested, 5 for each different experiment: raw, hole, 1 turn, 3 turn, and 5 turn. The only samples that were reinforced with the metal rods were the 1 turn, 3 turn, and 5 turn. For all these samples, the metal rod was slide through the hole and a washer and a nut were placed on both ends of the metal rod. The nuts were tightened manually up to a point where it would only be possible to be further tighten using a wrench. After tightened manually, the 1 turn sample had the nut tightened an extra complete full rotation, while the 3 turns and the 5 turns samples had 3, had 5 complete full rotation of the nut, respectively. Each full rotation corresponds to 2.265 mm displacement which is the pitch of a 2-56# thread, meaning that the displacements were 2.265 mm, 6.795 mm, and 11.325 mm respectively for the 1 turn, 3 turns, and 5 turns samples.

All the specimens were tested using the same grip used to test the metal rods. Starting with the raw sample, hole, and 1, 3, and 5 turn in sequence. The samples were gripped into the machine according to code provided by ASTM D638 [113] with the distance between grips of  $115 \pm 5$  mm. The parameters set on the MTS 810 (Material Test System 810, MTS Systems Corporation) were the same as used for testing the metal rods. All the reinforced samples were tightened right before tested to avoid creeping of the metal rod. The specimens were all tested until its breakage, which all happened on the 3D printed ABS (dog bone). The data acquisition and processing were done same as the metal rod.

### **Three-point bending tests**

The MTS 810 (Material Test System 810, MTS Systems Corporation) was also used for the bending tests, however, the setup of the machine was slightly different as compared to the tensile

tests, as mentioned earlier in this chapter. The Figure 17 below shows in detail the experiment setup of the 3-point bending test. As shown in Figure 17 instead of the grips used for the tensile tests, a support base with two columns was attached to the bottom head of the machine. The columns were separated by the distance of 140 mm, where the sample was placed on. The top head of the machine had a single column attached to it. The top column was responsible for applying the load onto the specimens that were being tested.

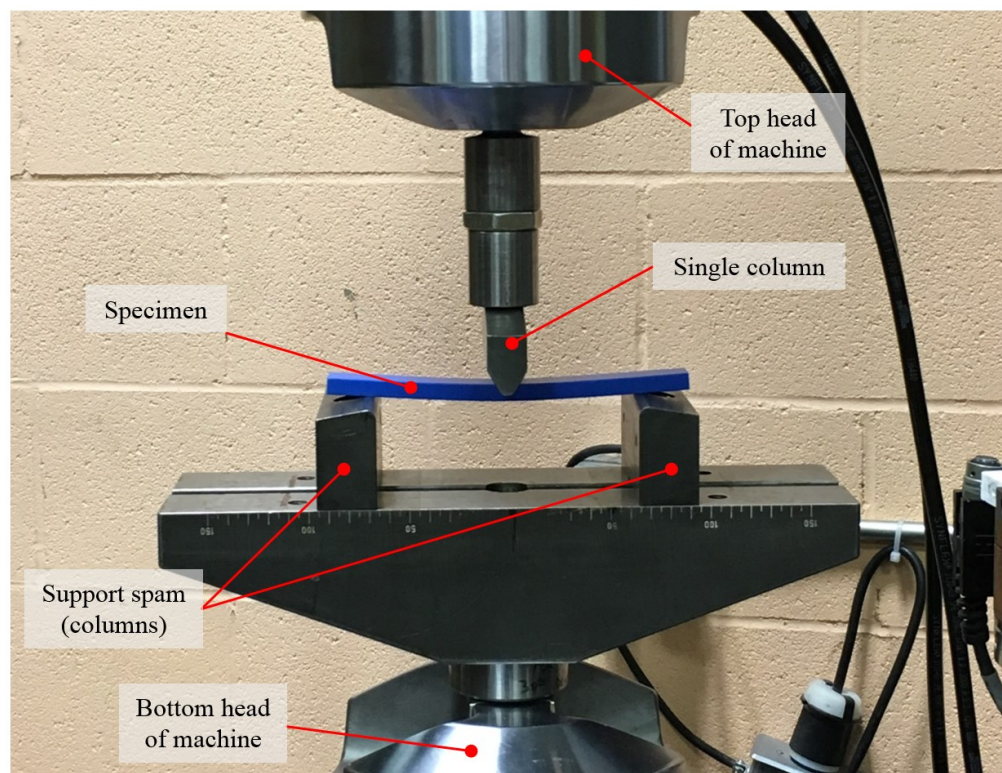


Figure 17: Setup of the MTS 810 for the 3-point bending tests.

There were four different samples tested: raw, hole, 3 turns, and 5 turns. Even though, the samples had a different geometry when compared to the tensile samples, due to the different standards, the same procedure was used on the bending tests, where the samples would only be reinforced right before being tested. The bending samples were designed according to the ISO 178, where there were some specific requirements related to the sample and to the three point support. Based on this standard, it was required that the specimen's width need to be  $\leq 1/4''$  of the support

spam, also that the overhanging on both ends need to be  $\geq 10\%$  of the support spam, but never less than 6.4 mm on each end. The support spam had to be  $16 \pm 1$  times the depth of the specimen.

The tests ran until the specimens broke, either completely or on the tension side of it, which in this case was on the bottom surface of the sample. The speed of the machine used for the experiments was 5 mm/min with a frequency of 20 Hz for the data acquisition. The data collected was composed by stroke (mm), axial load (N), and time (sec). The data for the bending tests had to be corrected as well, since the different position of the heads were generating offsets on the results, and that difference was due to the start position of the top head that had to be set manually each time a new specimen was going to be tested. The collected data was processed using an in-house code, where it generated Axial load (N) vs Stroke (mm) graphs.

## 2.4 Uncertainty analysis

Different sources of uncertainty were considered for each of the measurements performed in this study. Major identified error sources are related to pressure test, application and rating of external load, and strain measurement. Random and bias errors were included in the calculation of the reported uncertainties which are all at the confidence level of 95% [116][117].

Errors in the pressure were related to the study on the sealing performance while variations in load and strain were regarding the investigations on the reinforcement. The pressure transducer (Validyne DP15-50, Validyne Engineering) had a manufacturer-specified uncertainty of  $\pm 0.5\%$  of the full scale of the measurement. The calculations for the tensile and bending tests were done based on the set of equations provided in standard measurement and testing protocols [116]. Accordingly, for  $N$  number of samples having standard deviation of  $s_X$ , the uncertainty  $s_{\bar{X}}$  is calculated as:

$$s_{\bar{X}} = \frac{S_X}{\sqrt{N}} \quad (1)$$

It can be seen that equation ((1) only includes errors from repetitions which only correspond to random errors but not bias errors. In the case of having multiple sources of random error, equation ((2) can be used such that:

$$s_{\bar{X}} = \frac{1}{\sqrt{N}} \left[ \sum_{k=1}^K (s_{\bar{X}_k})^2 \right]^{\frac{1}{2}} \quad (2)$$

where  $K$  is the total number of random error sources, and  $s_{\bar{X}_k}$  is the elemental random standard uncertainty of the  $k^{th}$  source.

The bias and combined uncertainties were calculated using equations ((3) and ((4), respectively. All the bias uncertainties expressed had the same 95% level of confidence maintained, given by equation ((5). The equations are given as:

$$b_{\bar{X}} = \left[ \sum_{k=1}^K (b_{\bar{X}_k})^2 \right]^{\frac{1}{2}} \quad (3)$$

$$u_{\bar{X}} = \sqrt{(b_{\bar{X}})^2 + (s_{\bar{X}})^2} \quad (4)$$

$$U_{95} = 2u_{\bar{X}} \quad (5)$$

where  $b_{\bar{x}}$  is the bias uncertainty of measurement,  $b_{\bar{x}_k}$  is the bias uncertainty due to the  $k^{th}$  source, and  $u_{\bar{x}}$  is the combined standard uncertainty. The values thus calculated for all uncertainties considered are summarized in Table 5. The uncertainty on the extensometer used was not taken into consideration because it would negligibly affect the results.

Table 5: Error sources, error types, and their standard uncertainty.

Error Source	Error Type	Standard Uncertainty	Reference
Pressure Transducer (Validyne DP15-50, Validyne Engineering)	Bias	$\pm 0.75$ psi	[118]
Load cell (Force Transducer 661.20E-03, MTS Systems Corporation)	Random	$\pm 4.2$ N	[119]
Caliper (150 mm Digital Vernier Caliper, Mastercraft Tools)	Bias	$\pm 0.005$ mm	[120]

# Chapter 3. Effect of Coating on the Pressure Withstanding Capacity of 3D Printed ABS Cylinder

The purpose of this study is to demonstrate the effect of coating on the sealing performance of ABS 3D printed parts by developing a unique pressure test technique. The experiment was done by designing a pressure vessel able to fit and seal a 3D printed ABS cylinder and quantify the strengthening and sealing ability of spray painting and epoxy as coatings. To achieve the goal of this study, the pressure withstanding capacity of the two different coatings, epoxy and spray painting, and the effect of the thickness of the cylinders on the sealing performance were compared. The group of samples used on the experiment is shown in Figure 18.



Figure 18: The three different cylinder samples with a wall thickness of 1/8” used on the pressure measurement.

This chapter is divided into two subsections for two different cylinder wall thickness, where the results for the 1/8” cylinders are shown first, and it is followed by the 1/16”. A comparison is also undertaken between the two configurations for each type of coating trying to make clear the difference and improvement on the sealing performance that was obtained from the different

samples. An extra test was also completed where the 1/16” thickness cylinder was printed using 110% infill, instead of 100%. Conclusions were made based on the results found in which are illustrated by graphs showed throughout this chapter.

### 3.1 Results

#### 3.1.1 Cylinders with wall thickness of 1/8”

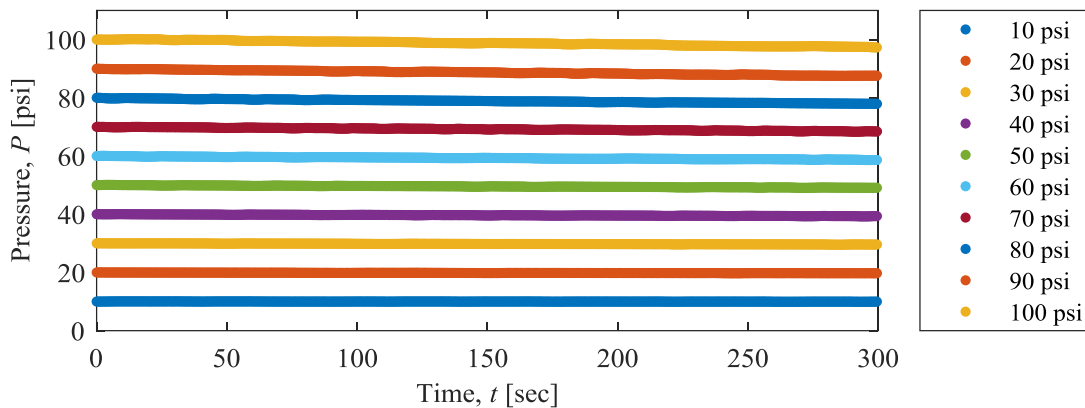


Figure 19: The change in pressure with respect to time for the raw sample with a wall thickness of 1/8”.

In this study, the raw, uncoated sample was the first one to be tested in order to have a reference for the comparison of the sealing performance amongst the different configurations. Figure 19 shows the change in the pressure of the system with respect to time for different set-point pressures. As shown, when the pressure load increases, the pressure withstanding capability of the raw sample decreases. This decrease in the pressure was more significant for higher pressures when compared to lower pressures, which can be due to more leakage in the system at higher pressure loads. However, for lower pressures, such as 10, 20 psi, the pressure remained constant throughout the 5 min test. Therefore, it can be concluded that for a minimum of 5 min of the test at lower pressures, the raw samples did not leak and had a good sealing performance. For

higher pressures, for example, 100 psi, there is a minor pressure drop, showing that as the set pressure increases the material tends to leak more.

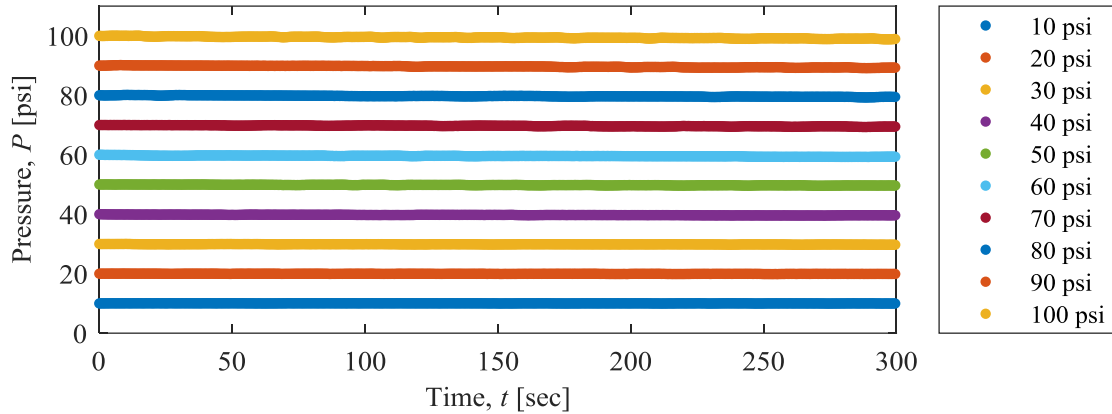


Figure 20: The change in pressure with respect to time for the spray painted sample with a wall thickness of 1/8”.

Figure 20 shows the results for cylinders that were coated with spray painting, illustrating their change in pressure with respect to time for different set-point pressures. Initial observations shown that the coating did not result in a significant improvement on the sealing performance when compared to the raw sample. However, looking closely to the results, it is notable that the coating improved the sealing performance of lower pressures especially the range of 10 to 40 psi. In this ranges of pressure, constant, unchanging pressure over the time period of the experiment was measured inside the cylinder. The overall trend of the leakage was the same as the raw sample. As the set pressure was increased a higher change in pressure was measured. The spray painting improved its sealing performance as compared to the raw sample but didn’t completely seal the sample at higher pressures.

The 1/8” cylinders were also tested with an epoxy coating. As shown in Figure 21, the change in pressure with the respect to time for the epoxy samples was zero, meaning that no leakage was found. Therefore, this highlights that the epoxy coated sample had the best results when compared to the other two cylinders, the raw and the spray painted. Figure 21 illustrates that the epoxy

coating was capable of completely sealing the 3D printed part throughout the 5 min for all range of pressures tested. Therefore, it can be concluded that to have a better sealing performance of the 3D printed parts with the thickness of the wall of 1/8", one layer of the epoxy needs to be applied onto the outer surface of an FFF ABS 3D printed part.

The main expected reason for the increase in sealing that the epoxy was able to achieve was a result of it being able to cover all the air gaps throughout the part. This created during the layer by layer process, a better seal in a stronger manner when compared to the spray painted samples. Even though the spray painted samples were also able to cover all the air gaps, it was not strong enough to withstand the pressure applied and ended up giving in to higher pressure loads.

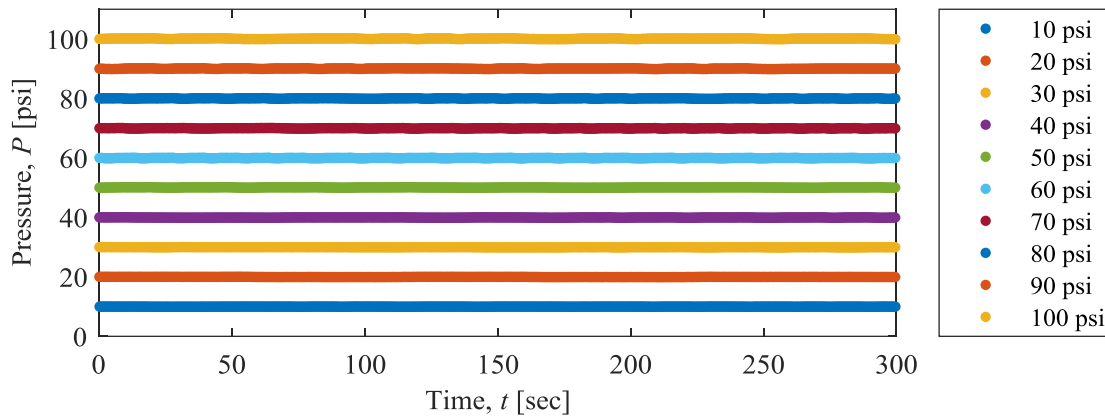


Figure 21: The change in pressure with respect to time for the epoxy coated sample with a wall thickness of 1/8".

To have a clear understanding of the change in the pressure of the highest tested pressure, the change in the pressure with respect to time of the three different samples with a cylinder wall thickness of 1/8" at 100 psi are plotted in Figure 22. It can be seen that the epoxy sample had a better sealing performance as the pressure increases, followed by the spray painted and raw samples. As shown in Figure 22, the pressure of the epoxy sample remained at the 100 psi during the entire 5 min of the test. The pressure of the spray painted samples and the raw samples decreased to ~ 99 psi and ~ 97 psi respectively.

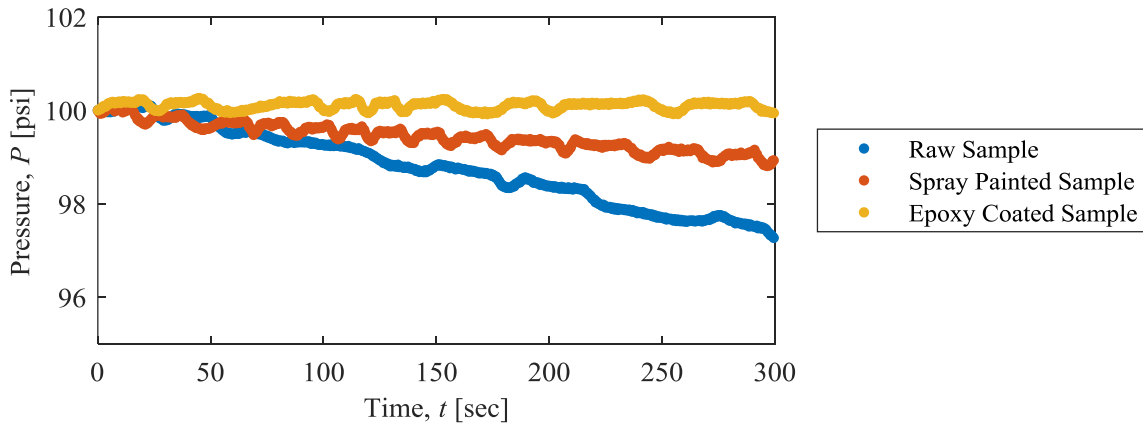
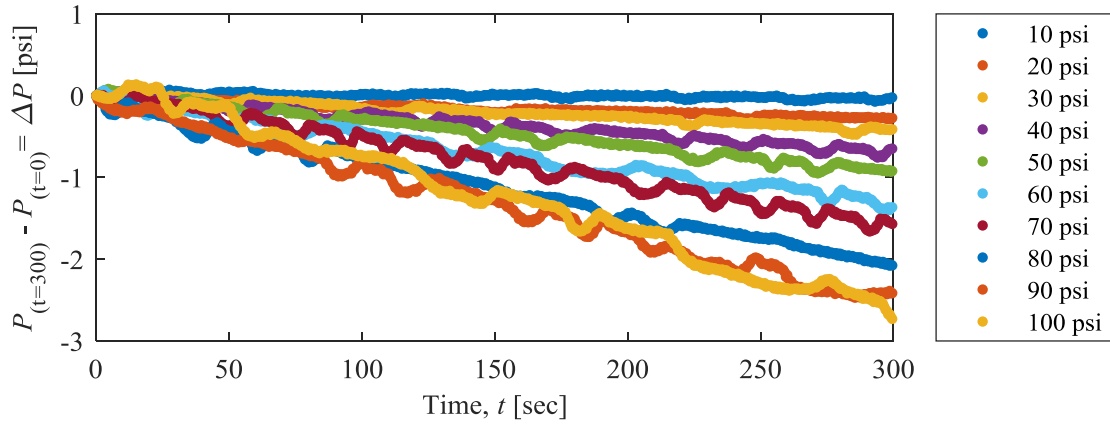
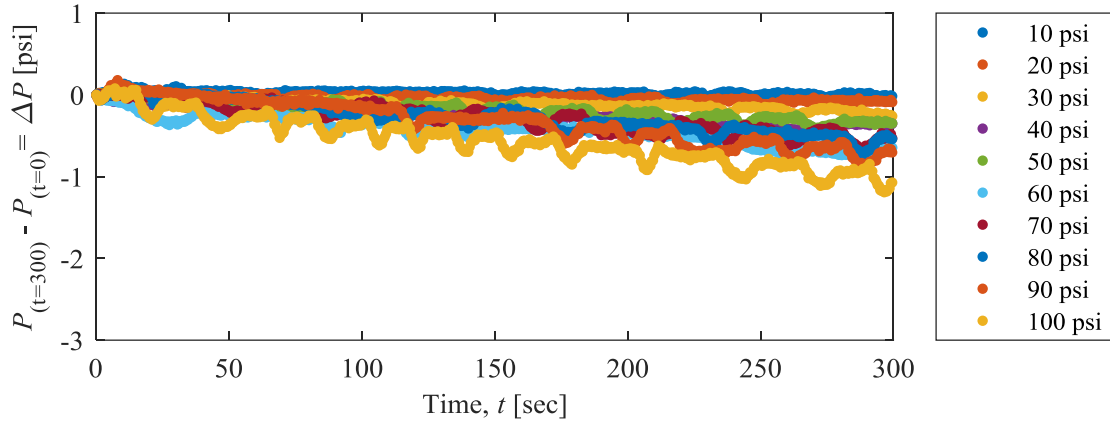


Figure 22: Comparison amongst the three different samples with a wall thickness of  $1/8''$ , showing the effect of the coatings in the sealing performance with respect to time.

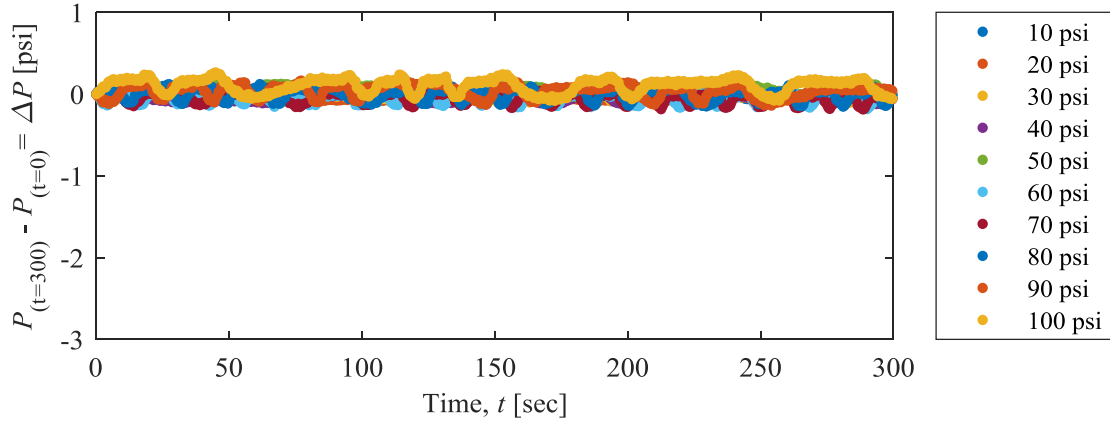
Figure 23 shows the trends in pressure drop with respect to time for all the three samples tested. It illustrates how the sealing performance improves when going from the not coated sample to the epoxy coated one, as well as the constant trend in pressure drop as the pressure increases. The raw sample seemed to withstand pressure loads up to 10 psi without leaking throughout the 5 min of the experiment. However, for higher pressures, such as 100 psi, it had a pressure drop of  $\sim 2.5$  psi. The spray painted sample, as mentioned earlier in this chapter, had an improvement on the sealing performance when compared to the not coated sample, where it could withstand low pressures up to 20 psi without leaking. At higher pressures, such as 100 psi, for example, it showed a pressure drop of  $\sim 1.0$  psi. While the not coated and the spray painted samples had small leakages at higher pressures, the epoxy coated sample seemed to be able to seal throughout the 5 min for all the pressures set, including at the maximum pressure load of 100 psi.



(a)



(b)



(c)

Figure 23: Comparison of the pressure drop for the (a) raw, (b) spray painted, and (c) epoxy coated samples with a wall thickness of 1/8", showing the effect of the coatings in the sealing performance with respect to time.

All the samples had very similar results and the trend in pressure drop. It is important to compare them all in one graph where an actual comparison of the improvement can be seen for each set point pressure with the pressure measured after the 5 min of the experiment. Figure 24 shows the difference in pressure drop for each sample after 5 min. The sample that had the best sealing performance was the epoxy sample, followed by the spray painted, and raw.

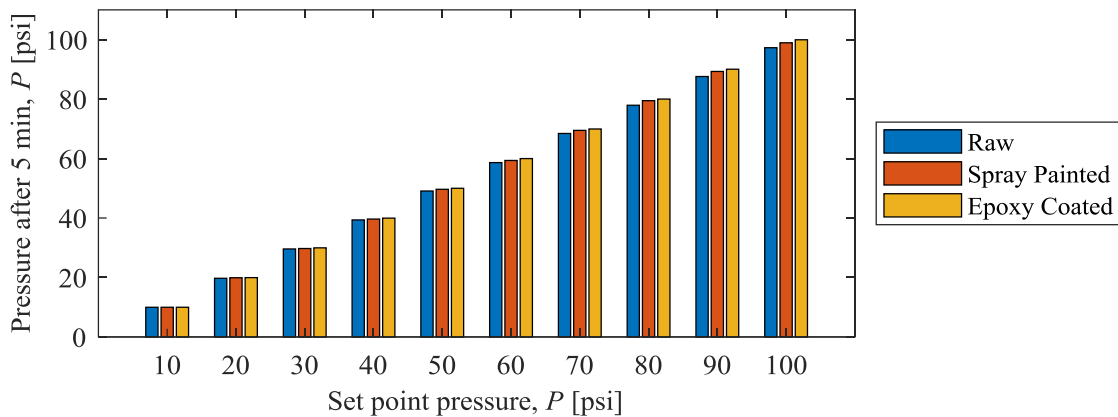


Figure 24: Comparison of the change in pressure with respect to time amongst the samples with a wall thickness of 1/8” for each pressure setting.

### 3.1.2 Cylinders with wall thickness of 1/16”

The results of the sealing performance of the cylinders with wall thickness of 1/16” are shown in this section. It is expected that due to the smaller wall thickness of the cylinders that the coatings will have a higher effect on the sealing performance when compared to the 1/8” cylinders. Figure 25 shows the results of the change in pressure with respect to time of the raw cylinder for different set-point pressures. As shown in Figure 25, it's notable that the raw sample could not maintain any pressure and it would start leaking as soon as the pressure was applied. Overall, the pressure inside the cylinder would decrease to the atmospheric pressure after 200 sec of the applied pressure. The results indicated that for thinner wall samples, the air gaps in between layer start to have a bigger influence on the sealing performance of a 3D printed part.

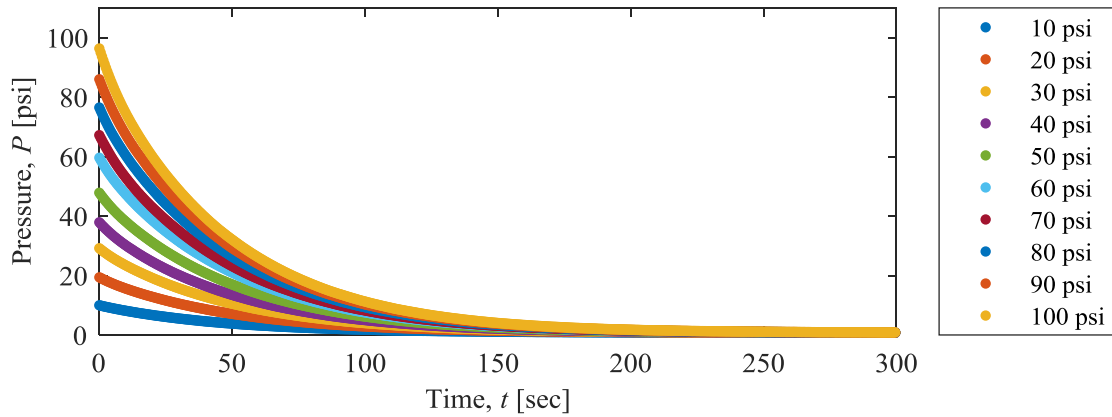


Figure 25: The change in pressure with respect to time for the raw sample with a wall thickness of 1/16”.

The change in pressure with respect to time for the spray painted samples is shown in Figure 26, and it demonstrates that coating the cylinder with spray painting, improved the sealing performance when compared to the raw sample. However, leaking was still observed which shows that the system is not able to withstand pressure in both high and low pressures. The lowest set of pressure applied, which was 10 psi, had a drop from 10 psi to 7 psi, which corresponds to a 30% loss in pressure. For the highest pressure applied in the measurement, which was 100 psi, it had a pressure drop from 100 psi to about 60 psi, corresponding to about 40% loss in pressure. Coating the sample with filler primer and spray paint on the post manufacturing stage seemed to have an influence on filling the air gaps that were contributing to all the leakage observed on the raw sample, in which did not have any coating applied onto its outer surface. This influence, however, was not enough to completely seal the cylinder.

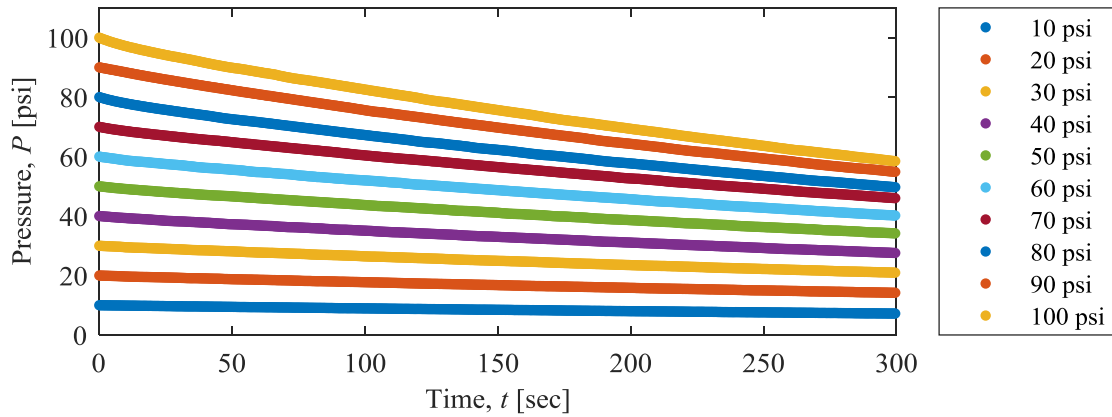


Figure 26: The change in pressure with respect to time for the spray painted sample with a wall thickness of 1/16”.

The epoxy coated sample results are showed in Figure 27 where the change in pressure with respect to time is illustrated. The epoxy coated sample had the best sealing performance amongst the three different samples with a wall thickness of 1/16”. The coating appeared to fill in all the air gaps that were responsible for the leaking. Both for higher or lower pressures, the epoxy was able to hold to pressure inside the cylinder and no leakage was observed.

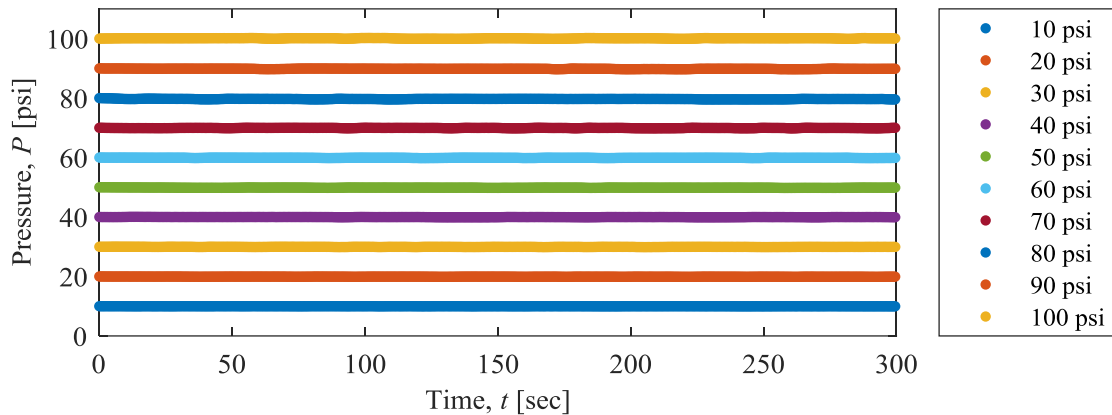


Figure 27: The change in pressure with respect to time for the epoxy coated sample with a wall thickness of 1/16”.

Figure 28 shows the comparison amongst the three different samples with respect to the change in pressure over time, in a way to clarify and make clearer the importance of the coating on the sealing performance of a 3D printed part, especially for thinner walls parts. The plot shows

the set-point pressure, which corresponds to the pressure that was applied at the beginning of the experiment, and the pressure measured after the 5 min of the experiment. It is easy to tell that the raw sample had the worst sealing performance by not holding any pressure throughout the experiment, followed by the spray painted, and the epoxy coating having the best sealing performance, being able to hold all the pressure loads applied into it.

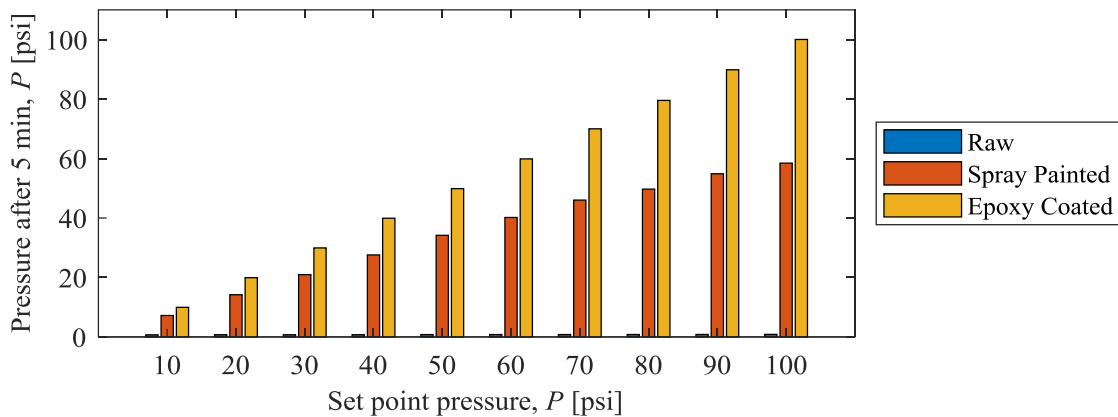


Figure 28: Comparison of the change in pressure with respect to time amongst the samples with a wall thickness of 1/16” for each pressure setting.

All the samples for this experiment, for both 1/8” and 1/16” wall thickness, were printed with 100% infill, as mentioned earlier in Chapter 2. It is notable when analyzing the performance of the raw sample, that the air gaps were present and working against the sealing performance. Therefore, an extra sample of the cylinder was printed using 110% infill instead of 100%. The idea was to add more overlapping between each filament deposition, thus reducing the air gaps and improving the sealing performance. The change in pressure with respect to time for the 110% infill raw sample with a wall thickness of 1/16” is shown in Figure 29. It illustrates that increasing the overlapping between each filament deposition helps on the sealing performance of a 3D printed part. However, it still leaks and does not completely seal the 3D printed part.

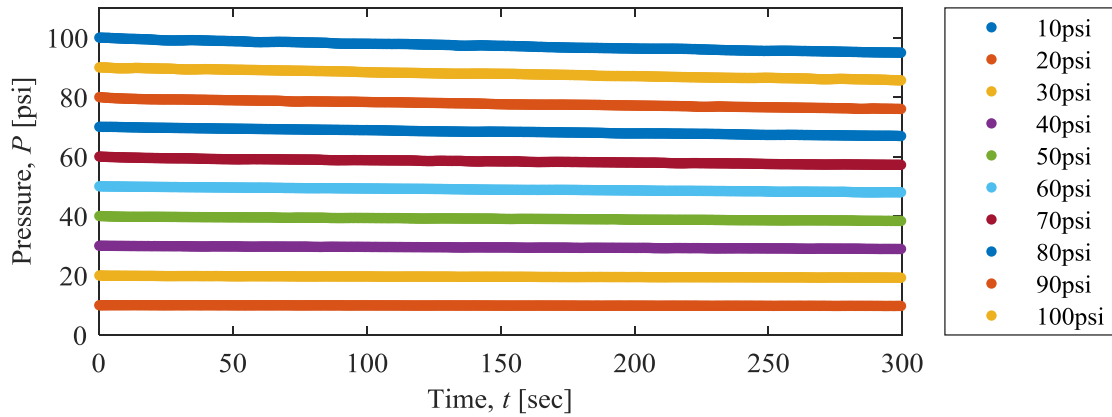


Figure 29: The change in pressure with respect to time for the 110% infill raw sample with a wall thickness of 1/16”.

### 3.2 Conclusion

The essence of this work was to understand how to make 3D printed parts more functional when it comes to sealing applications. The results that were found helped on understanding the effects of coatings on the sealing performance. Based on the results provided, conclusions were taken and given below.

#### 3.2.1 1/8” samples

The thicker samples showed that the coatings had a negligible effect on the sealing performance. However, a small drop in pressure could still be seen when comparing the three samples at higher pressures, especially at 100 psi, showing that the coatings helped to improve the sealing performance. The raw sample had the least sealing performance, followed by the spray painted, and by the epoxy coated where no leak was observed. Therefore, based on the negligible difference amongst the three samples, it can be said that 3D printed parts with 1/8” of thickness seem to be the threshold for sealing purposes.

### 3.2.2 1/16" samples

The thinner samples showed clearer the effect of the coatings by having three completely different results on the sealing performance. Again, the raw sample had the least sealing performance where no pressure could be held, followed by the spray painted and the epoxy coated having the best performance where no leak was observed.

There were two crucial aspects to understand the sealing performance of the samples. First, the epoxy with the best sealing performance where no leak was detected by applying only one layer of epoxy on the outer surface of the samples. Second, the number of wall lines of the samples that could define a threshold on the sealing performance. The thicker sample had about 4 lines on the wall while the thinner had only 2 lines. Since just a small leak was detected on the thicker raw sample, it can be assumed that 4 wall lines are the threshold when it comes to sealing purposes, when using a 0.8mm nozzle diameter.

# Chapter 4. Effect of Reinforcing 3D Printed ABS Parts

This chapter will show the results obtained from the experiments done in 3D printed samples using a metal rod as reinforcement. The purpose of this study is to understand the effects of adding reinforcement to 3D printed parts. The specimens were tested under bending and axial loads by running tensile and 3-point bending experiments. Comparisons were done amongst the samples to understand the effects on their mechanical properties such as tensile and flexural strength, and elastic and the flexural modulus. The results of the tensile tests done in the metal rod itself will be also provided and used for calculations. In addition, a conclusion will be stated by the end of this chapter.

## 4.1 Tensile tests

### 4.1.1 Metal rods

The metal rods used as reinforcement for the 3D printed samples were tested under tension, and the results are provided in Figure 30 which illustrates the stress-strain curve of five different specimens. The results showed a consistent data where the ultimate tensile strength was found to be around  $1.73 \pm 0.01$  GPa and the elastic modulus of  $87.01 \pm 7.52$  GPa. The elastic modulus and tensile strength were calculated based on the average of all tested samples.

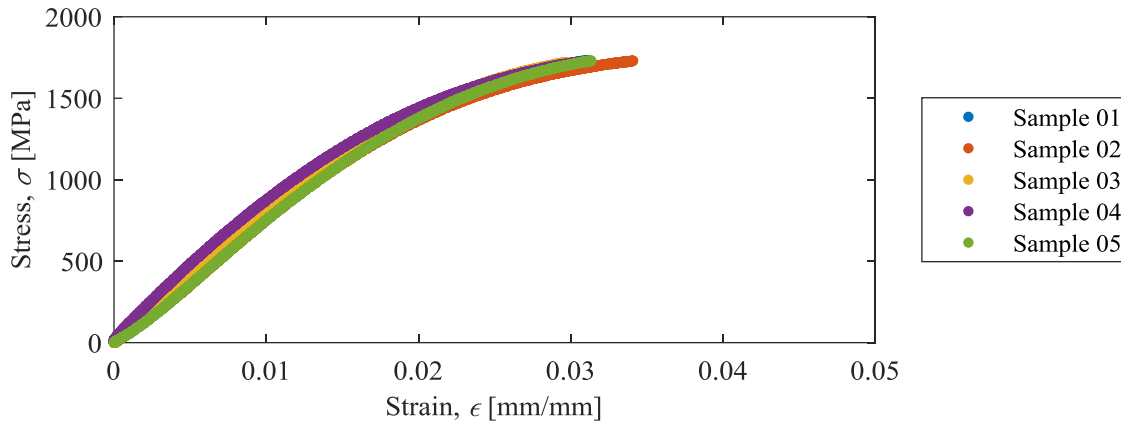


Figure 30: The stress-strain curve showing the results of the tensile tests done on five different samples of the metal rod.

Before testing the metal rods in the tensile machine, as mentioned earlier in Chapter 2, the metal rods were tested in the lab to check how many turns of the nut the rod could withstand without breaking. The results from that experiment showed that the rods were breaking in average after 7 full rotations plus 90° degree of turn, in which corresponds to a total displacement of 7.25 times the pitch of the #2-56 thread. By taking into consideration that the pitch of a #2-56 thread is equal to 0.453 mm, the total displacement of the nut would be 3.28 mm. Therefore, those results could be compared and applied to the results found in the tensile experiment. This comparison is shown in Figure 31, where it shows the location that each turn corresponds to in the stress-strain curve of the metal rod based on the stress-strain curve of the mean.

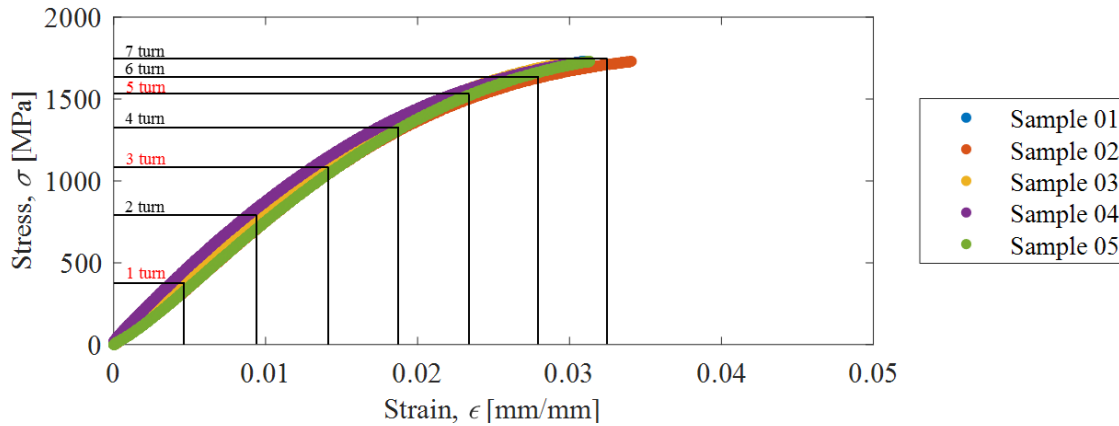


Figure 31: The stress-strain curve of the metal rod samples illustrating the position that each turn of the nut would represent in the curve.

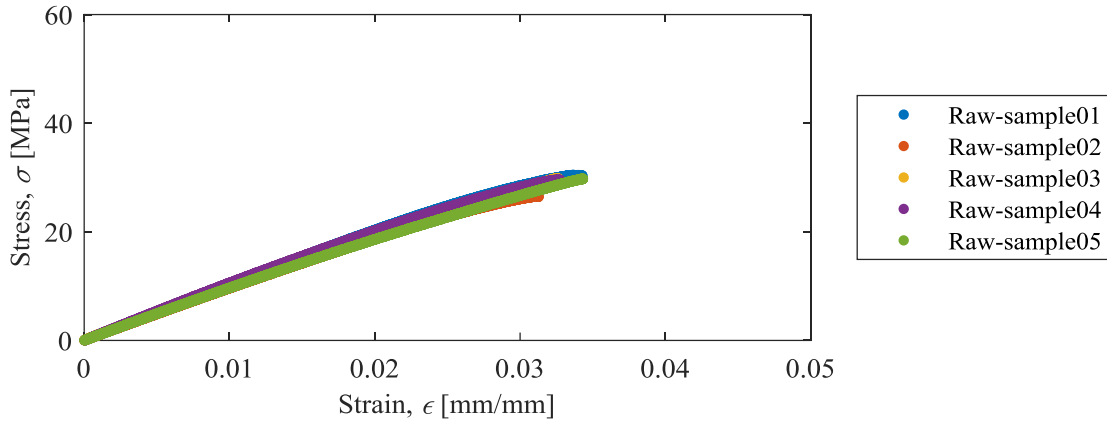
It is notable that the 1, 3, and 5 turns are marked with a red color. These three different torques were chosen to be the ones used for the experiment. The idea was to understand how different compressive loads could effect on the mechanical properties of the 3D printed samples by taking the lowest, middle, and highest torques. However, in order to be safe that the metal rods would not break while tightening the nuts during the experiment, the highest torque used was the one with 5 turn.

#### 4.1.2 Longitudinal samples

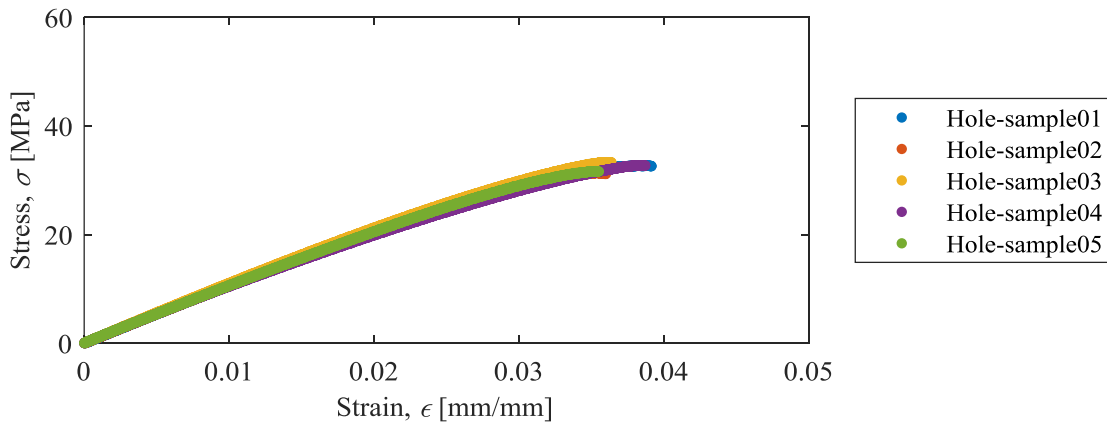
##### Raw and hole samples

The raw and hole samples had very similar results with negligible differences. The results are provided in Figure 32 where it is shown the stress-strain curve for each sample in two different figures. They both had almost the same elastic modulus and tensile strength. The raw sample had an elastic modulus of  $1.01 \pm 0.04$  GPa and a tensile strength of  $29.10 \pm 1.52$  MPa while the hole had  $1.07 \pm 0.02$  GPa and  $32.34 \pm 0.86$  MPa, respectively. These results can be explained by the fact that the hole that goes through the samples is very small compared to the rest of the 3D printed part cross-section. Therefore, the cross sectional area of the sample is mostly composed by the 3D

printed part which represents 98.5% of the total area, while the hole area only represents 1.5% of the total area. The elastic modulus and tensile strength were calculated based on the average of all the tested samples.



(a)



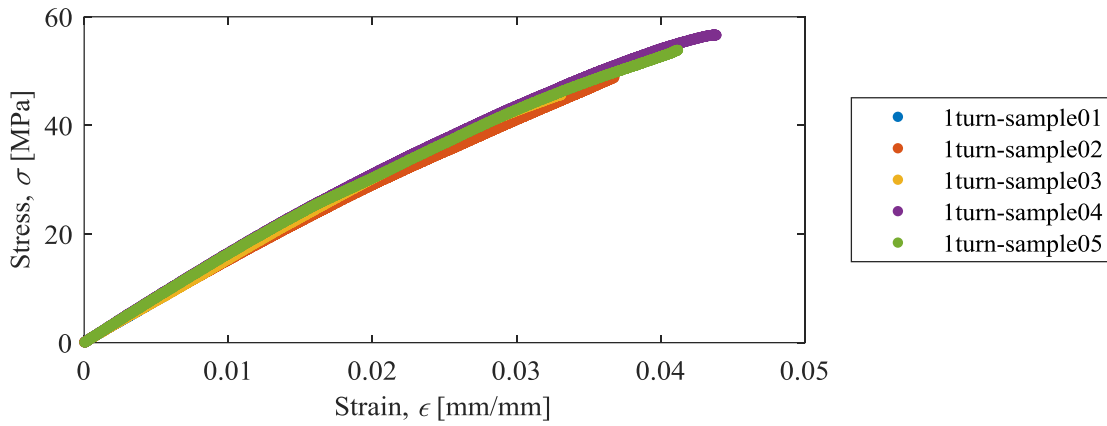
(b)

Figure 32: The stress-strain curve showing the results of the tensile tests for the (a) raw, and (b) hole longitudinal samples.

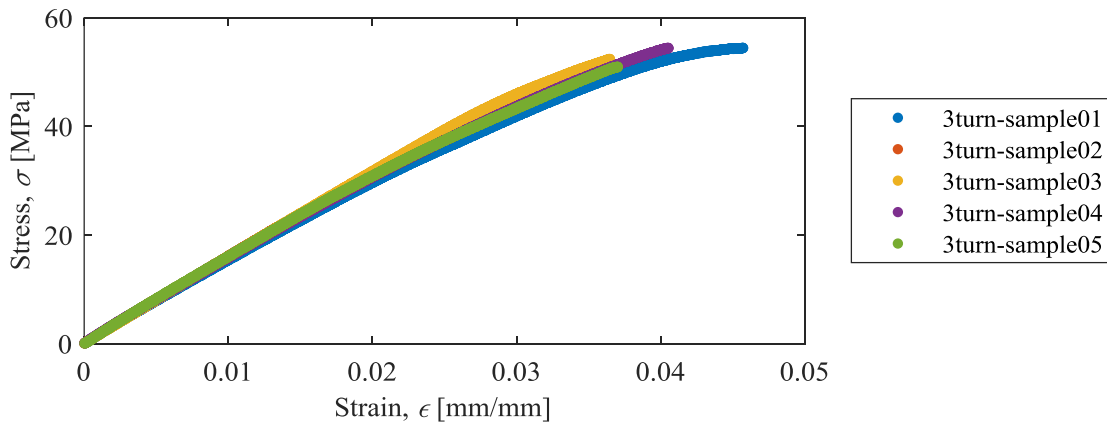
## Reinforced samples

This subsection will show the results of the reinforced samples with 1, 3 and 5 turns. Also, providing detailed information regarding their improvement/effect on the mechanical properties of the 3D printed parts. A comparison was done amongst the three results to see which one provided the best results.

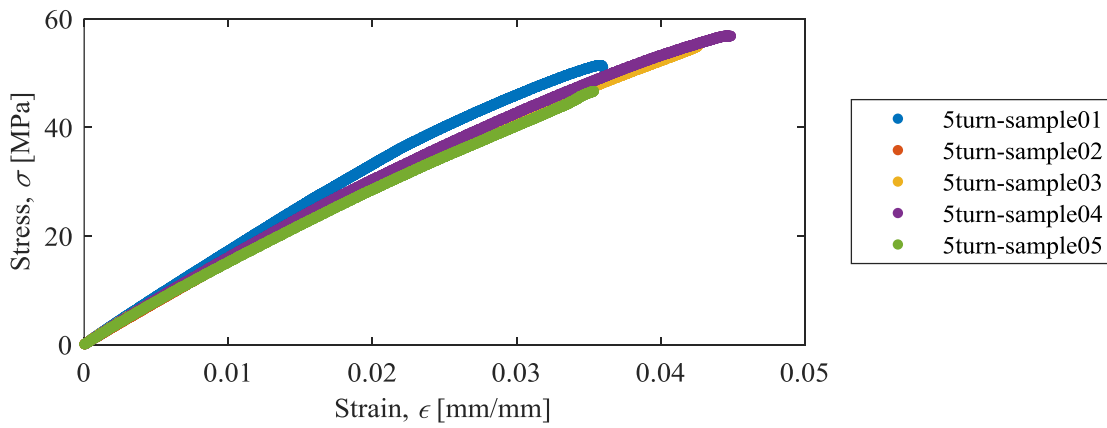
Figure 33 shows the stress-strain curve of the results found on the tensile tests for each of the reinforced samples. It is noticed that regardless the amount of turns, the results seemed to be very similar to each other. However, adding the metal rod to the 3D printed part greatly improved their mechanical properties. The tensile strength of the samples was found to  $50.64 \pm 4.59$  MPa,  $52.74 \pm 1.71$  MPa, and  $49.6 \pm 7.54$  MPa, respectively for the 1 turn, 3 turn, and 5 turn samples. By taking the tensile strength of the 1 turn samples and comparing it to the raw sample, it shows that the tensile strength increased from  $29.10 \pm 1.52$  MPa, which is the value found for the raw sample, to  $50.64 \pm 4.59$  MPa, corresponding to about 75% improvement on the tensile strength.



(a)



(b)



(c)

Figure 33: The stress-strain curve showing the results of the tensile tests for the (a) 1 turn, (b) 3 turn, and (c) 5 turn longitudinal samples.

The elastic modulus also increased from  $1.01 \pm 0.04$  GPa to  $1.59 \pm 0.08$  GPa which corresponds to the raw and 5 turn, respectively. The elastic modulus was calculated based on the average of all tested samples. Once again, the difference on the elastic modulus amongst the reinforced samples is negligible, since all samples had almost the same results. Table 6 shows the elastic modulus of each sample and compares it to the values found for the raw and hole samples, while Table 7 shows the comparison of the tensile strength found for each sample. Figure 34 and Figure 35 illustrate the results of the elastic modulus, and tensile strength, respectively, where the error bars are the standard deviation of the mean.

Table 6: Overall comparison amongst the elastic modulus for the longitudinal samples.

Samples	Elastic Modulus (MPa)	Standard Deviation ( $\pm$ )
Raw	1011.33	45.10
Hole	1068.33	22.30
1 turn	1574.67	58.77
3 turn	1592.67	32.60
5 turn	1593.89	82.22

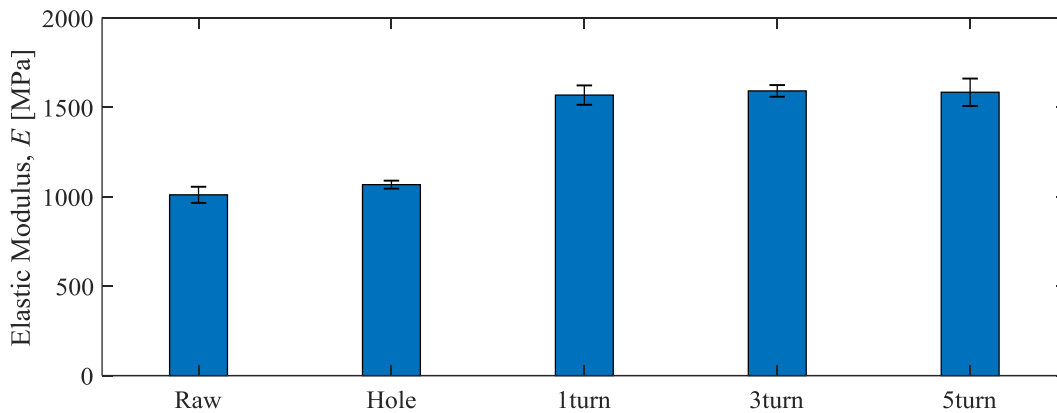


Figure 34: Overall comparison of the elastic modulus for the longitudinal samples where the error bars are the standard deviation of the mean

Table 7: Overall comparison amongst the tensile strength for the longitudinal samples.

Samples	Tensile Strength (MPa)	Standard Deviation ( $\pm$ )
Raw	29.10	1.52
Hole	32.34	0.86
1 turn	50.64	4.59
3 turn	52.74	1.71
5 turn	49.60	7.54

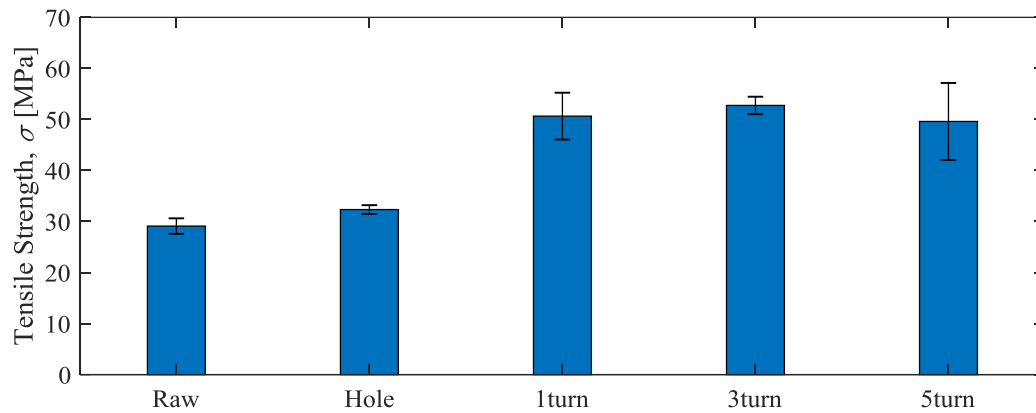


Figure 35: Overall comparison of the tensile strength for the longitudinal samples where the error bars are the standard deviation of the mean.

The improvement on the tensile strength and on the elastic modulus is explained by fact that the metal rod has a much higher value for each property than the 3D printed part itself, including tensile strength and elastic modulus. The tensile strength and the elastic modulus of the metal rod are respectively,  $1726 \pm 5.48$  MPa and  $87.01 \pm 7.52$  GPa, while the values of the same mechanical properties for the hole longitudinal 3D printed sample, for example, are  $32.34 \pm 0.86$  MPa and  $1.07 \pm 0.02$  GPa. Therefore, when the metal rod is added to the cross section of the 3D printed part, it starts sharing the load according to its fraction of area in the cross section. For example, if having a larger diameter of a metal rod, the tensile strength and elastic modulus of the reinforced 3D printed part would also increase, since now the area of the metal rod that is sharing the load is larger. This calculation is done based on the equivalent areas method approach. The equivalent

areas method starts from the derivation of equation (6) which assumes that the strain is the same for both metal rod and 3D printed part when under tension or compression, and is defined as:

$$\varepsilon_{cm} = \varepsilon_f = \varepsilon_m \quad (6)$$

where  $\varepsilon_{cm}$  is the strain of the composite material composed by the metal rod plus the 3D printed part,  $\varepsilon_f$  is the strain of the fiber which, in this case, is the metal rod, and  $\varepsilon_m$  is the strain of the matrix which is the 3D printed part. It is also known that when under tension, the loads applied onto the reinforced sample can be described as:

$$P_{cm} = P_f + P_m \quad (7)$$

where  $P_{cm}$  is the load carried by the composite material,  $P_f$  is the load carried by the fiber (metal rod), and  $P_m$  is the load carried by the matrix (3D printed part). Knowing that load ( $P$ ) is equal to tension times the cross-sectional area, equation (7) can be derived as:

$$\sigma_{cm}A_{cm} = \sigma_f A_f + \sigma_m A_m \quad (8)$$

where the  $\sigma_{cm}$  and  $A_{cm}$  are the tension and the area of the cross section of the composite material,  $\sigma_f$  and  $A_f$  are the tension and area of the fiber (metal rod), also  $\sigma_m$  and  $A_m$  being the tension and area of the matrix (3D printed part), respectively. By applying the concept that tension is equal to elastic modulus times the strain, equation (8) can be derived as:

$$E_{cm}\varepsilon_{cm}A_{cm} = E_f\varepsilon_f A_f + E_m\varepsilon_m A_m \quad (9)$$

$$E_{cm} = E_f \left( \frac{\varepsilon_f A_f}{\varepsilon_{cm} A_{cm}} \right) + E_m \left( \frac{\varepsilon_m A_m}{\varepsilon_{cm} A_{cm}} \right) \quad (10)$$

where  $\varepsilon_{cm}$ ,  $\varepsilon_f$ , and  $\varepsilon_m$ , as mentioned earlier are equal to each other, therefore it can be cut out of the equation, and  $E_{cm}$ ,  $E_f$ , and  $E_m$  are the elastic modulus for the composite, fiber, and matrix respectively. Since, the area fraction is the same as the volume fraction, the final equation can be defined as:

$$E_{cm} = E_f V_f + E_m V_m \quad (11)$$

where  $V_f$  and  $V_m$  are the volume fraction of fiber (metal rod) and volume fraction of the matrix (3D printed part), respectively. The equation (11) helps on calculating the elastic modulus of the composite material, according to how much of the cross-sectional area is taken by the metal rod and how much it is taken by the 3D printed part.

The elastic modulus for the reinforced samples was found to be  $E_{cm} = 2.37$  GPa when calculated using values from the metal rod, and hole sample tensile tests. The  $E_c$  was obtained by taking into consideration values for  $A_f$ ,  $A_m$ , and  $A_{cm}$  that were given by the solid model in SolidWorks. The values used for the areas were  $2.84 \text{ mm}^2$ ,  $182.93 \text{ mm}^2$ , and  $185.77 \text{ mm}^2$ , respectively for  $A_f$ ,  $A_m$ , and  $A_{cm}$ . The elastic modulus  $E_f$ , and  $E_m$  used in the calculation were the ones obtained from the tensile tests of the metal rod by itself, and from the hole sample, being them  $87.01 \pm 7.52$  GPa, and  $1.07 \pm 0.02$  GPa, respectively. The calculation of the volume ratio was done according to equations (12) and (13).

$$V_f = \frac{A_f}{A_f + A_m} \quad (12)$$

$$V_m = \frac{A_m}{A_f + A_m} \quad (13)$$

### Comparisons amongst longitudinal samples

The first comparison in this subsection is between the raw and the hole sample, willing to see how much the hole going through the sample would affect on the mechanical properties. The Figure 36 shows the stress-strain curve of both samples combined. As illustrated, the results are very similar and there is not much of a difference between the two samples. The average of the elastic modulus for both samples were found to be almost the same, as shown in Table 6 earlier in this chapter. There is only a small difference on the tensile strength that can be neglected due to the uncertainty of the experiments.

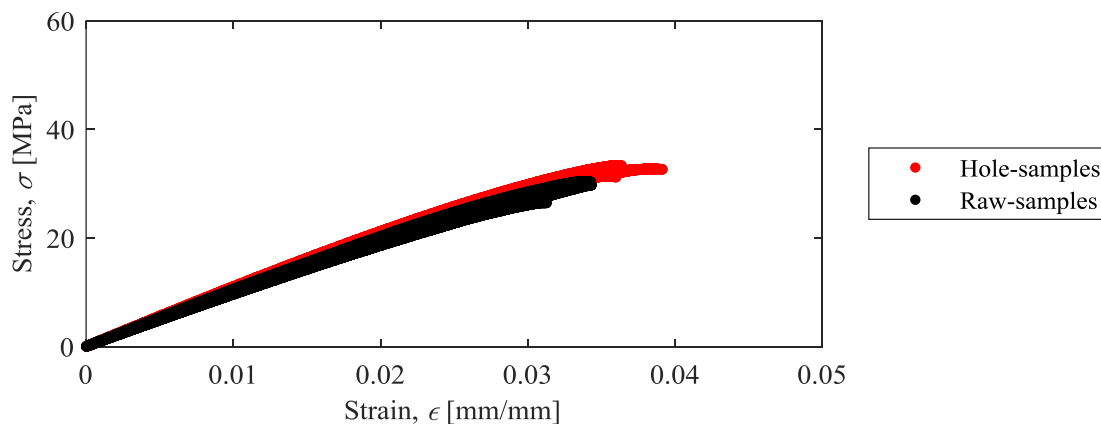


Figure 36: The stress-strain curve comparing the results of the tensile tests between the raw, and the hole longitudinal samples.

The second comparison was done with the results of two extremes samples, the raw and 5 turn, illustrated on a stress-strain curve in Figure 37. As expected, the raw has a lower elastic modulus  $1.01 \pm 0.04$  GPa when compared to the 5 turn sample  $1.59 \pm 0.08$  GPa. The tensile strength is also much higher for the 5 turn samples than to the raw one with values of  $49.60 \pm 7.54$  MPa, and  $29.10 \pm 1.52$  MPa, respectively. This difference in the elastic modulus and the tensile strength is due to the presence of the metal rod that, as explained earlier in this chapter, carries most of the load applied to the samples.

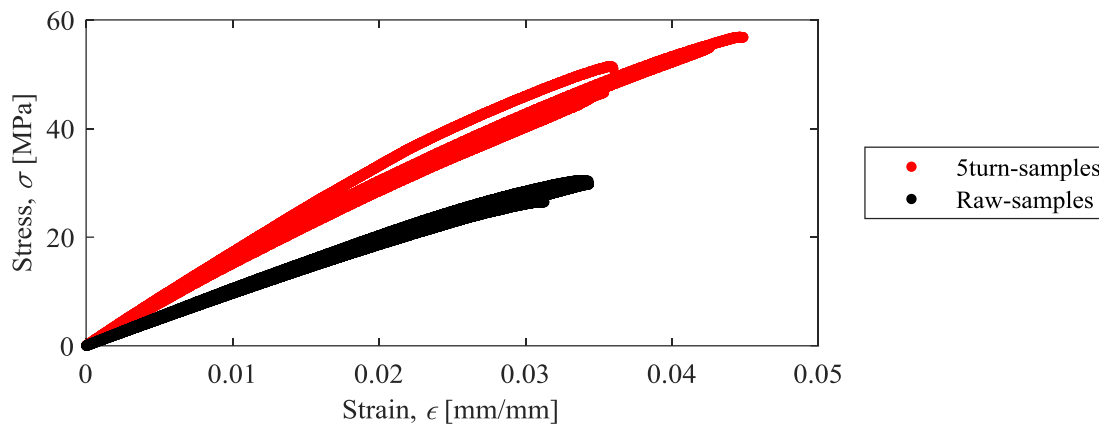


Figure 37: The stress-strain curve comparing the results of the tensile tests between the raw, and the 5 turn longitudinal samples.

There were three different types of reinforced samples: 1 turn, 3 turn, and 5 turn. The results of the tensile tests of these three samples are compared in Figure 38 on a stress-strain curve. It was observed that changing the torque applied onto the samples does not change the final mechanical properties of the parts. All the samples had very similar results for both tensile strength, and elastic modulus.

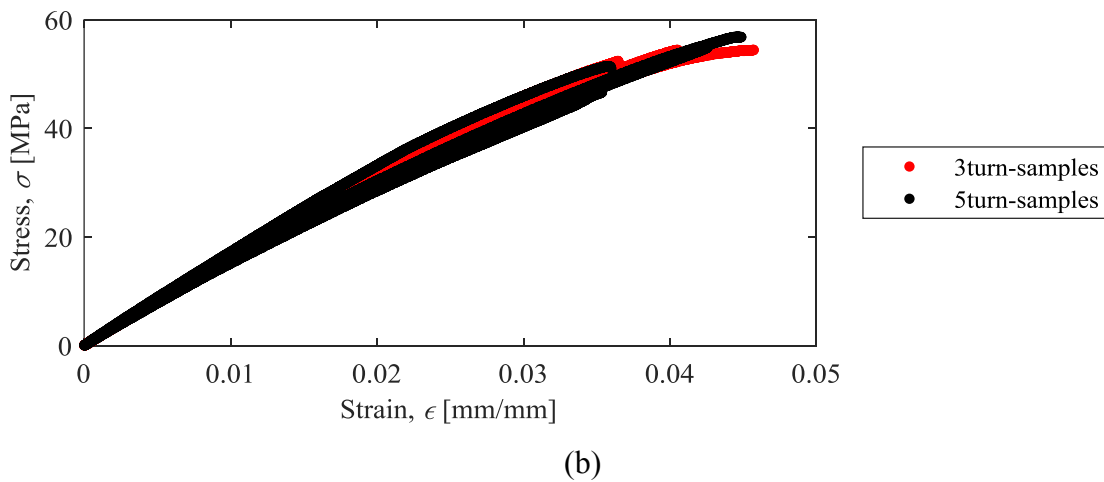
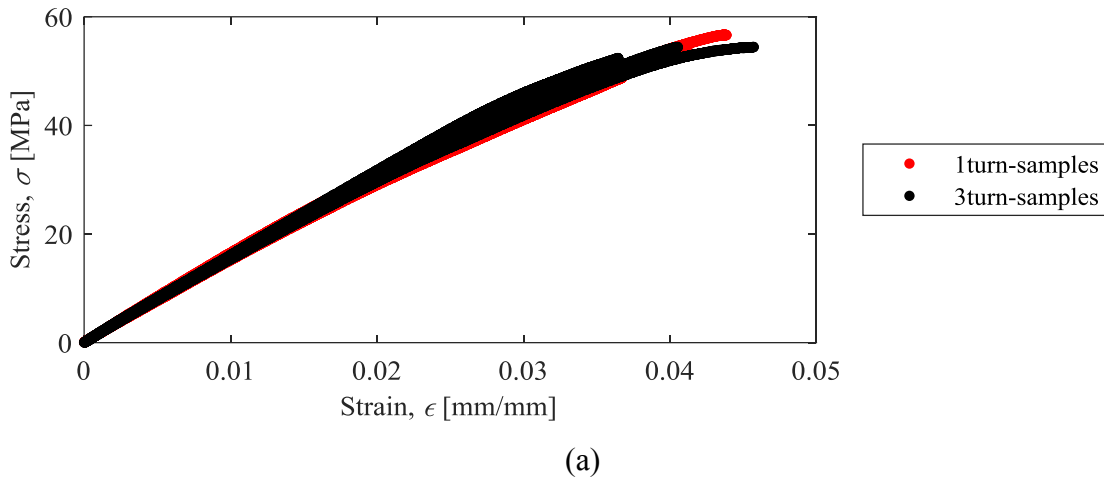


Figure 38: The stress-strain curve comparing the results of the tensile tests between the (a) 1 turn and 3 turn, and the (b) 3 turn and 5 turn longitudinal samples.

The final comparison in this subsection is amongst the raw, 1 turn, and 5 turn, shown in Figure 39 on a stress-strain curve. This comparison was done to show the improvement that just by adding a metal rod could provide, also to show that even if different amount of torques are done, the improvement is going to be the same. The elastic modulus is higher for the 1 turn and 5 turn samples,  $1.57 \pm 0.06$  GPa and  $1.59 \pm 0.08$  GPa, respectively, than for the raw one which is  $1.01 \pm 0.04$  GPa. The tensile strength of the raw samples is also lower than the reinforced samples, with  $29.10 \pm 1.52$  MPa, while the 1 turn, and 5 turn have  $50.64 \pm 4.59$  MPa and  $49.60 \pm 7.54$  MPa, respectively.

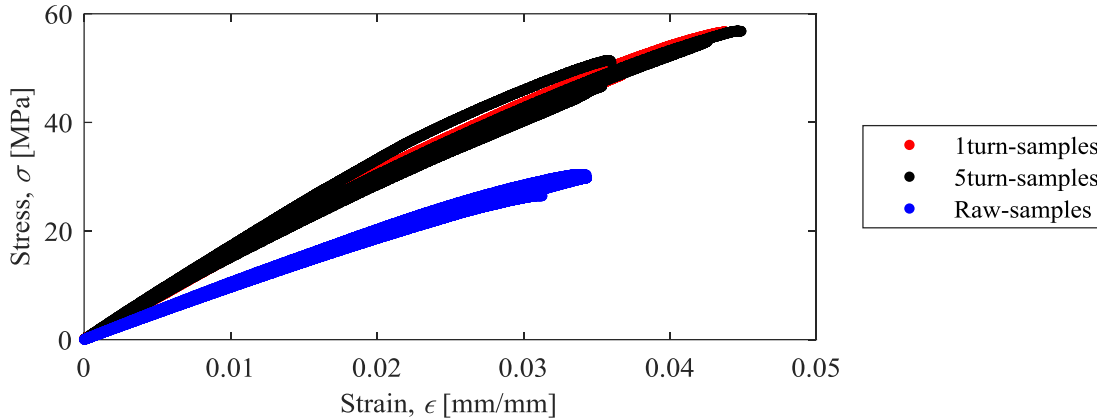
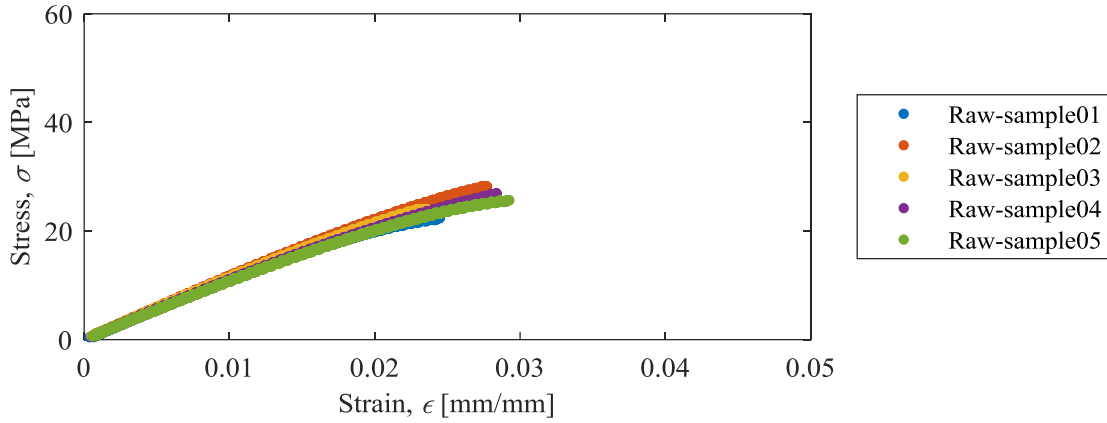


Figure 39: The stress-strain curve comparing the results of the tensile tests amongst the raw, 1 turn, and the 5 turn longitudinal samples.

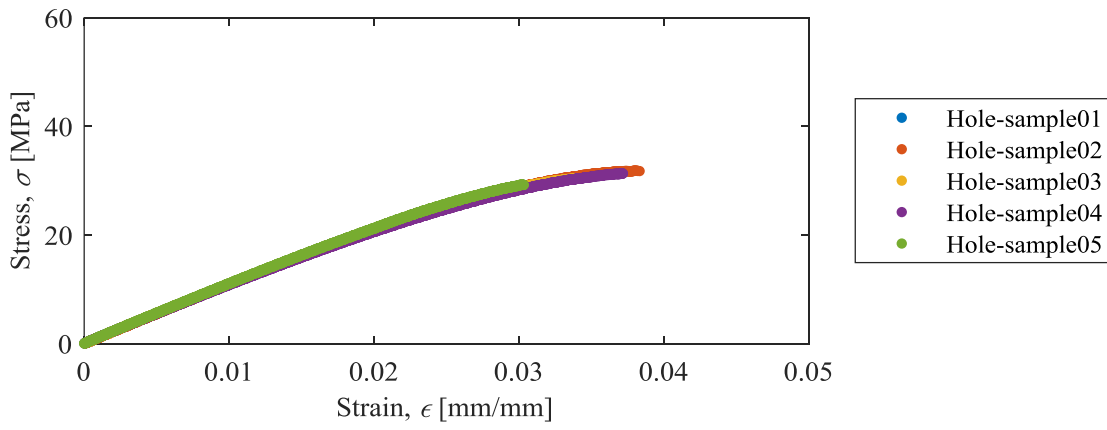
### 4.1.3 Z-direction samples

#### Raw and hole samples

The raw and hole samples were tested on a tensile machine and the results are provided using a stress-strain curve illustrated in Figure 40. The results, once again, just like what happened to the longitudinal samples, had a negligible difference when it comes to tensile strength and elastic modulus. The raw sample had an elastic modulus of  $1.11 \pm 0.04$  GPa and a tensile strength of  $25.54 \pm 2.36$  MPa while the hole had  $1.09 \pm 0.01$  GPa and  $30.78 \pm 1.02$  MPa, respectively. The elastic modulus and tensile strength were calculated based on the average of all the samples used on the experiment. The similarity in the results can be explained by the fact that the hole that goes through the part only corresponds to 1.5% to the total area of the cross section. Therefore, it does not affect much on the performance of the part under tension. The samples, however, had a small difference on the strain at breakage where the hole samples were breaking at a higher strain than the raw ones.



(a)



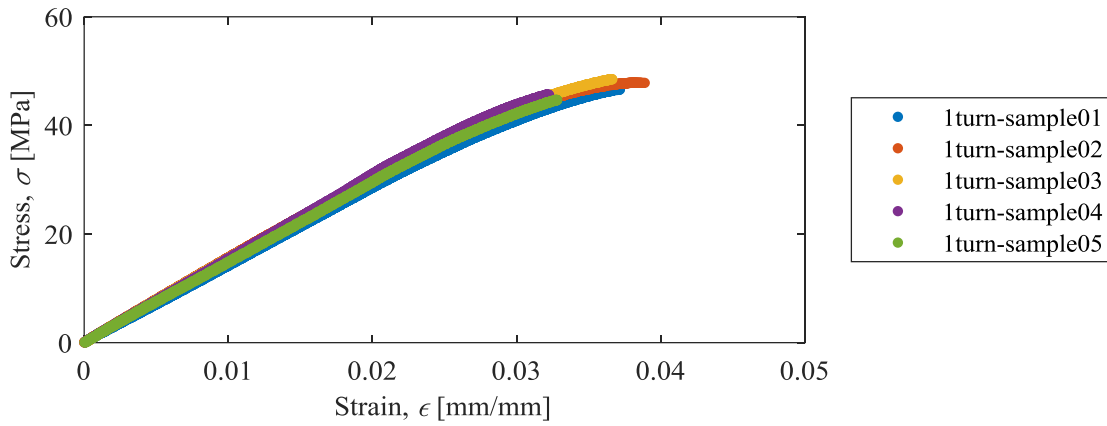
(b)

Figure 40: The stress-strain curve showing the results of the tensile tests for the (a) raw, and (b) hole  $z$ -direction samples.

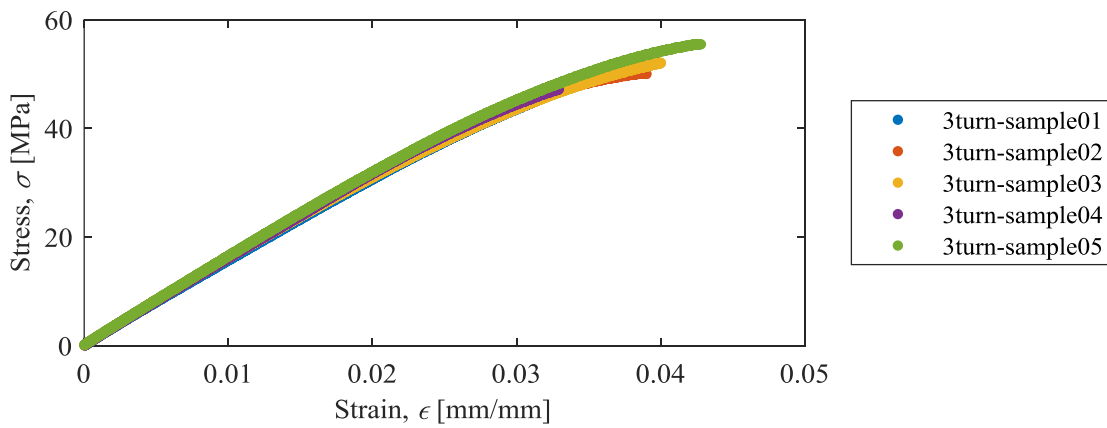
## Reinforced samples

The same types of reinforced samples used on the longitudinal direction parts are going to be used for the  $z$ -direction samples. This subsection will provide the results for the  $z$ -direction reinforced samples with 1 turn, 3 turn, and 5 turn. The results will provide a better understand on how the post tensioning technique could affect on the mechanical properties of the  $z$ -direction samples.

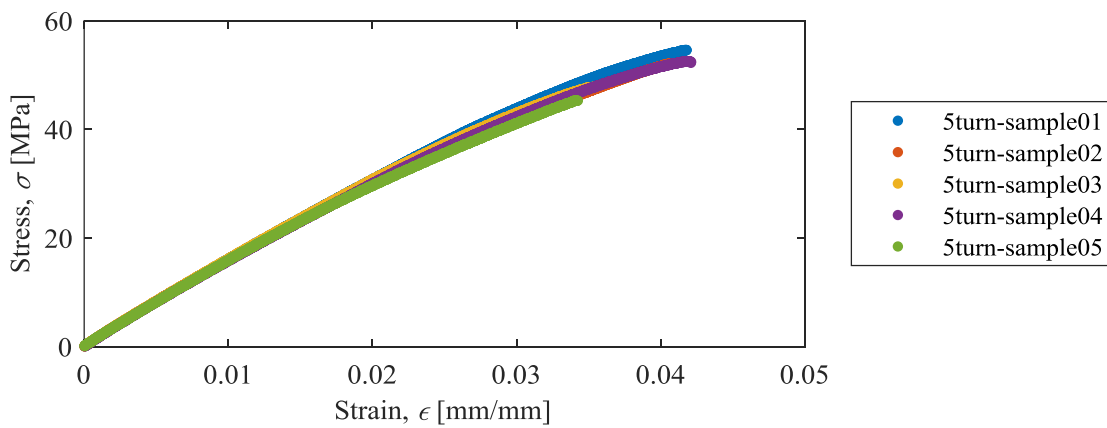
The results of the tensile tests for the 1 turn, 3 turn, and 5 turn are provided in Figure 41 with a stress-strain curve. The results showed that adding the metal rod as a reinforcement highly improved the mechanical strength and increased the elastic modulus when compared to the raw and hole samples. The improvement can be quantified by comparing the two extremes case scenarios, which are the raw sample and the 5 turn. The tensile strength increased from  $25.54 \pm 2.36$  MPa to  $50.42 \pm 3.76$  MPa, and the elastic modulus from  $1.11 \pm 0.04$  GPa to  $1.61 \pm 0.04$  GPa, for the raw, and 5 turn samples, respectively. However, it is notable the similarity of the results amongst the reinforced samples themselves, showing that the different amount of torque applied onto the 3D printed part did not have an impact on their mechanical properties.



(a)



(b)



(c)

Figure 41: Stress-strain curve showing the results of the tensile tests for the (a) 1 turn, (b) 3 turn, and (c) 5 turn z-direction samples.

Table 8 shows the elastic modulus for each different group of the  $z$ -direction samples, which is also provided in Figure 42, that illustrates the change in the elastic modulus when the reinforcement is added. Also, showing that the amount of torque applied did not affect on the elastic modulus of the 3D printed part, since all the reinforced samples had almost the same elastic modulus. Table 9 and Figure 43 show the tensile strength comparison amongst the  $z$ -direction samples, where the improvement when adding the metal rod can be quantified and illustrated.

Table 8: Overall comparison amongst the elastic modulus for the  $z$ -direction samples.

Samples	Elastic modulus (MPa)	Standard deviation ( $\pm$ )
Raw	1111.11	38.67
Hole	1092.78	10.64
1 turn	1510.44	54.46
3 turn	1624.44	25.90
5 turn	1616.00	38.61

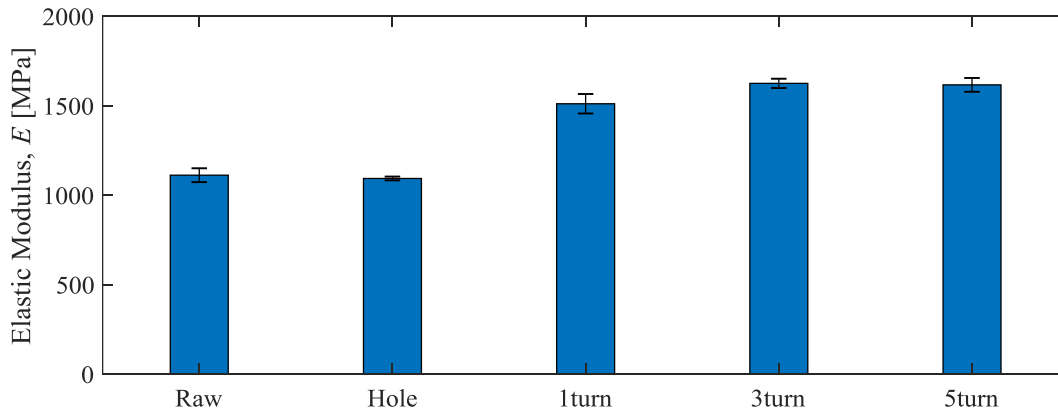


Figure 42: Overall comparison amongst the elastic modulus for the  $z$ -direction samples where the error bars are the standard deviation of the mean.

Table 9: Overall comparison amongst the tensile strength for the  $z$ -direction samples.

Samples	Tensile Strength (MPa)	Standard deviation ( $\pm$ )
Raw	25.54	2.36
Hole	30.78	1.02
1 turn	46.58	1.58
3 turn	50.20	3.72
5 turn	50.42	3.76

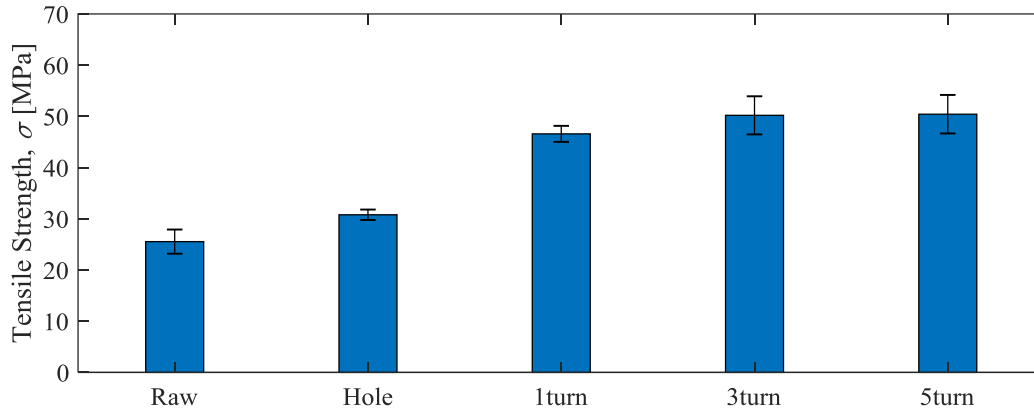


Figure 43: Overall comparison amongst the tensile strength for the z-direction samples where the error bars are the standard deviation of the mean.

### Comparisons amongst z-direction samples

As mentioned earlier in this chapter, the raw and hole samples had a very similar tensile tests result. A comparison is illustrated in Figure 44 where both raw and hole samples results are combined on the same plot using a stress-strain curve. The hole going through the sample had a negligible effect on the mechanical properties of the part since its fraction of area on the cross section of the part is very small, only 1.5% of the total. The difference in strain can be related to the different batch the samples were printed with.

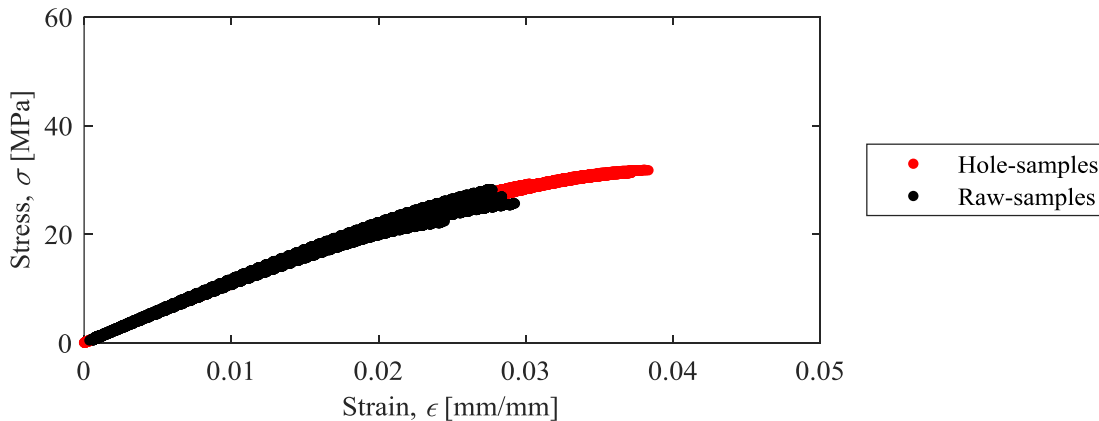


Figure 44: The stress-strain curve comparing the results of the tensile tests between the raw, and the hole z-direction samples.

The second comparison was done by taking the two extremes, which are the raw and the 5 turn samples, and combining them on the sample plot. Figure 45 shows the results of the two different specimens on a stress-strain curve. This comparison is important to see the actual effect of using a metal rod as a reinforcement to 3D printed parts. The tensile strength increased from  $25.54 \pm 2.36$  MPa to  $50.42 \pm 3.76$  MPa when adding the reinforcement. Besides the tensile strength, there was also a change on the elastic modulus of the part, going from  $1.11 \pm 0.04$  GPa to  $1.62 \pm 0.04$  GPa.

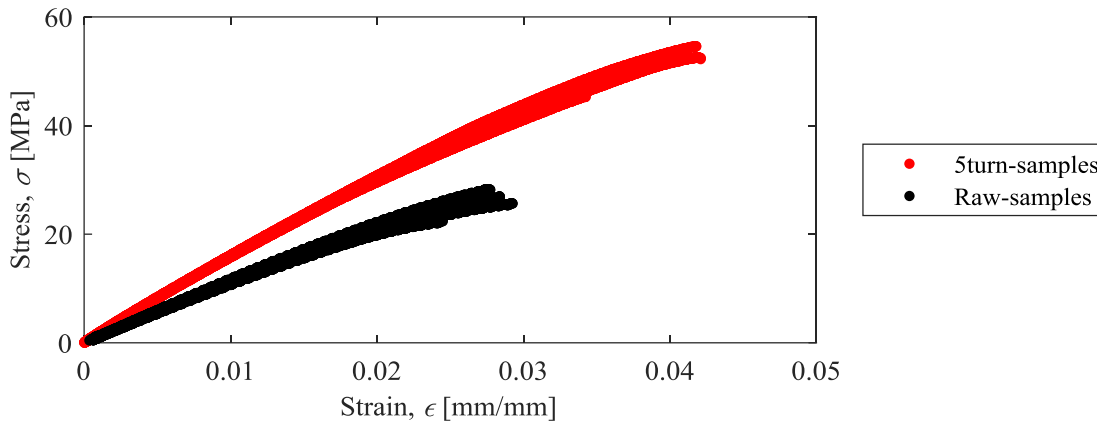
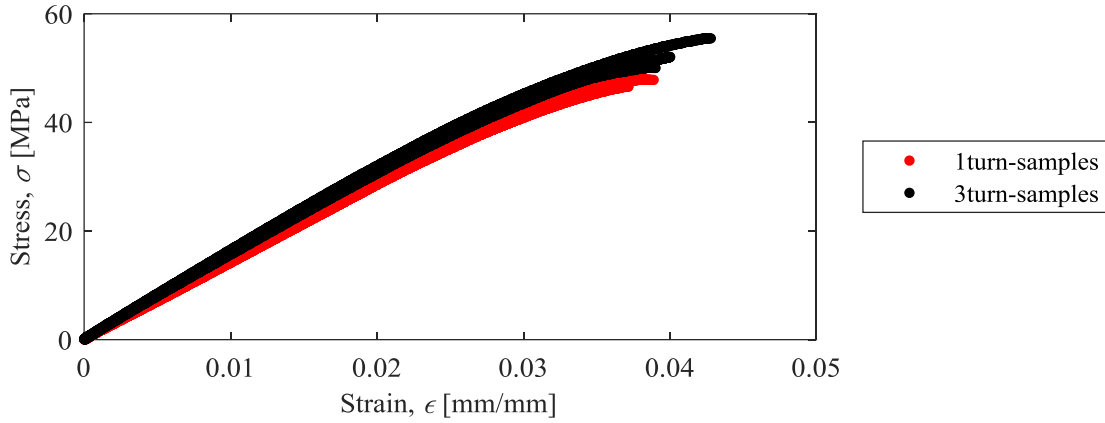
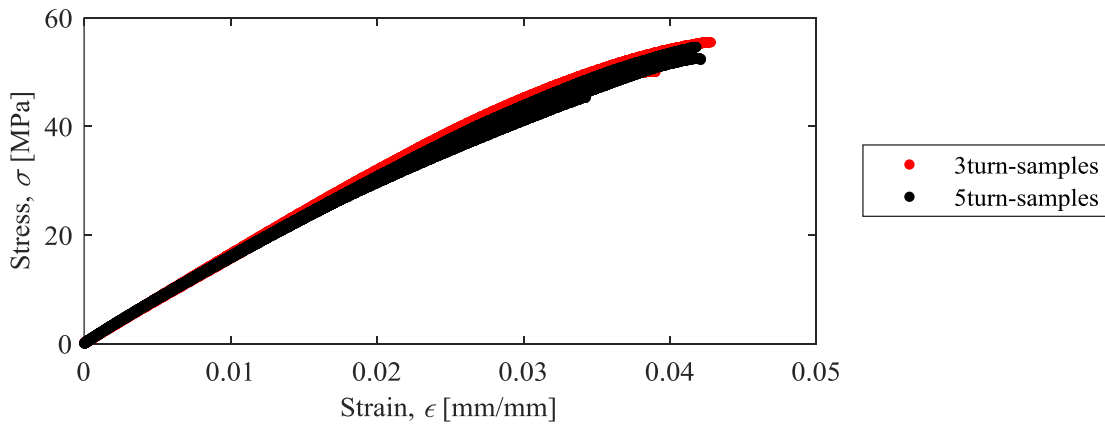


Figure 45: The stress-strain curve comparing the results of the tensile tests between the raw, and the 5 turn z-direction samples.

The third comparison was done amongst the three different reinforced samples, 1 turn, 3 turn, and 5 turn in order to understand the effect that adding different amount of torques to the samples would have. Figure 46 illustrates the comparison between the 1 turn, and 3 turn, also the comparison between the 3 turn, and 5 turn samples using a stress-strain curve. The different amount of compressive loads applied onto the 3D printed parts did not have any effect or change on the mechanical property of the samples. The three reinforced samples had almost the same tensile strength,  $46.58 \pm 1.56$  MPa,  $50.20 \pm 3.72$  MPa, and  $50.42 \pm 3.76$  MPa, also almost the same elastic modulus,  $1.51 \pm 0.05$  GPa,  $1.62 \pm 0.03$  GPa, and  $1.62 \pm 0.04$  GPa, respectively for the 1 turn, 3 turn, and 5 turn samples.



(a)



(b)

Figure 46: The stress-strain curve comparing the results of the tensile tests between the (a) 1 turn and 3 turn, and the (b) 3 turn and 5 turn  $z$ -direction samples.

Figure 47 shows the last comparison for the  $z$ -direction samples showing the results of the raw, 1 turn, and 5 turn samples. It illustrates, using a stress-strain curve, the change in the mechanical properties of the 3D printed part when using a metal rod as reinforcement. The tensile strength increased from  $25.54 \pm 2.36$  MPa to  $50.42 \pm 3.76$  MPa, based on the values of the raw, and 5 turn samples, respectively. There was also a change in the elastic modulus where it went from  $1.11 \pm 0.04$  GPa to  $1.62 \pm 0.04$  GPa, using the raw, and the 5 turn samples, respectively. However, as mentioned before, the different compressive loads did not have much effect on the mechanical properties, as can be seen when comparing the 1 turn, and 5 turn samples.

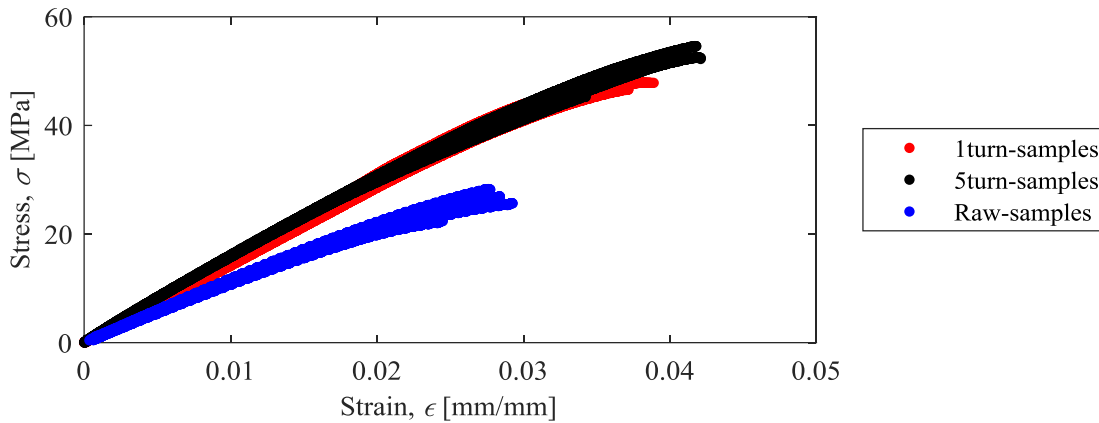


Figure 47: The stress-strain curve comparing the results of the tensile tests amongst the raw, 3 turn, and the 5 turn  $z$ -direction samples.

#### 4.1.4 Comparison between longitudinal and $z$ -direction samples

Comparisons between the longitudinal and  $z$ -direction samples will be discussed in the next subsection. The idea behind these comparisons is to understand the effect of printing 3D printed parts in different orientations, also comparing the results of the reinforced samples. The tensile strength and elastic modulus will also be compared.

#### Raw and hole samples

The first comparison was done between the raw and hole samples. Figure 48 illustrates the results of the two different configurations for each specimen, using a stress-strain curve. The different layer orientation did not have great impact on the mechanical properties for neither raw nor hole samples. The specimens had a negligible difference on the tensile strength and on the elastic modulus between them.

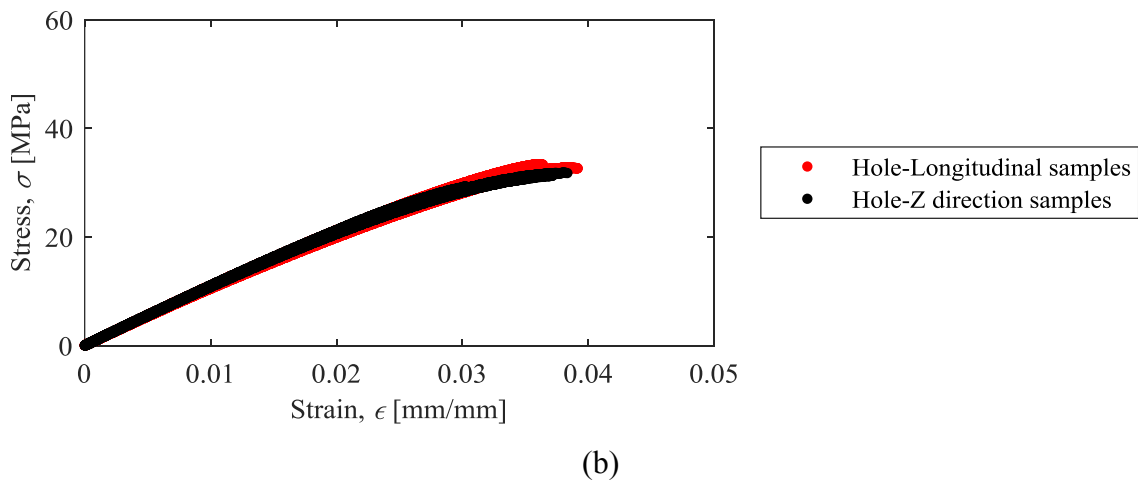
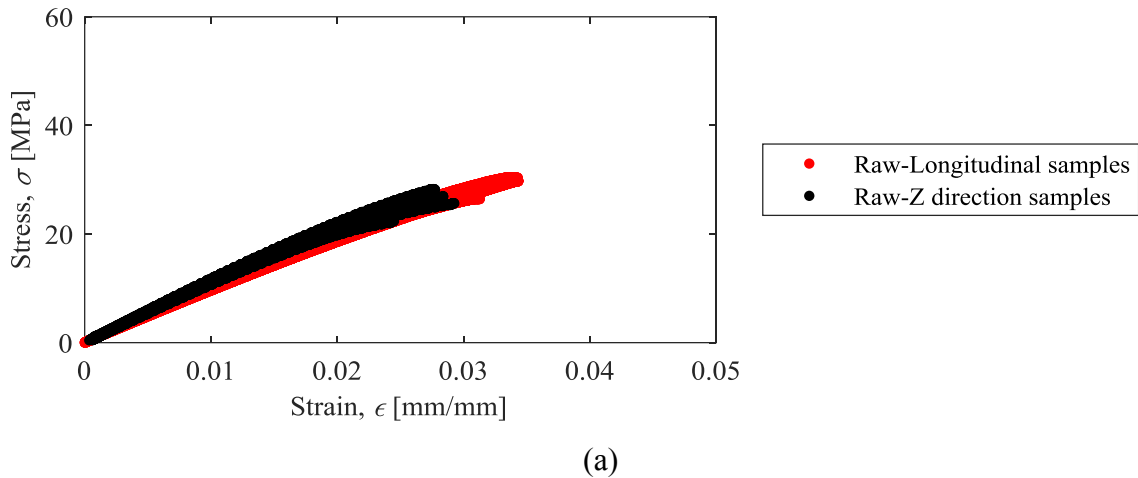
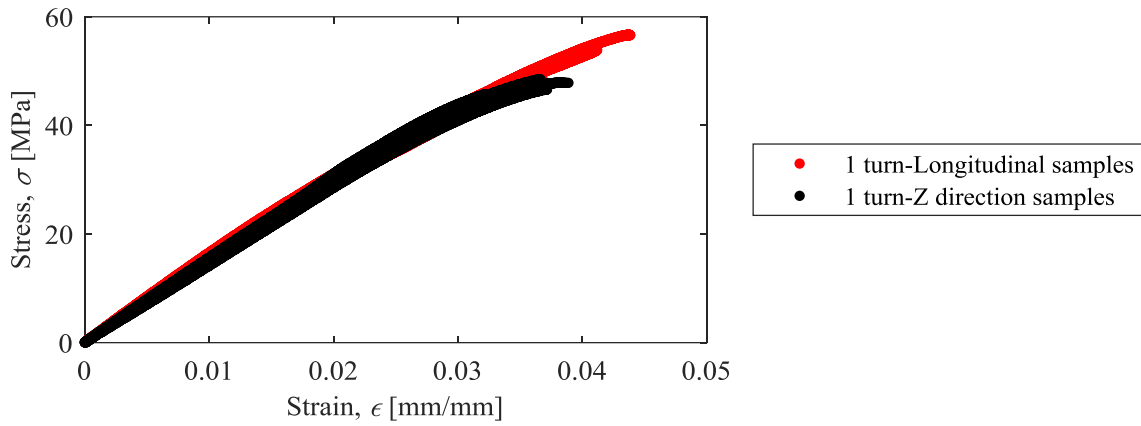


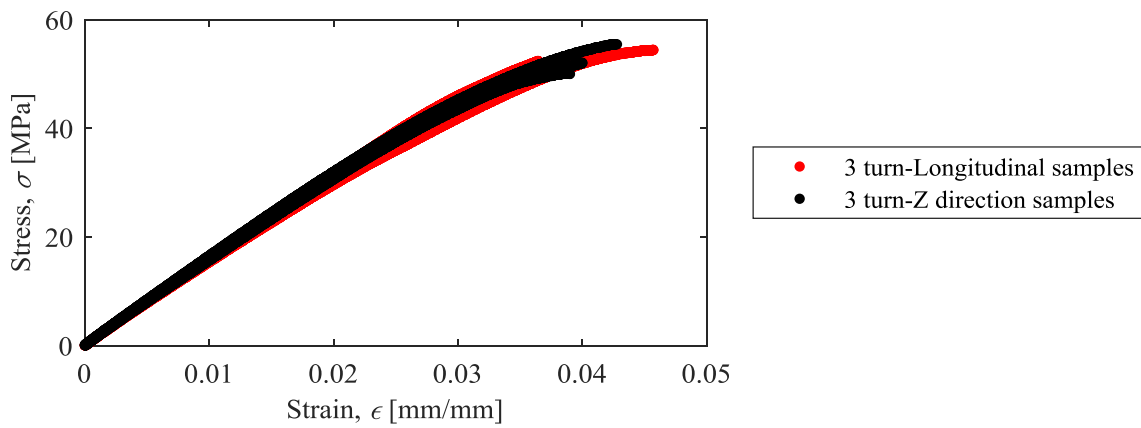
Figure 48: The stress-strain curve comparing the results of the tensile tests between the (a) raw, and the (b) hole samples for the longitudinal and z-direction.

### Reinforced samples

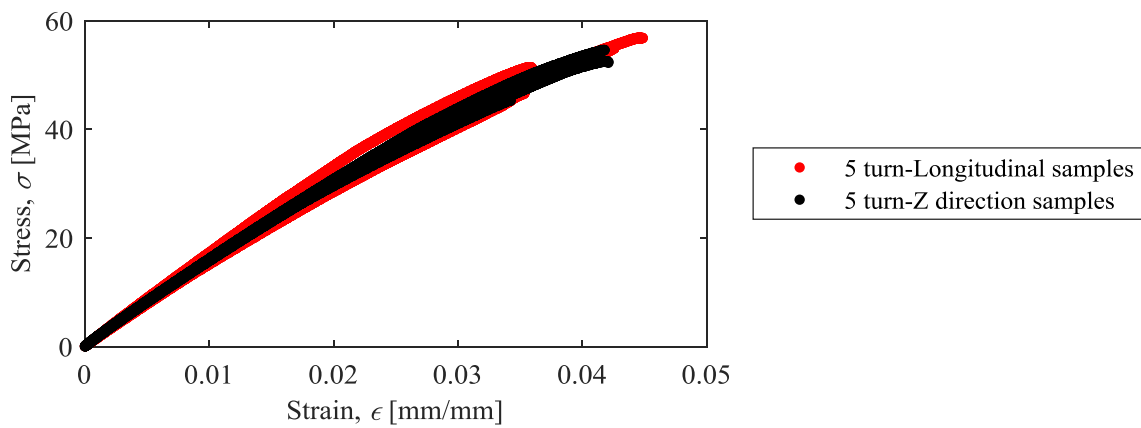
Figure 49 shows, using a stress-strain curve, the second comparison between the longitudinal and z-direction samples when it comes to the effect that each reinforcement sample had on the 3D printed part. The different layer orientation or different amount of torque applied did not change the improvement obtained by adding the metal rod. The tensile strength was almost the same for all the samples, as well as the elastic modulus.



(a)



(b)



(c)

Figure 49: The stress-strain curve comparing the results of the tensile tests amongst the (a) 1 turn, (b) 3 turn, and (c) 5 turn samples for the longitudinal and z-direction.

## Extreme samples

The last comparison will be done comparing the two extreme case scenarios, which are the raw and the 5 turn samples. Figure 50 shows the two extremes for each type of printing orientation using a stress-strain curve. When comparing the same type of sample for different printing orientation, it does not show great difference and the results are very similar. However, when it comes to the comparison between the raw and the 5 turn samples, it is notable the improvement that adding the metal rod as a reinforcement brought. Both tensile strength, and elastic modulus increased from  $25.54 \pm 2.36$  MPa to  $49.60 \pm 7.54$  MPa, and  $1.11 \pm 0.04$  GPa to  $1.59 \pm 0.08$  GPa, respectively, when comparing the  $z$ -direction raw sample to the longitudinal 5 turn sample, respectively.

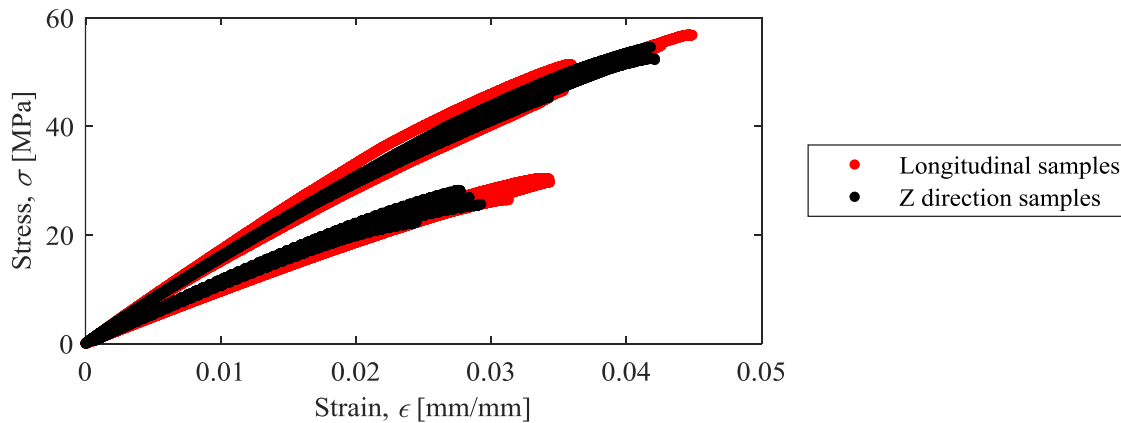
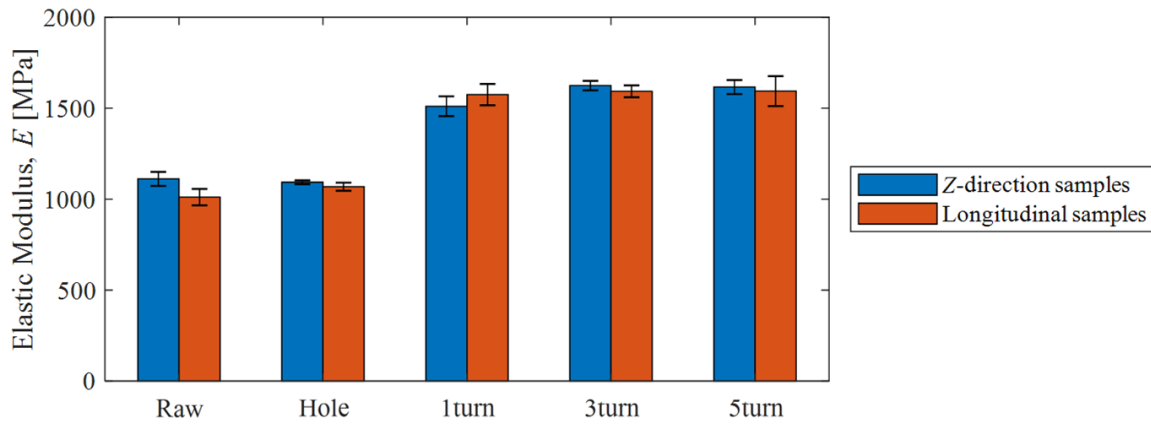


Figure 50: The stress-strain curve comparing the results of the tensile tests between the raw, and the 5 turn longitudinal and  $z$ -direction samples, where the samples with higher tensile strength are the 5 turn, and the ones with lower tensile strength are the raw samples.

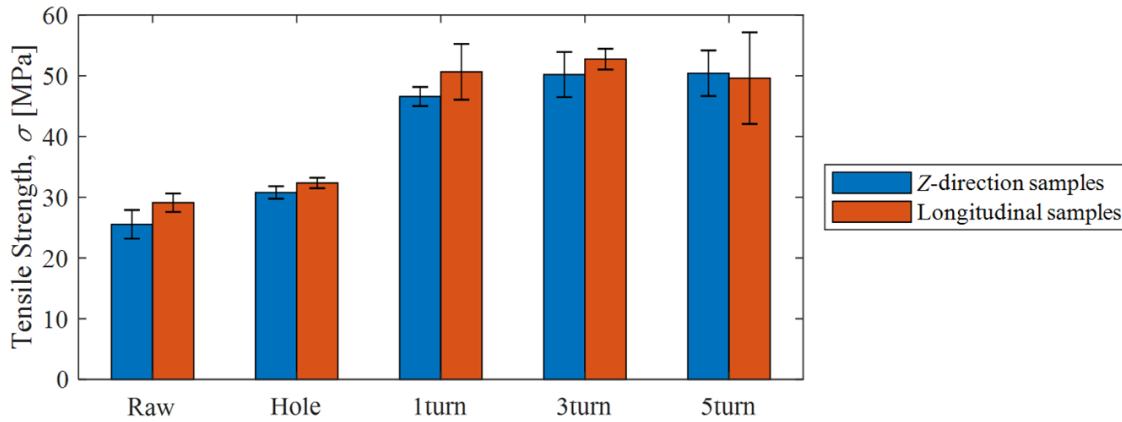
## Overall comparison amongst the tensile tests

Figure 51 shows the comparison amongst all the results from the tensile tests for both longitudinal and  $z$ -direction samples. It illustrates the elastic modulus and tensile strength obtained for each group of samples. The results showed that adding reinforcement to the 3D printed parts, helped on increasing both elastic modulus and tensile strength. However, the improvement was

very similar when comparing the longitudinal to the  $z$ -direction samples. The samples that were not reinforced such as raw and hole, had a lower elastic modulus and tensile strength when compared to the 1,3, and 5 turn samples. The error bars illustrate the standard deviation of the mean result.



(a)



(b)

Figure 51: The comparison of results from the tensile tests for both longitudinal and  $z$ -direction samples. It compares the (a) elastic modulus, and (b) tensile strength amongst all samples for both printing orientations.

## 4.2 Bending tests

The bending tests results will be provided in this subsection. The bending samples were divided into two different groups of samples: longitudinal and  $z$ -direction. First, the results for the longitudinal samples are shown and compared amongst them, followed by the results obtained from the  $z$ -direction specimens. The subsection is concluded with an overall comparison of the results amongst all samples for both printing orientations.

### 4.2.1 Longitudinal samples

#### Raw and hole samples

Figure 52 shows the results for the raw and hole samples in an axial load-stroke curve. Both samples had a very similar result with negligible difference. The flexural modulus and flexural strength were almost the same, having the values of  $1726.76 \pm 71.58$  MPa, and  $1769.37 \pm 73.83$  MPa for the flexural modulus and,  $55.61 \pm 2.69$  MPa, and  $55.22 \pm 1.25$  MPa, for the flexural strength, respectively to the raw and hole samples. This similarity can be explained by that fact that both samples had almost the same design, being the hole going through the sample, the only difference. The center of the hole was located on the neutral axis of the cross section, which helps reducing the effect of the hole on the mechanical properties of the part. The results also showed that the experiment was very consistent with repeatable results.

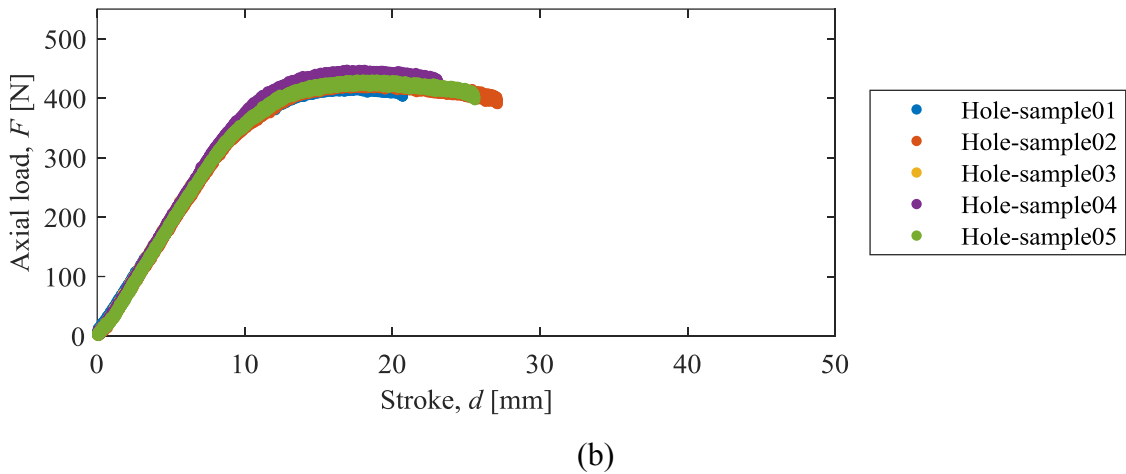
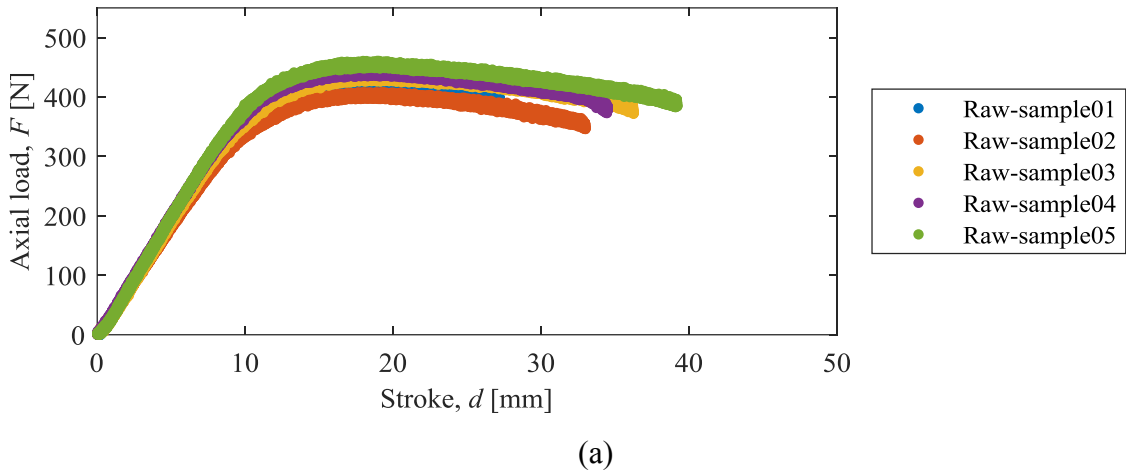
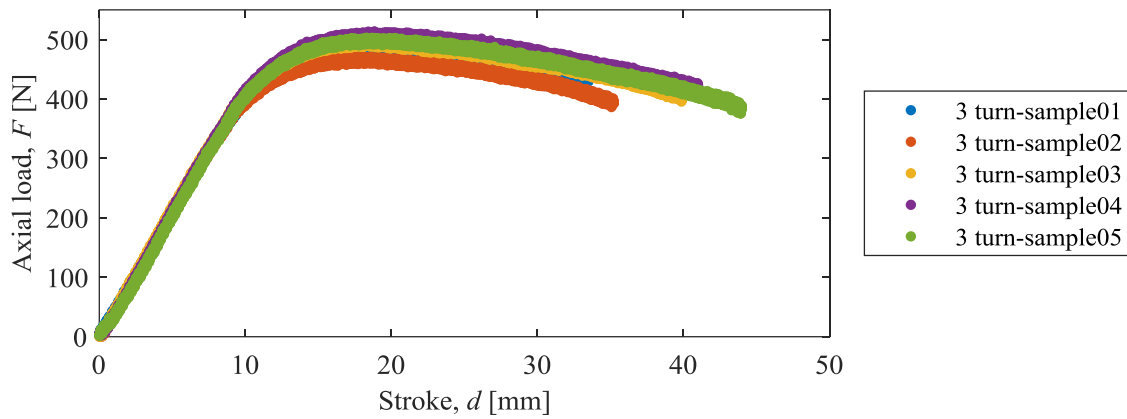


Figure 52: The axial load-stroke curve showing the results of the 3 point bending tests for the (a) raw, and (b) hole longitudinal samples.

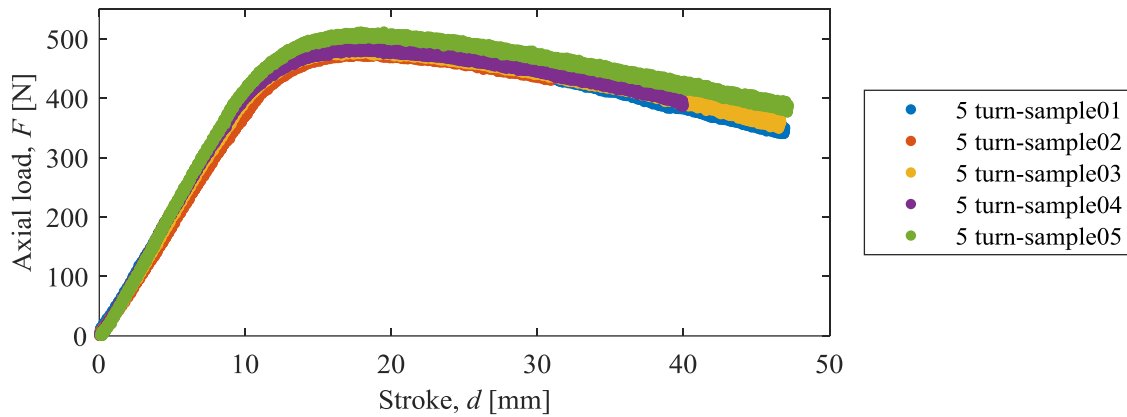
### Reinforced samples

There were two different types of reinforced samples for the three point bending tests: 3 turn, and 5 turn. Figure 53 shows the results for the 3 turn and 5 turn samples, using an axial load-stroke curve. There was a small improvement on the performance, since that the raw and hole samples had their maximum flexural strength around 55 MPa while the reinforced samples ranged from  $61.44 \pm 4.26$  MPa to  $63.26 \pm 2.49$  MPa, for the 5 turn and 3 turn, respectively. The flexural modulus and flexural strength were calculated based on the average of all tested samples, also obtaining

their standard deviation. This improvement is related to the compressive load applied into the sample, therefore increasing the flexural strength. The effect of the compressive load will be explained in detail later in this chapter. It is also noticeable that the amount of turns does not change much on the mechanical properties, since the results for both 3 and 5 turns were very similar.



(a)



(b)

Figure 53: The axial load-stroke curve showing the results of the 3 point bending tests for the (a) 3 turn, and (b) 5 turn longitudinal samples.

Table 10: Overall comparison amongst the flexural modulus for the longitudinal samples.

Samples	Flexural Modulus (MPa)	Standard Deviation ( $\pm$ )
Raw	1726.76	71.58
Hole	1769.37	73.83
3 turn	1858.50	85.60
5 turn	1823.74	100.96

Table 11: Overall comparison amongst the flexural strength for the longitudinal samples.

Samples	Flexural Strength (MPa)	Standard Deviation ( $\pm$ )
Raw	55.61	2.69
Hole	55.22	1.25
3 turn	63.26	2.49
5 turn	63.13	1.69

The flexural modulus,  $E_{fm}$ , was calculated based on equation (14) [121], where  $L_s$  is the support span length,  $F$  is the load applied onto the middle of the specimen,  $d$  is the deflection of the sample due to  $F$ , and  $I$  is the second moment of area. The second moment of area is dependent on geometry of the cross section. Equation (15) [121] shows the second moment of area for rectangular cross sections, and equation (16) [121] shows the second moment of area for circular cross sections,

$$d = \frac{L_s^3 F}{48IE_{fm}} \quad (14)$$

$$I_r = \frac{wh^3}{12} \quad (15)$$

$$I_c = \frac{\pi r^4}{4} \quad (16)$$

where,  $w$  and  $h$  are the width and the height of the specimen, respectively, and  $r$  is the radius of the circle (metal rod). Since, the metal rod is in the neutral axis of the samples, it will be neglected

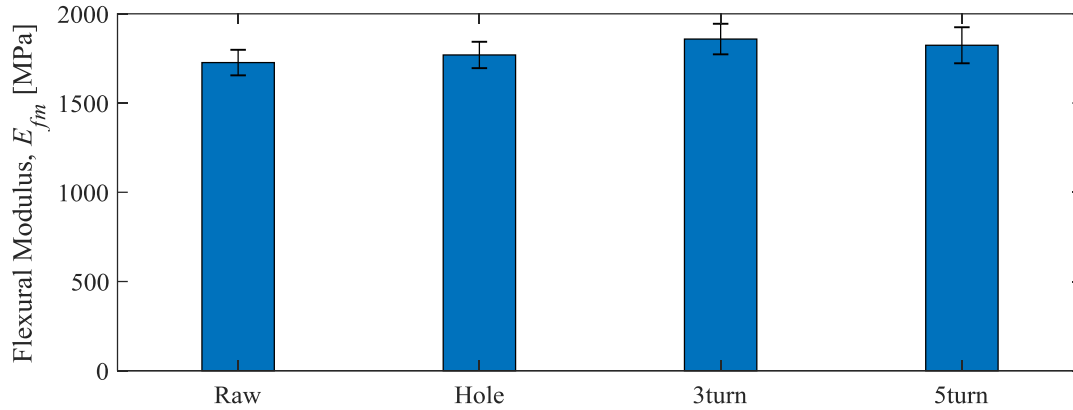
from the calculation. Therefore, by replacing equation (15) in equation (14), it is found the final equation used to calculate the flexural modulus of the specimens, which is represented below by equation (17).

$$E_{fm} = \frac{L_s^3 F}{4wh^3d} \quad (17)$$

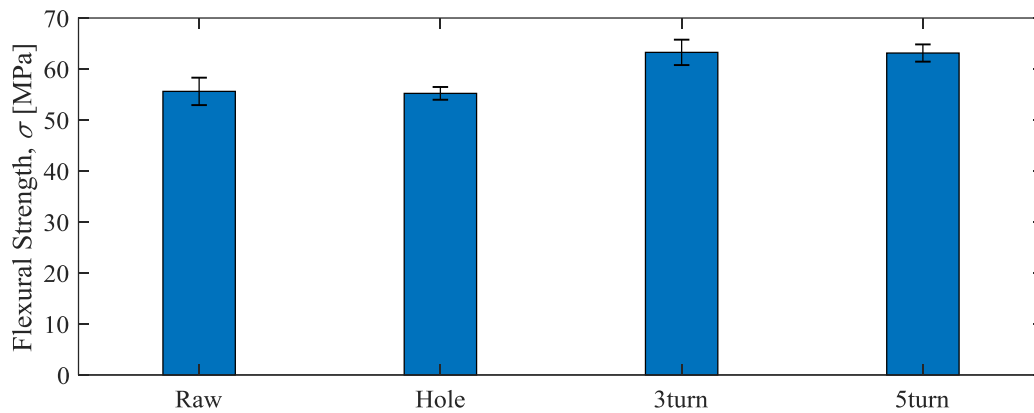
The flexural strength was calculated based on equation (18) [121], where,  $\sigma_{fs}$  is the flexural strength,  $M$  is the bending moment, and  $y$  is the distance from the neutral axis. The final equation used to calculate the flexural strength, represented by equation (19), was found by replacing the  $M$ , which is equal to  $\frac{FL}{4}$ , and  $y$  that is equal to  $\frac{h}{2}$ . Figure 54 shows the comparisons on the flexural strength and modulus, respectively, amongst the longitudinal samples.

$$\sigma_{fs} = \frac{My}{I_r} \quad (18)$$

$$\sigma_{fs} = \frac{3FL_s}{2wh^2} \quad (19)$$



(a)



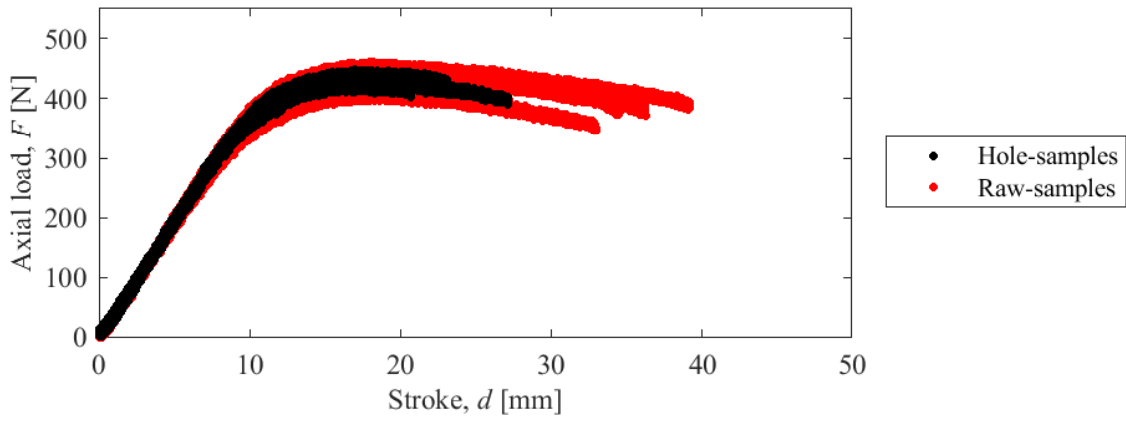
(b)

Figure 54: Comparison of the (a) flexural modulus, and (b) flexural strength amongst all the longitudinal samples. The error bars represent the standard deviation of the mean.

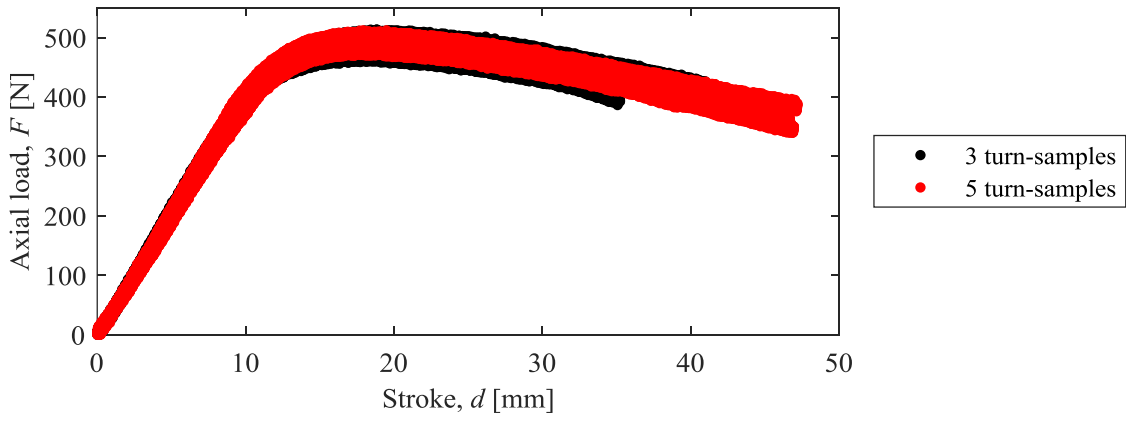
### Comparison amongst longitudinal samples

The raw and hole sample, as mentioned earlier in this chapter, had very similar results and did not seem to have a clear difference on their mechanical properties. Figure 55 compares both 3 point bending results in the same plot, so that it is easier to see the negligible difference between the two specimens where the raw and hole samples had a flexural modulus of  $1726.76 \pm 71.58$  MPa and  $1769.37 \pm 73.83$  MPa, and a flexural strength of  $55.61 \pm 2.69$  MPa and  $55.22 \pm 1.25$  MPa, respectively. Figure 55 also shows the comparison done for the reinforced samples, with the purpose of illustrating the similarity of the results and the improvement on the mechanical

properties of the 3D printed samples when compared to the raw and hole samples. The 3, and 5 turn samples had a flexural modulus of  $1858.50 \pm 85.60$  MPa and  $1823.74 \pm 100.96$  MPa, and a flexural strength of  $63.26 \pm 2.49$  MPa and  $63.13 \pm 1.69$  MPa, respectively.



(a)



(b)

Figure 55: The axial load-stroke curve comparing the results of the 3 point bending tests for the (a) raw and hole samples, and for the (b) 3 turn and 5 turn longitudinal samples.

The last comparison amongst the longitudinal samples was done with the raw and the 3 turn samples. Figure 56 shows the improvement on the mechanical properties of the 3D printed part, illustrated by an axial load-curve obtained from the 3 point bending test. The improvement can be quantified by flexural strength in which corresponded to  $55.61 \pm 2.69$  MPa and  $63.26 \pm 2.49$  MPa,

respectively to the raw and 3 turn samples. The flexural modulus was almost the same, being  $1726.76 \pm 71.58$  MPa and  $1858.50 \pm 85.60$  MPa, for the raw and 3 turn samples, respectively.

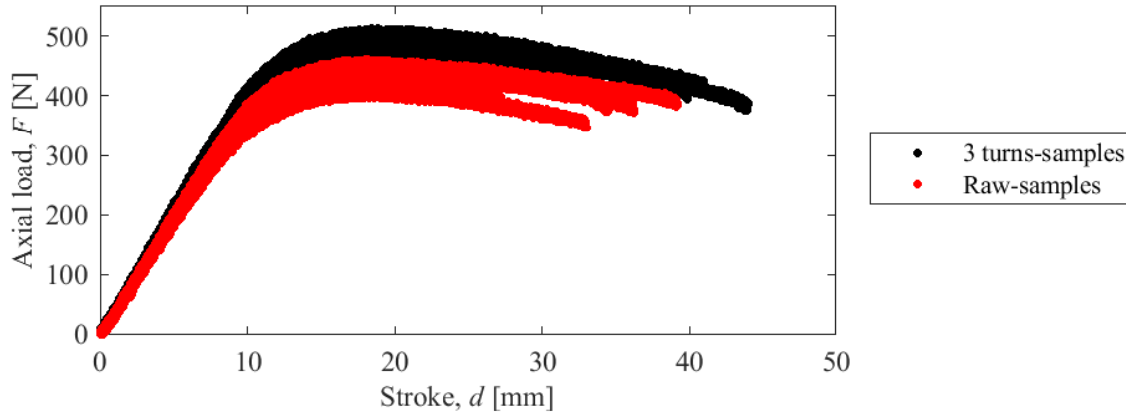


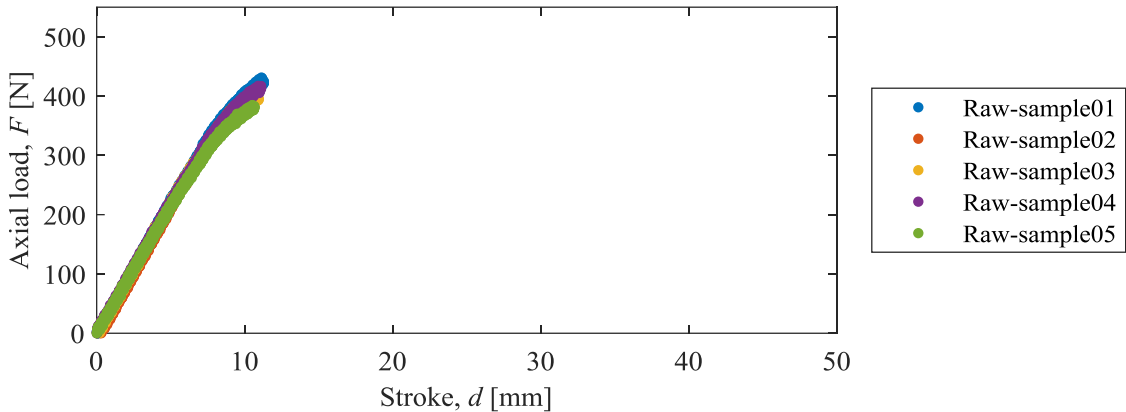
Figure 56: The axial load-stroke curve comparing the results of the 3 point bending tests for the raw, and 3 turn longitudinal samples.

#### 4.2.2 Z-direction samples

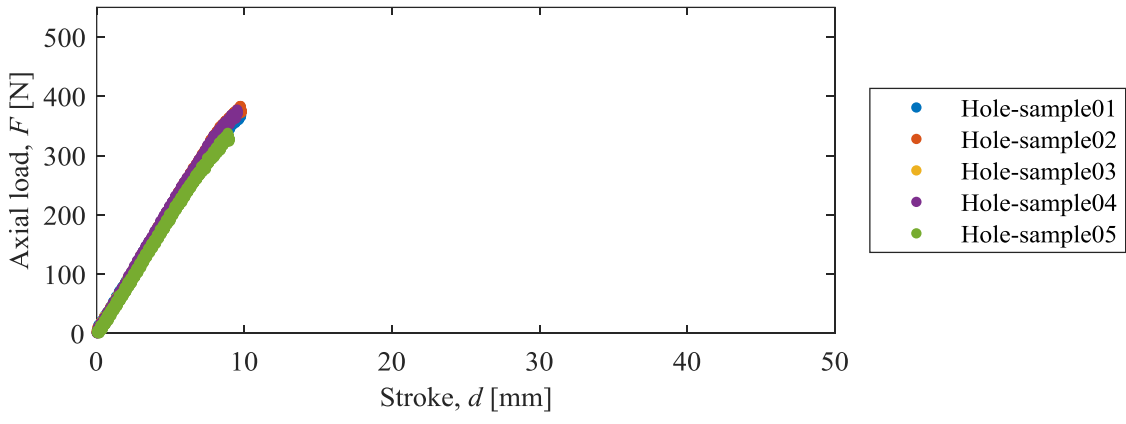
##### Raw and hole samples

The raw and hole results from the 3-point bending tests are shown in Figure 57 by an axial load-stroke curve. The raw and hole samples had a very similar flexural modulus with values of  $2010.11 \pm 41.08$  MPa, and  $1899.02 \pm 85.96$  MPa, respectively. There was a small, but negligible, difference on the flexural strength where the values were  $52.11 \pm 2.32$  MPa, and  $46.15 \pm 2.80$  MPa for the raw and hole samples, respectively. The similarity in the results can be explained by the fact that the hole that goes through the entire part is located on the neutral axis, which does not affect much on the flexural strength, since the holes are very small (3 mm). It is interesting to mention that for the longitudinal samples, after the samples reached their maximum flexural strength, it would still bend for about 25 mm more until it breaks. However, for the *z*-direction samples it would not bend that much, since the samples were printed on the *z*-direction its bonding between layers are very weak. Therefore, when a small crack was created it is going to propagate

easily through the cross section, since there is nothing to stop it from moving forward. For the longitudinal samples, when a crack is created, and a filament is broken, there is still many more filaments that the crack needs to break through in order to break the 3D printed part. This fact explains the difference in the stroke after the maximum flexural strength.



(a)



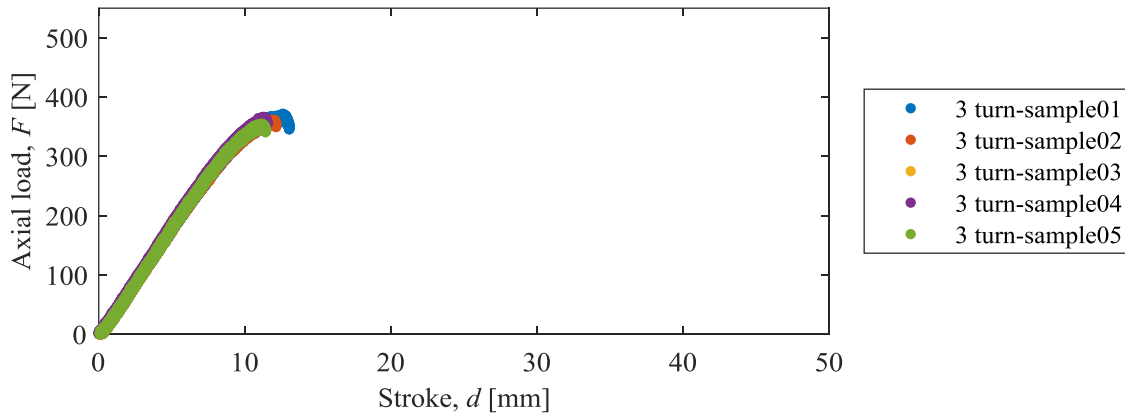
(b)

Figure 57: The axial load-stroke curve showing the results of the 3 point bending tests for the (a) raw, and (b) hole z-direction samples.

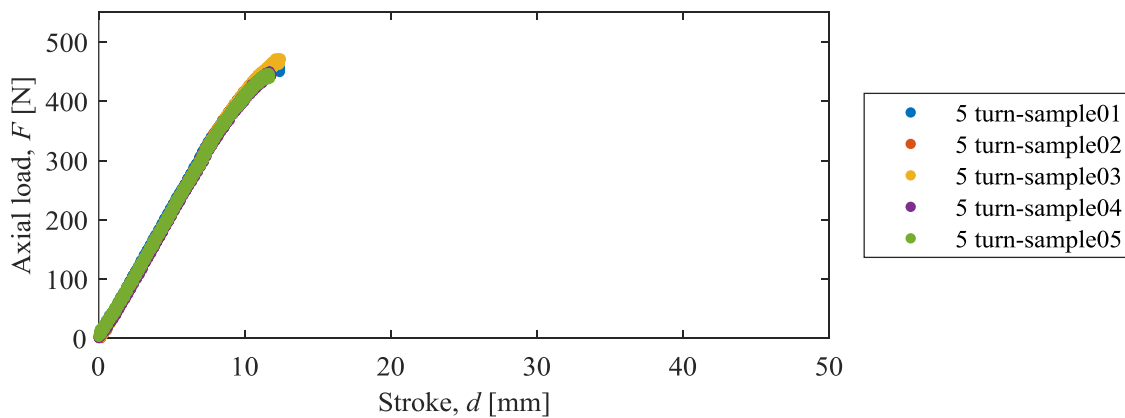
**Reinforced samples**

Figure 58 shows the results for the reinforced samples with 3 and 5 turns on an axial load-stroke curve. The two specimens had a modest difference on both flexural modulus, and flexural strength. The results found for the flexural modulus are  $1652.53 \pm 46.02$  MPa, and

1919.93±51.21 MPa, respectively for the 3, and 5 turn samples. The flexural strength had a higher difference on the results with values of 46.15±0.85 MPa, and 58.20±1.80 MPa, respectively for the 3, and 5 turn samples. Those differences on the results were not expected and are assumed to come from the different printing batch where the build plate might have had a different leveling, therefore, influencing on the repeatability of the printing properties of the specimens. However, there was an improvement on the tensile strength when comparing the 5 turn samples to the raw and hole. The hole sample, for example, had a flexural strength 46.15±2.80 MPa, while the 5 turn had a value of 58.20±1.80 MPa, which corresponds to about 25% improvement on their capability of withstand bending loads without failing.



(a)



(b)

Figure 58: The axial load-stroke curve showing the results of the 3 point bending tests for the (a) 3 turn, and (b) 5 turn *z*-direction samples.

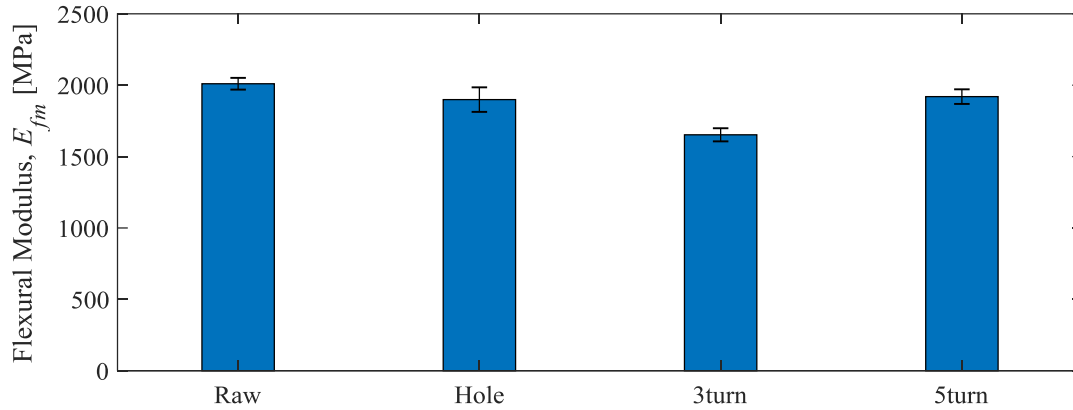
The flexural modulus and strength were calculated the same way as per the longitudinal samples. Table 12 and Table 13 compare the flexural modulus, and flexural strength amongst the four different groups of specimens, respectively. Figure 59 helps on illustrating the improvement/difference on the results provided on the tables below for the *z*-direction samples.

Table 12: Overall comparison amongst the flexural modulus for the *z*-direction samples.

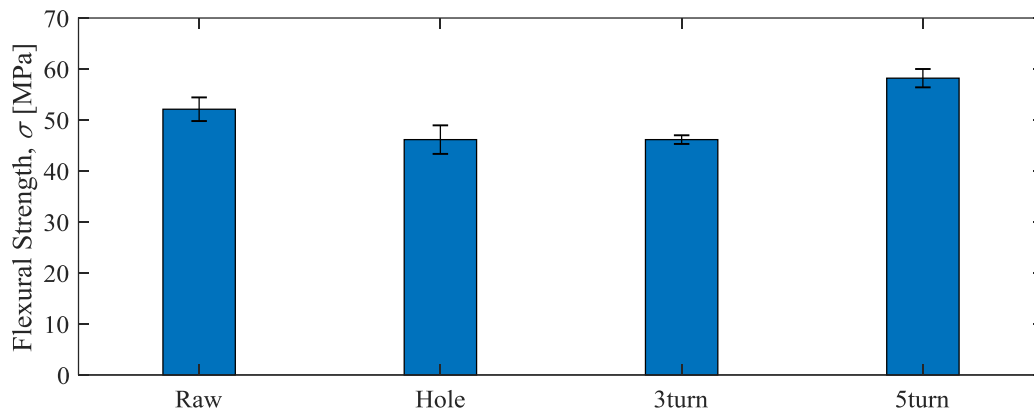
Samples	Flexural Modulus (MPa)	Standard Deviation ( $\pm$ )
Raw	2010.11	41.08
Hole	1899.02	85.96
3 turn	1652.53	46.02
5 turn	1919.93	51.21

Table 13: Overall comparison amongst the flexural strength for the *z*-direction samples.

Samples	Flexural Strength (MPa)	Standard Deviation ( $\pm$ )
Raw	52.11	2.32
Hole	46.15	2.80
3 turn	46.15	0.85
5 turn	58.20	1.80



(a)



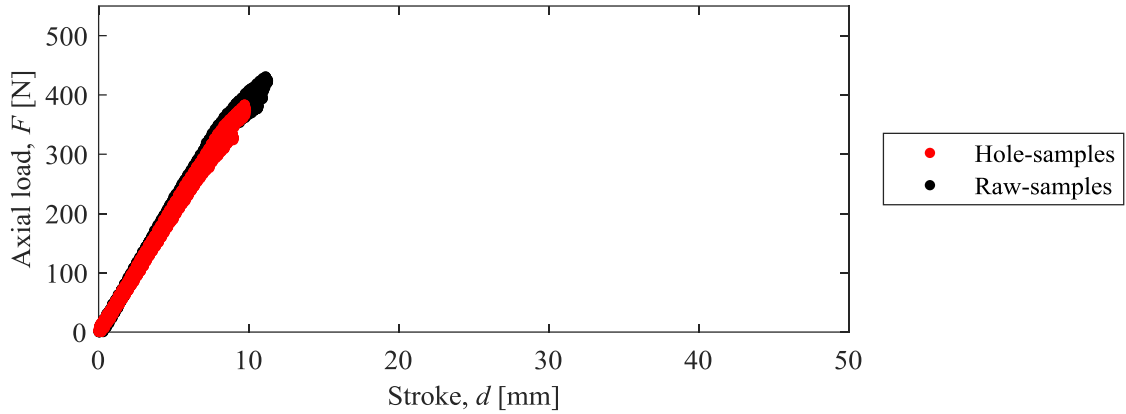
(b)

Figure 59: Comparison of the (a) flexural modulus, and (b) flexural strength amongst all the  $z$ -direction samples. The error bars represent the standard deviation of the mean

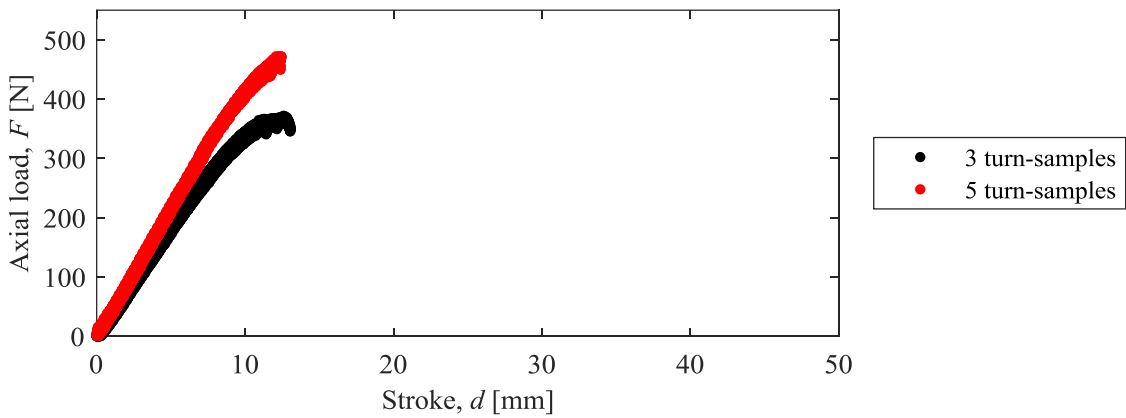
### Comparison amongst the $z$ -direction samples

Few comparisons were done amongst the  $z$ -direction samples to understand what the differences in mechanical properties for each type of specimen are. The first comparison is between the raw and hole sample. As mentioned before, these two samples had a very similar result, having negligible differences on the both flexural modulus and strength. The similarity can be seen in Figure 60, where both samples were plotted in the same graph using an axial load-stroke curve. The other comparison was done between the two reinforced samples. As mentioned earlier,

the 3 turn sample had a non-expected result. However, the 5 turn sample showed 25% improvement on the flexural strength when compared to the hole sample, for example.



(a)



(b)

Figure 60: The axial load-stroke curve comparing the results of the 3 point bending tests for the (a) raw and hole samples, and for the (b) 3 turn and 5 turn for the  $z$ -direction samples.

The reinforced samples showed the potential to improve the capability of 3D printed to withstand bending loads. Figure 61 quantifies that improvement by showing the difference in maximum flexural strength between the raw and the 5 turn samples on an axial load-stroke curve. The improvement between the raw, and 5 turn samples was found to be around 10% on the flexural strength. However, the highest improvement on the flexural strength was found to be between the hole, and 5 turn samples, with 25% improvement.

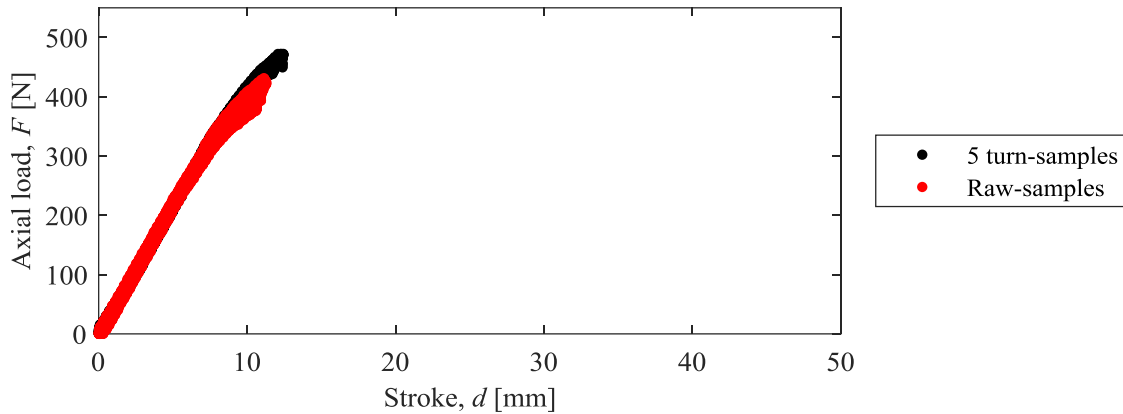


Figure 61: The axial load-stroke curve comparing the results of the 3 point bending tests for the raw, and 5 turn  $z$ -direction samples.

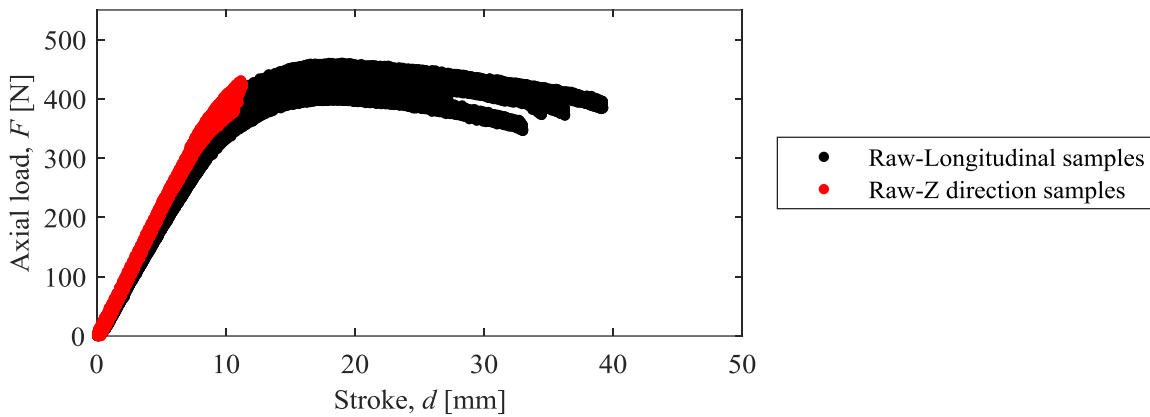
### 4.2.3 Comparison between longitudinal and $z$ -direction samples

The following section will include comparisons between the two different printing orientation samples, longitudinal and  $z$ -direction. These comparisons will help on understanding the effects that different printing orientations have on the flexural modulus and flexural strength, and the effects that adding reinforcement to it has. The flexural modulus and flexural strength will be compared in order to quantify the change in the mechanical properties of the 3D printed parts.

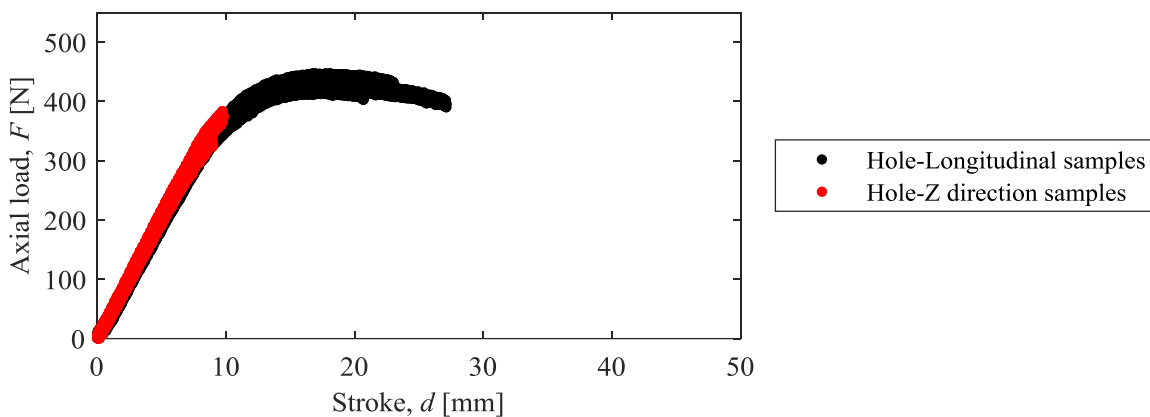
#### Raw and hole samples

The first comparison is between the raw and hole samples. Figure 62 shows the results for the raw and hole samples, for both longitudinal and  $z$ -direction samples on an axial load-stroke curve. The two different printing orientation seemed to have similar mechanical properties. The longitudinal samples had flexural strength and flexural modulus of  $55.61 \pm 2.69$  MPa and  $1726.76 \pm 71.58$  MPa for the raw sample, and  $55.22 \pm 1.25$  MPa, and  $1769.37 \pm 73.83$  MPa for the hole ones, respectively, while the  $z$ -direction samples had values of  $52.11 \pm 2.32$  MPa and  $2010.11 \pm 41.08$  MPa for the raw, and values of  $46.15 \pm 2.80$  MPa and  $1899.02 \pm 85.96$  MPa for the hole samples, respectively. That modest difference on the flexural strength is related to the way

the samples were printed. During a 3 point bending test, the  $z$ -direction samples for example, have a lower flexural strength than the longitudinal samples because there is nothing reinforcing the bonding between layers, therefore, when a small crack is created, it can easily propagate through the entire cross section. However, for the longitudinal samples, if a crack is created, it will not propagate very easy through the sample because there will be a lot of filaments that need to be broken in order to the complete failure of the part occur. That is also the reason why the longitudinal samples could withstand a higher stroke than the  $z$ -direction samples.



(a)

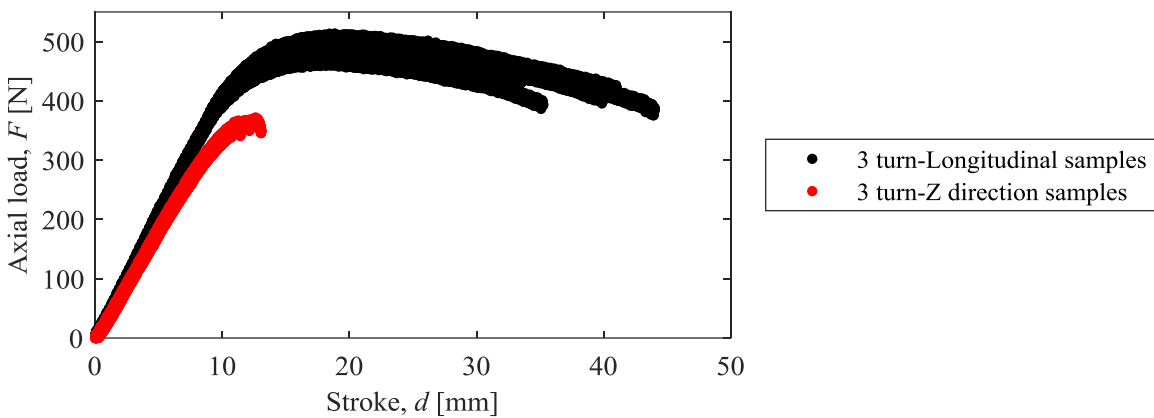


(b)

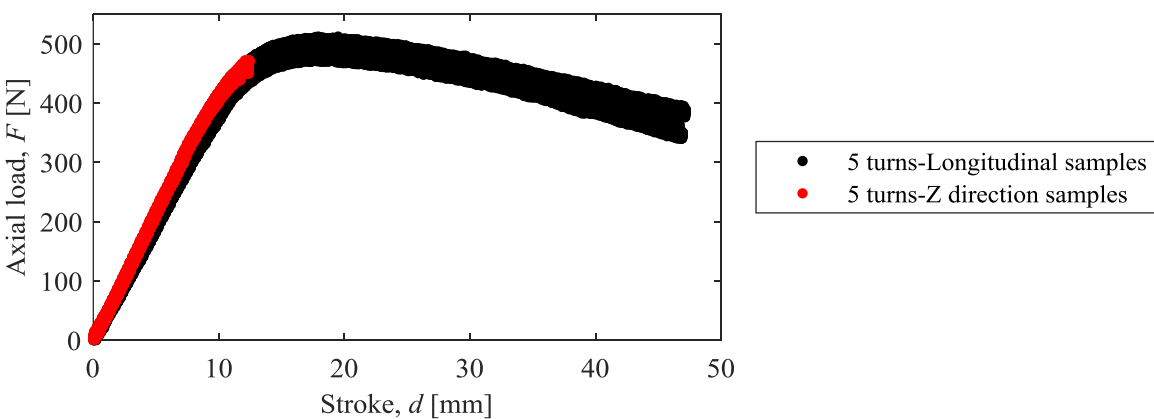
Figure 62: The axial load-stroke curve comparing the results of the 3 point bending tests between the (a) raw, and the (b) hole samples for the longitudinal and  $z$ -direction.

## Reinforced samples

The results for the 3 point bending tests for the 3 turn, and 5 turn samples are illustrated in Figure 63 by an axial load-stroke curve comparison. This second comparison shows that there was an increase on the flexural strength for both longitudinal, and  $z$ -direction samples when compared to the raw, and hole samples. However, the difference in torque did not seem to change the flexural strength of the samples. Once again, the results from the 3 turn  $z$ -direction sample were not expected.



(a)

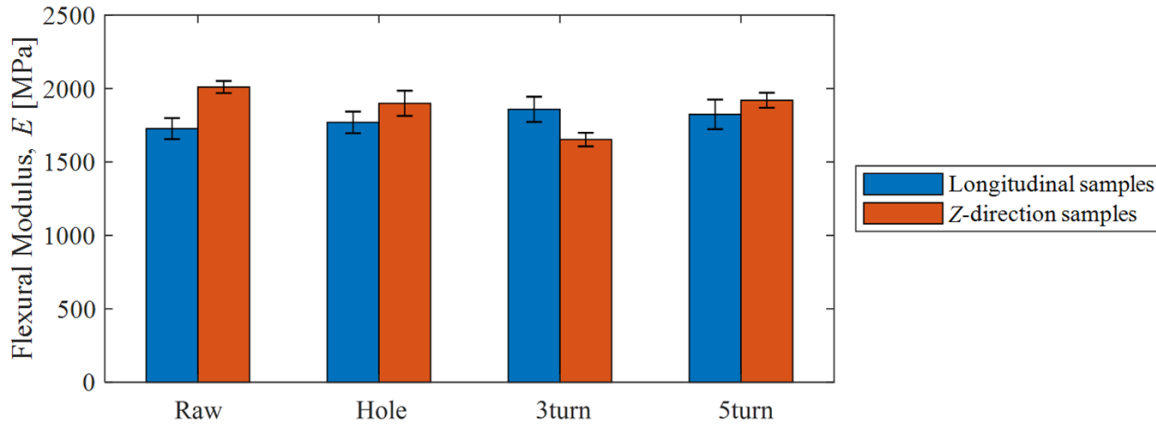


(b)

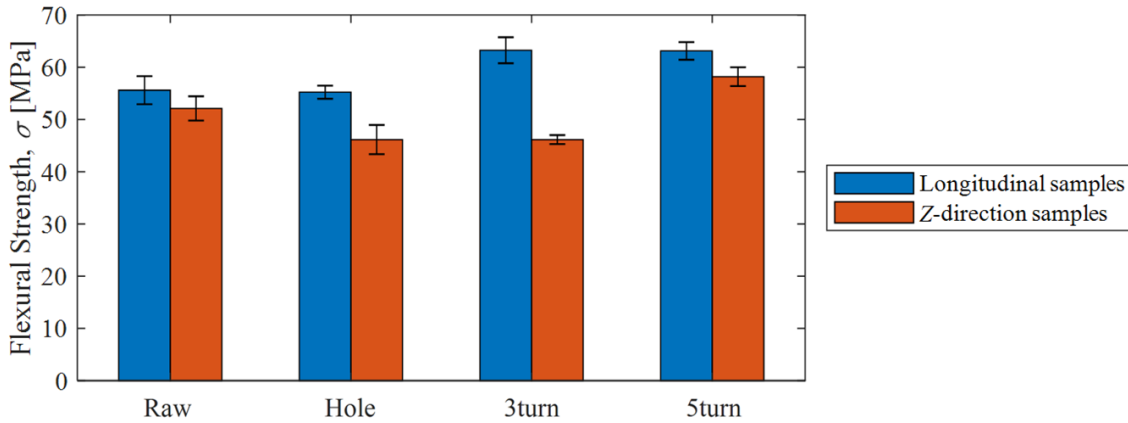
Figure 63: The axial load-stroke curve comparing the results of the 3 point bending tests between the (a) 3 turn, and (b) 5 turn samples for the longitudinal and  $z$ -direction.

## Overall comparison amongst the bending tests

Figure 64 shows the comparison for the flexural modulus, and flexural strength amongst all the samples used on the 3-point bending tests, which are the raw, hole, 3, and 5 turn samples for both longitudinal and  $z$ -direction printing orientation. The flexural modulus was almost the same for all the samples tested, meaning that either the printing orientation or the reinforcement used did not have an influence in it. The similarity on the flexural modulus can be explained by the fact that the hole that goes through the hole, 3, and 5 turn samples, is located on the neutral axis of the cross section, therefore it does not interfere either on the compression or the extension part of the beam tested. It can be proved by using the elastic beam theory, represented by equation (14) [121], for the two different geometries, meaning, using the second moment of area for the rectangle and for the circular geometry (metal rod) separately. It can be done by assuming the 3D printed ABS samples and the metal rods to be homogeneous and isotropic. It was found that for the same load applied, the deflection of the hole sample only represented 3.09% of the total deflection of the metal rod. Therefore, it can be stated that the metal rod had a negligible influence on the flexural modulus.



(a)



(b)

Figure 64: The comparison of results from the 3-point bending tests for both longitudinal and z-direction samples. It compares the (a) flexural modulus, and (b) flexural strength amongst all samples for both printing orientations.

The flexural strength seemed to be affected by the presence of the metal rod where an improvement was obtained when comparing the raw and hole samples to the reinforced ones. This improvement can be explained due to the uniform compressive loads added to the sample, coming from the washers that would compress the samples as the nuts were tightened. The difference in mechanical behavior between the samples is explained in Figure 65, where it shows how the compressive load helped on the improvement of the flexural strength for the reinforced samples. Figure 65 shows that the compressive stress,  $\sigma_c$ , shifts the stress distribution to the right, meaning that, in order to reach the same tensile stress,  $\sigma_t$ , that was required to the sample to fail, there will need to have a higher deflection, therefore, requiring a higher load to be applied to the sample.

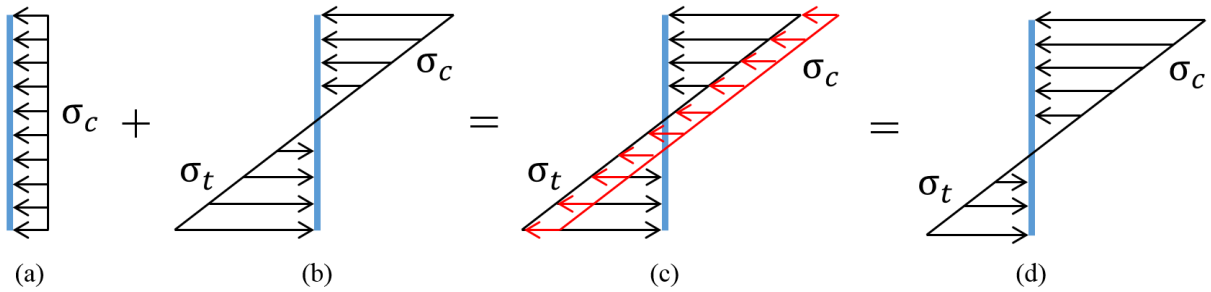


Figure 65: The stress distribution showing the effects of the compressive loads applied on the reinforced samples and how it improved their flexural strength, assuming the rod has negligible effect on it. Figure (a) demonstrates the uniform distribution of the compressive loads applied from the washers through the tightening of the nuts; (b) stress distribution of the hole sample during the bending test at its failure point; (c) shows the effect of the compressive loads on the normal stress distribution of the hole sample; (d) the final stress distribution of the combined stresses applied to the reinforced samples.

The result obtained from the 3 turn samples printed in the  $z$ -direction was not expected and the reason for it might be the different printing batch where the build plate might have suffered small displacements, therefore affecting on the printing repeatability. Another interesting fact on the tensile strength is that the  $z$ -direction samples seemed to have a lower tensile strength when compared to the longitudinal samples. It can be explained by the fact that when a crack initiates on the samples, it propagates easier on the  $z$ -direction samples than on the longitudinal ones, therefore any small uniformity on the samples could initiate a crack.

## 4.3 Conclusion

### 4.3.1 Tensile tests

The tensile tests showed that when using the post tensioning technique on 3D printed ABS parts it can improve its mechanical properties, for both elastic modulus and tensile strength. However, there was not seen a great difference between the longitudinal and  $z$ -direction samples and that happened because when 3D printing on the longitudinal direction, some air gaps were

created at the radius of the dog bones during the printing process. Those spots weakened the parts and therefore the results were similar with the  $z$ -direction samples, while it was expected to have a higher mechanical property.

The reinforcement provided a better performance under tension, however the difference in improvement when comparing the three different reinforced samples was negligible, since the 1 turn, 3 turn, and 5 turn had almost the same results. Once again, the metal rods used were not much stronger when compared to the 3D printed plastic itself, they both have a very similar strength and could withstand almost the same load, due to the difference in the cross sectional area each had. It is important to mention that using a stronger material as a rod or with a larger area would not improve the mechanical properties of the 3D printed parts tested, since all the samples broke on the plastic.

#### **4.3.2 Bending tests**

The bending test showed that adding reinforcement to the samples did not affect the flexural modulus, where both printing orientations had very similar results amongst all samples. However, the flexural strength seemed to slightly increase when comparing the 3, and 5 turn samples to the raw and hole ones. The small improvement on the flexural strength can be explained by the compressive loads that were applied onto the sample. The two different samples that had reinforcement, the 3 turn and 5 turn, did not show a lot of difference, showing that the amount of compression applied did not influence the mechanical properties of the reinforced samples themselves. However, when compared to the unreinforced samples, a small improvement could be noticed.

It is also important to mention the difference on the stroke while testing the samples, where the longitudinal samples could withstand to a higher displacement when compared to the  $z$ -direction ones. This can be explained by the fact that  $z$ -direction samples do not have a strong bonding between each printed layer, differently than the longitudinal samples. If a crack is initiated on a longitudinal sample, for example, it would have to break through many strings of filaments in order to have the sample to fail, while for the  $z$ -direction samples there is no need for that, since the strings are not going through the cross sectional area. That explains why the longitudinal samples would withstand to longer displacements than the  $z$ -direction ones.

## Chapter 5. Conclusion and Future Work

The effects of adding coatings, and using the post tensioning technique, during the post manufacturing stage, were studied for FFF 3D printed parts. The coatings were used, trying to obtain an improvement on the sealing performance of parts manufactured using this type of technology. The post tensioning technique was done looking for better mechanical properties, including flexural and tensile strength. Therefore, getting as a result of the experiments, 3D printed parts to be functional when it comes to applications where sealing and higher mechanical properties are required.

Chapter 3 showed that 3D printed parts can have a better sealing performance when the proper post processing technique is applied. Depending on the load applied, even using priming and spray painting seemed to be enough to seal the 3D printed part. However, for loads up to 100 psi, the epoxy coating demonstrated to completely seal the part. The difference in sealing performance is clearly seen when comparing the raw to the epoxy coated sample, quantifying the improvement on the sealing performance.

Chapter 4 helped on understanding the effect of the reinforcement to the mechanical properties of a 3D printed part. The tensile tests showed an improvement of 70%, and 97% on the tensile strength for the raw and 5 turn longitudinal, and z-direction samples, respectively. It was also shown an increase on the elastic modulus of 58%, and 45% respectively, to the longitudinal and z-direction samples, when comparing the same group of samples. The bending tests showed that adding the reinforcement on the neutral axis of the samples did not altered the flexural modulus. However, it did show an increase of 14%, and 12% on the flexural strength when

comparing the raw and the 5 turn samples for the longitudinal and  $z$ -direction samples, respectively.

Those results proved that 3D printed parts can turn into a more functional part, specially, when it comes to sealing purposes and applications where a higher mechanical strength is required. Techniques like epoxy coating and post tensioning seemed to be a reliable way of doing it, with very consistent results. However, there are still improvements that could be done to this research. Next section will include ideas and options for future work related to this area.

## **5.1 Future work**

The conclusions taken from the results of this study are believed to contribute on making 3D printed parts more functional. The topics below give ideas for future work that could help on making 3D printed parts to be used in a broader range of applications.

- Apply the pressure test to 3D printed parts that have different shapes, including sharp corners, and more complex geometries.
- Run the same experiments in a controlled temperature environment, to have a better understand of the behavior of 3D printed parts for temperatures different than the room temperature.
- Use the Digital Image Correlation (DIC) on the tensile, and bending tests, to have a better understanding on how the parts break and on the elastic/plastic behavior of 3D printed parts.
- Combine both experiments by creating a new pressure vessel able to fit cylinders reinforced if metal rods, looking for applications where both good sealing and mechanical properties are required.

## References

- [1] B. Redwood, F. Schoffer, and B. Garret, *The 3D Printing Handbook*. Amsterdam, The Netherlands: 3D Hubs, 2017.
- [2] C. Borg Costanzi, Z. Y. Ahmed, H. R. Schipper, F. P. Bos, U. Knaack, and R. J. M. Wolfs, “3D Printing Concrete on temporary surfaces: The design and fabrication of a concrete shell structure,” *Autom. Constr.*, vol. 94, pp. 395–404, Oct. 2018.
- [3] L. E. Murr *et al.*, “Metal Fabrication by Additive Manufacturing Using Laser and Electron Beam Melting Technologies,” *J. Mater. Sci. Technol.*, vol. 28, no. 1, pp. 1–14, Jan. 2012.
- [4] R. Singh, “Process capability study of polyjet printing for plastic components,” *J. Mech. Sci. Technol.*, vol. 25, no. 4, pp. 1011–1015, Apr. 2011.
- [5] H. Kim, J.-W. Choi, and R. Wicker, “Scheduling and process planning for multiple material stereolithography,” *Rapid Prototyp. J.*, vol. 16, no. 4, pp. 232–240, Jan. 2010.
- [6] H. Yin, M. Qu, H. Zhang, and Y. Lim, “3D Printing and Buildings: A Technology Review and Future Outlook,” *Technol. + Des.*, vol. 2, no. 1, pp. 94–111, Jan. 2018.
- [7] B. Campbell, Thomas Williams, Christopher Ivanova, Olga Garrett, “Strategic Foresight Report,” pp. 3–7, 2012.
- [8] R. Sharma, “The 3D Printing Revolution You Have Not Heard About,” *Forbes*, pp. 1–9, 2013.
- [9] The Economist, “From dental braces to astronauts’ seats; 3D printing,” *Econ.*, vol. 408, no.

- 8852, p. 14, 2013.
- [10] J. Zuniga *et al.*, “Cyborg beast: A low-cost 3d-printed prosthetic hand for children with upper-limb differences,” *BMC Res. Notes*, vol. 8, no. 1, 2015.
- [11] T. Kellner, “Jet Engines with 3D-Printed Parts Power Next-Gen Airbus Passenger Jet,” *GE Reports*, pp. 1–5, 2015.
- [12] A. L. L. The and W. A. Y. To, “ORBIT NEXT LAUNCH SPACEX ’ S SUPERDRACO ENGINE : ABORT CAPABILITY,” pp. 1–8, 2018.
- [13] H. F. The, “This is how Hollywood makes its props in 2016,” 2018.
- [14] I. Gibson, T. Kvan, and L. W. Ming, “Rapid prototyping for architectural models,” *Rapid Prototyp. J.*, vol. 8, no. 2, pp. 91–99, 2002.
- [15] I. Christopher *et al.*, “( 12 ) United States Patent ( 10 ) Patent No .:,” vol. 2, no. 12, 2015.
- [16] J. Brecht, A. Fan, K. Lee, B. Pruitt, and P. Williams, “Dimensional Printing: Rapid Tooling and Prototypes Directly from CAD Representation,” *Solid Free. Fabr. Symp.*, pp. 481–488, 1992.
- [17] I. Gibson, D. W. Rosen, and B. Stucker, “Additive manufacturing technologies: Rapid prototyping to direct digital manufacturing,” *Addit. Manuf. Technol. Rapid Prototyp. to Direct Digit. Manuf.*, pp. 1–459, 2010.
- [18] J. Zhang and B. Khoshnevis, “Optimal machine operation planning for construction by Contour Crafting,” *Autom. Constr.*, vol. 29, pp. 50–67, Jan. 2013.
- [19] J. Faludi, C. Bayley, S. Bhogal, and M. Iribarne, “Comparing environmental impacts of additive manufacturing vs traditional machining via life-cycle assessment,” *Rapid Prototyp.*

- J.*, vol. 21, no. 1, pp. 14–33, Jan. 2015.
- [20] M. Kreiger and J. M. Pearce, “Environmental Life Cycle Analysis of Distributed Three-Dimensional Printing and Conventional Manufacturing of Polymer Products,” *ACS Sustain. Chem. Eng.*, vol. 1, no. 12, pp. 1511–1519, Dec. 2013.
- [21] S. A. M. Tofail, E. P. Koumoulos, A. Bandyopadhyay, S. Bose, L. O’Donoghue, and C. Charitidis, “Additive manufacturing: scientific and technological challenges, market uptake and opportunities,” *Mater. Today*, vol. 21, no. 1, pp. 22–37, 2018.
- [22] T. O. Cost, E. Through, and S. S. Manufacturing, “a Sculpteo Guide.”
- [23] Sculpteo, “3D Printing and Traditional Manufacturing Methods: overview.” [Online]. Available: <https://www.sculpteo.com/en/3d-printing/3d-printing-and-traditional-manufacturing-processes/>.
- [24] C. Ziemian, M. Sharma, and S. Ziemian, “Anisotropic Mechanical Properties of ABS Parts Fabricated by Fused Deposition Modelling,” 2007.
- [25] S. H. Ahn, M. Montero, D. Odell, S. Roundy, and P. K. Wright, *Anisotropic material properties of fused deposition modeling ABS*, vol. 8, no. 4. 2002.
- [26] J. H. D. Fasel, D. D. Malis, C. Wiederer, and N. Hagenbuch, “3D printing of anatomical models for surgeons: an investigation on repeatability,” *Int. J. Interact. Des. Manuf.*, vol. 12, no. 2, pp. 621–627, May 2018.
- [27] D. T. Pham and C. Ji, “Design for stereolithography,” *Proc. Inst. Mech. Eng. Part C J. Mech. Eng.*, vol. 214, no. 5, pp. 635–640, 2000.
- [28] D. Pranzo, P. Larizza, D. Filippini, and G. Percoco, “Extrusion-Based 3D Printing of Microfluidic Devices for Chemical and Biomedical Applications: A Topical Review,”

*Micromachines*, vol. 9, no. 8, p. 374, 2018.

- [29] Sculpteo, “Most used 3D printing technologies in 2017 and 2018,” *Statista 2019*. [Online]. Available: <https://www.statista.com/statistics/560304/worldwide-survey-3d-printing-top-technologies/>.
- [30] E. Cuan-Urquizo, E. Barocio, V. Tejada-Ortigoza, R. Pipes, C. Rodriguez, and A. Roman-Flores, “Characterization of the Mechanical Properties of FFF Structures and Materials: A Review on the Experimental, Computational and Theoretical Approaches,” *Materials (Basel)*, vol. 12, no. 6, p. 895, 2019.
- [31] Ultimaker BV, “How to print with Ultimaker ABS.” [Online]. Available: <https://ultimaker.com/en/resources/22226-how-to-print-with-ultimaker-abs>.
- [32] E. Tyson, “PLA 3D Printing Filament - Everything You Need to Know,” *Rigid.ink*. [Online]. Available: <https://rigid.ink/blogs/news/3d-printing-basics-how-to-get-the-best-results-with-pla-filament>.
- [33] P. M. Pandey, N. V. Reddy, and S. G. Dhande, “Improvement of surface finish by staircase machining in fused deposition modeling,” *J. Mater. Process. Technol.*, vol. 132, no. 1–3, pp. 323–331, Jan. 2003.
- [34] T. Serra, J. A. Planell, and M. Navarro, “High-resolution PLA-based composite scaffolds via 3-D printing technology,” *Acta Biomater.*, vol. 9, no. 3, Mar. 2013.
- [35] S. Ahn, M. Montero, and P. K. Wright, “Anisotropic material properties of fused deposition modeling ABS,” 2014.
- [36] N. Hill and M. Haghi, “Deposition direction-dependent failure criteria for fused deposition modeling polycarbonate,” *Rapid Prototyp. J.*, vol. 20, no. 3, 2014.

- [37] J. M. Chacón, M. A. Caminero, E. García-Plaza, and P. J. Núñez, “Additive manufacturing of PLA structures using fused deposition modelling: Effect of process parameters on mechanical properties and their optimal selection,” *Mater. Des.*, vol. 124, pp. 143–157, 2017.
- [38] M. F. Arif, S. Kumar, K. M. Varadarajan, and W. J. Cantwell, “Performance of biocompatible PEEK processed by fused deposition additive manufacturing,” *Mater. Des.*, vol. 146, pp. 249–259, May 2018.
- [39] H. N. Chia and B. M. Wu, “Recent advances in 3D printing of biomaterials,” *J. Biol. Eng.*, vol. 9, no. 1, p. 4, Mar. 2015.
- [40] X. Deng, Z. Zeng, B. Peng, S. Yan, and W. Ke, “Mechanical properties optimization of poly-ether-ether-ketone via fused deposition modeling,” *Materials (Basel)*, vol. 11, no. 2, 2018.
- [41] B. Brenken, E. Barocio, A. Favaloro, V. Kunc, and R. B. Pipes, “Fused filament fabrication of fiber-reinforced polymers: a review,” *Addit. Manuf.*, vol. 21, May 2018.
- [42] F. Ning, W. Cong, J. Qiu, J. Wei, and S. Wang, “Additive manufacturing of carbon fiber reinforced thermoplastic composites using fused deposition modeling,” *Compos. Part B Eng.*, vol. 80, pp. 369–378, Oct. 2015.
- [43] H. L. Tekinalp *et al.*, “Highly oriented carbon fiber-polymer composites via additive manufacturing,” *Compos. Sci. Technol.*, vol. 105, pp. 144–150, 2014.
- [44] L. J. Love *et al.*, “The importance of carbon fiber to polymer additive manufacturing,” *J. Mater. Res.*, vol. 29, no. 17, pp. 1893–1898, 2014.
- [45] J. Castro, E. A. Rojas-Nastrucci, A. Ross, T. M. Weller, and J. Wang, “Fabrication,

- Modeling, and Application of Ceramic-Thermoplastic Composites for Fused Deposition Modeling of Microwave Components,” *IEEE Trans. Microw. Theory Tech.*, vol. 65, no. 6, pp. 2073–2084, Jun. 2017.
- [46] J. Mireles, D. Espalin, D. Roberson, B. Zinniel, F. Medina, and R. Wicker, “Fused deposition modeling of metals,” *23rd Annu. Int. Solid Free. Fabr. Symp. - An Addit. Manuf. Conf. SFF 2012*, pp. 836–845, 2012.
- [47] V. E. Kuznetsov, A. N. Solonin, O. D. Urzhumtsev, R. Schilling, and A. G. Tavitov, “Strength of PLA components fabricated with fused deposition technology using a desktop 3D printer as a function of geometrical parameters of the process,” *Polymers (Basel)*, vol. 10, no. 3, 2018.
- [48] M. S. Uddin, M. F. R. Sidek, M. A. Faizal, R. Ghomashchi, and A. Pramanik, “Evaluating Mechanical Properties and Failure Mechanisms of Fused Deposition Modeling Acrylonitrile Butadiene Styrene Parts,” *J. Manuf. Sci. Eng.*, vol. 139, no. 8, p. 081018, 2017.
- [49] B. Stephens, P. Azimi, Z. El Orch, and T. Ramos, “Ultrafine particle emissions from desktop 3D printers,” *Atmos. Environ.*, vol. 79, pp. 334–339, Nov. 2013.
- [50] UL’s Prospector, “Acrylonitrile Butadiene Styrene (ABS) Typical Properties Generic ABS.” [Online]. Available: <https://plastics.ulprospector.com/generics/1/c/t/acrylonitrile-butadiene-styrene-abs-properties-processing>.
- [51] J. C. Middleton and A. J. Tipton, “Synthetic biodegradable polymers as orthopedic devices,” *Biomaterials*, vol. 21, no. 23, pp. 2335–2346, 2000.
- [52] Xu Zhang *et al.*, “Large-scale 3D printing by a team of mobile robots,” *Autom. Constr.*, vol. 95, Nov. 2018.

- [53] D. Horvath, R. Noorani, and M. Mendelson, "Improvement of surface roughness on ABS 400 polymer materials using design of experiments (DOE)," *Mater. Sci. Forum*, vol. 561–565, 2007.
- [54] B. Vasudevarao, D. P. Natarajan, and M. Henderson, "Sensitivity of Rp Surface Finish To Process," *Solid Free. Fabr. Proc.*, pp. 251–258, 2000.
- [55] E. Tyson, "What 3D Printer Nozzle Should I Use? - The Pros and Cons...," *Rigid.ink*. [Online]. Available: <https://rigid.ink/blogs/news/what-3d-printer-nozzle-size-should-i-use-the-pros-and-cons>.
- [56] Y. Zhang and K. Chou, "A parametric study of part distortions in fused deposition modelling using three-dimensional finite element analysis," *Proc. Inst. Mech. Eng. Part B J. Eng. Manuf.*, vol. 222, no. 8, pp. 959–967, 2008.
- [57] A. H. Nickel, D. M. Barnett, and F. B. Prinz, "Thermal stresses and deposition patterns in layered manufacturing," *Mater. Sci. & Eng. A (Structural Mater. Prop. Microstruct. Process.)*, vol. A317, no. 1–2, Oct. 2001.
- [58] Q. Sun, G. M. Rizvi, C. T. Bellehumeur, and P. Gu, "Effect of processing conditions on the bonding quality of FDM polymer filaments," *Rapid Prototyp. J.*, vol. 14, no. 2, 2008.
- [59] C. W. Ziemian and P. M. Crawn III, "Computer aided decision support for fused deposition modeling," *Rapid Prototyp. J.*, vol. 7, no. 3, pp. 138–147, 2001.
- [60] M. K. Agarwala, V. R. Jamalabad, N. A. Langrana, A. Safari, P. J. Whalen, and S. C. Danforth, "Structural quality of parts processed by fused deposition," *Rapid Prototyp. J.*, vol. 2, no. 4, pp. 4–19, 1996.
- [61] Bin Huang and S. Singamneni, "Raster angle mechanics in fused deposition modelling," *J.*

*Compos. Mater.*, vol. 49, no. 3, Feb. 2015.

- [62] M. Fernandez-Vicente, W. Calle, S. Ferrandiz, and A. Conejero, “Effect of Infill Parameters on Tensile Mechanical Behavior in Desktop 3D Printing,” *3D Print. Addit. Manuf.*, vol. 3, no. 3, pp. 183–192, 2016.
- [63] M. Shojib Hossain, D. Espalin, J. Ramos, M. Perez, and R. Wicker, “Improved Mechanical Properties of Fused Deposition Modeling-Manufactured Parts Through Build Parameter Modifications,” *J. Manuf. Sci. Eng.*, vol. 136, no. 6, p. 061002, 2014.
- [64] MakerBot Industries, “How to sand your 3D prints,” *MakerBot*, 2015. [Online]. Available: <https://www.makerbot.com/professional/post-processing/sanding/>.
- [65] D. Evans, “Ultimate guide to finishing 3D printed parts,” *fictiv*, 2017. [Online]. Available: <https://www.fictiv.com/hwg/fabricate/ultimate-guide-to-finishing-3d-printed-parts>.
- [66] L. M. Galantucci, F. Lavecchia, and G. Percoco, “Experimental study aiming to enhance the surface finish of fused deposition modeled parts,” *CIRP Ann. - Manuf. Technol.*, vol. 58, no. 1, pp. 189–192, 2009.
- [67] E. Bélanger, S. A. Lévesque, G. Anctil, A.-S. Poulin-Girard, and P. Marquet, “Low-cost production and sealing procedure of mechanical parts of a versatile 3D-printed perfusion chamber for digital holographic microscopy of primary neurons in culture,” *Quant. Phase Imaging III*, vol. 10074, no. February 2017, p. 100741S, 2017.
- [68] and G. N. L. M. Schmid, C. Simon, “Finishing of SLS-parts for rapid manufacturing (RM) - A comprehensive approach,” pp. 1–10, 2009.
- [69] L. M. Galantucci, F. Lavecchia, and G. Percoco, “Quantitative analysis of a chemical treatment to reduce roughness of parts fabricated using fused deposition modeling,” *CIRP*

- Ann. - Manuf. Technol.*, vol. 59, no. 1, pp. 247–250, 2010.
- [70] G. Percoco, F. Lavecchia, and L. M. Galantucci, “Compressive properties of FDM rapid prototypes treated with a low cost chemical finishing,” *Res. J. Appl. Sci. Eng. Technol.*, vol. 4, no. 19, pp. 3838–3842, 2012.
- [71] A. S. Rao, M. A. Dharap, J. V. L. Venkatesh, and D. Ojha, *Investigation of post processing techniques to reduce the surface roughness of fused deposition modeled parts*, vol. 3. 2012.
- [72] C. C. Kuo and R. C. Mao, “Development of a Precision Surface Polishing System for Parts Fabricated by Fused Deposition Modeling,” *Mater. Manuf. Process.*, vol. 31, no. 8, pp. 1113–1118, 2016.
- [73] A. Garg, A. Bhattacharya, A. Batish, A. Garg, A. Bhattacharya, and A. Batish, “On Surface Finish and Dimensional Accuracy of FDM Parts after Cold Vapor Treatment On Surface Finish and Dimensional Accuracy of FDM Parts after Cold Vapor Treatment,” *LMMP*, vol. 31, no. 4, pp. 522–529, 2016.
- [74] W. R. Priedeman Jr. and D. T. Smith, “Smoothing method for layered deposition modeling,” *US patent 8,123,999*. 2012.
- [75] D. Espalin, F. Medina, K. Arcaute, B. Zinniel, T. Hoppe, and R. Wicker, *Effects of vapor smoothing on ABS part dimensions*. 2009.
- [76] M. Anthamatten, S. A. Letts, and R. C. Cook, “Controlling surface roughness in vapor-deposited poly (amic acid) films by solvent-vapor exposure,” *Langmuir*, vol. 20, no. 15, pp. 6288–6296, 2004.
- [77] F. Authors, “Pre and post processing techniques to improve surface characteristics of FDM parts : a state of art review and future applications,” 2017.

- [78] K. Raja, "A review on chemical processes for plastics substrates used in engineering industries," *Int. J. ChemTech Res.*, vol. 9, no. 7, pp. 354–365, 2016.
- [79] J. Mireles *et al.*, "Analysis of sealing methods for FDM-fabricated parts," *Solid Free. Fabr.*, no. February, pp. 185–196, 2011.
- [80] J. P. Thomas and J. E. Renaud, "Mechanical behavior of acrylonitrile butadiene styrene ( ABS ) fused deposition materials . Experimental investigation Âguez," 2006.
- [81] I. Durgun and R. Ertan, "Experimental investigation of FDM process for improvement of mechanical properties and production cost," *Rapid Prototyp. J.*, vol. 20, no. 3, pp. 228–235, 2014.
- [82] B. M. Tymrak, M. Kreiger, and J. M. Pearce, "Mechanical properties of components fabricated with open-source 3-D printers under realistic environmental conditions," *Mater. Des.*, vol. 58, pp. 242–246, 2014.
- [83] A. Rodríguez-Panes, J. Claver, and A. M. Camacho, "The influence of manufacturing parameters on the mechanical behaviour of PLA and ABS pieces manufactured by FDM: A comparative analysis," *Materials (Basel)*, vol. 11, no. 8, 2018.
- [84] C. A. Griffiths, J. Howarth, G. D. A. Rowbotham, and A. Rees, "Effect of Build Parameters on Processing Efficiency and Material Performance in Fused Deposition Modelling," *Procedia CIRP*, vol. 49, pp. 28–32, 2016.
- [85] J. T. Cantrell *et al.*, "Experimental characterization of the mechanical properties of 3D-printed ABS and polycarbonate parts," *Rapid Prototyp. J.*, vol. 23, no. 4, pp. 811–824, 2017.
- [86] G. C. Onwubolu and F. Rayegani, "Characterization and Optimization of Mechanical Properties of ABS Parts Manufactured by the Fused Deposition Modelling Process," *Int. J.*

- Manuf. Eng.*, vol. 2014, pp. 1–13, 2014.
- [87] N. A. Bin Sukindar, M. K. A. M. A. Bin, B. T. B. Hang Tuah Bin, C. N. A. J. Binti, and M. I. S. I. Bin, “Analysis on the impact process parameters on tensile strength using 3d printer repetier-host software,” *ARPJ. Eng. Appl. Sci.*, vol. 12, no. 10, pp. 3341–3346, 2017.
- [88] J. J. Laureto and J. M. Pearce, “Anisotropic mechanical property variance between ASTM D638-14 type i and type iv fused filament fabricated specimens,” *Polym. Test.*, vol. 68, no. April, pp. 294–301, 2018.
- [89] A. R. Torrado and D. A. Roberson, “Failure Analysis and Anisotropy Evaluation of 3D-Printed Tensile Test Specimens of Different Geometries and Print Raster Patterns,” *J. Fail. Anal. Prev.*, vol. 16, no. 1, pp. 154–164, 2016.
- [90] A. August, “Chapter 31 165,” pp. 165–170, 2013.
- [91] Z. Weng, J. Wang, T. Senthil, and L. Wu, “Mechanical and thermal properties of ABS/montmorillonite nanocomposites for fused deposition modeling 3D printing,” *Mater. Des.*, vol. 102, pp. 276–283, 2016.
- [92] F. Van Der Klift, Y. Koga, A. Todoroki, M. Ueda, Y. Hirano, and R. Matsuzaki, “3D Printing of Continuous Carbon Fibre Reinforced Thermo-Plastic (CFRTP) Tensile Test Specimens,” *Open J. Compos. Mater.*, vol. 06, no. 01, pp. 18–27, 2016.
- [93] D. Milan and D. Peal, “(12) Patent Application Publication (10) Pub . No .: US 2002/0187020 A1,” vol. 1, no. 19, 2013.
- [94] N. Li, Y. Li, and S. Liu, “Rapid prototyping of continuous carbon fiber reinforced polylactic acid composites by 3D printing,” *J. Mater. Process. Technol.*, vol. 238, pp. 218–225, 2016.
- [95] G. W. Melenka, B. K. O. Cheung, J. S. Schofield, M. R. Dawson, and J. P. Carey,

- “Evaluation and prediction of the tensile properties of continuous fiber-reinforced 3D printed structures,” *Compos. Struct.*, vol. 153, pp. 866–875, 2016.
- [96] T. K. Nguyen and B. K. Lee, “Post-processing of FDM parts to improve surface and thermal properties,” *Rapid Prototyp. J.*, vol. 24, no. 7, pp. 1091–1100, 2018.
- [97] K. H. Jo, Y. S. Jeong, J. H. Lee, and S. H. Lee, “A study of post-processing methods for improving the tightness of a part fabricated by fused deposition modeling,” *Int. J. Precis. Eng. Manuf.*, vol. 17, no. 11, pp. 1541–1546, 2016.
- [98] A. K. Sood, R. K. Ohdar, and S. S. Mahapatra, “Parametric appraisal of mechanical property of fused deposition modelling processed parts,” *Mater. Des.*, vol. 31, no. 1, pp. 287–295, 2010.
- [99] W. Wu, P. Geng, G. Li, D. Zhao, H. Zhang, and J. Zhao, “Influence of layer thickness and raster angle on the mechanical properties of 3D-printed PEEK and a comparative mechanical study between PEEK and ABS,” *Materials (Basel)*, vol. 8, no. 9, pp. 5834–5846, 2015.
- [100] O. Lužanin, D. Movrin, and M. Plan, “27. Effect of Layer Thickness , Deposition Angle , and Infill on Maximum Flexural Force in Fdm-Built Specimens,” *J. Technol. Plast.*, vol. 39, no. 1, pp. 49–58, 2014.
- [101] E. Cuan-Urquizo and A. Bhaskar, “Flexural elasticity of woodpile lattice beams,” *Eur. J. Mech. A/Solids*, vol. 67, pp. 187–199, 2018.
- [102] M. Somireddy, D. A. De Moraes, and A. Czekanski, “Flexural Behavior of Fdm Parts: Experimental, Analytical and Numerical Study,” *Solid Free. Fabr. Symp.*, pp. 992–1004, 2017.

- [103] A. W. Gebisa and H. G. Lemu, “Investigating effects of Fused-deposition modeling (FDM) processing parameters on flexural properties of ULTEM 9085 using designed experiment,” *Materials (Basel)*, vol. 11, no. 4, pp. 1–23, 2018.
- [104] I. Urieli and D. Berchowitz, *Stirling Cycle Engine Analysis*. Adam Hilger Ltd, 1984.
- [105] C. Stumpf, “Parameter Optimization of a Low Temperature Difference Gamma-Type Stirling Engine to Maximize Shaft Power,” University of Alberta, 2019.
- [106] R. Sier, *Reverend Robert Stirling, D.D.: A Biography of the Inventor of the Heat Economiser and Stirling Cycle Engine*. 1995.
- [107] J. Banks and N. B. Harris, “Geothermal potential of Foreland Basins: A case study from the Western Canadian Sedimentary Basin,” *Geothermics*, vol. 76, Nov. 2018.
- [108] E. J. McCullough and V. K. Yadavalli, “Surface modification of fused deposition modeling ABS to enable rapid prototyping of biomedical microdevices,” *J. Mater. Process. Technol.*, vol. 213, no. 6, pp. 947–954, 2013.
- [109] S. Zhang, J. Han, H. Kang, and B. Shin, “Thermo-mechanical properties of ABS parts fabricated by fused deposition modeling and vapor smoothing,” pp. 2–7, 2017.
- [110] “Post-Tensioning Tendon Installation and Grouting Manual,” no. May, 2013.
- [111] ASM International, *Engineered Materials Handbook Volume 2: Engineering Plastics*. ASM International, 1988.
- [112] S. A. Hinchliffe, K. M. Hess, and W. V. S. Iii, “Experimental and theoretical investigation of prestressed natural fiber-reinforced polylactic acid ( PLA ) composite materials,” *Compos. Part B*, vol. 95, pp. 346–354, 2016.

- [113] ASTM D638, “Standard Test Method for Tensile Properties of Plastics,” *Annu. B. ASTM Stand.*, pp. 1–15, 2004.
- [114] S. Provided and I. S. O. No, “INTERNATIONAL STANDARD properties,” vol. 2010, 2016.
- [115] ASTM INTERNATIONAL, “Standard Test Methods for Flexural Properties of Unreinforced and Reinforced Plastics and Electrical Insulating Materials. D790,” *Annu. B. ASTM Stand.*, no. January, pp. 1–12, 2002.
- [116] Joint Comitee for Guides in Metrology, JCGM100:2008, and GUM1995, “Evaluation of measurement data — Guide to the expression of uncertainty in measurement,” *JCGM 1002008 GUM 1995 with Minor Correct.*, vol. 50, no. September, p. 134, 2008.
- [117] S. Bell, “Good Practice Guide No. 11 Issue 2 - A Beginners Guide to Uncertainty of Measurement,” no. 11, p. 41, 2001.
- [118] W. Capability, “DP15,” no. 818.
- [119] S. W. Design, D. Performance, H. Output, H. Degree, O. Component, and R. O. Beams, “661.20 Force Transducer.”
- [120] Mastercraft, “Measuring: Tape measure, vernier caliper,” pp. 1–4, 2018.
- [121] J. E. Shigley, *Mechanical Engineering Design*. McGraw-Hill Book Company, Inc., 1963.
- [122] E. Penetrating, “Tc-1614 a / B Epoxy Penetrating,” no. 714, pp. 120–122, 2014.

# Appendix A: 3D printing parameters

The following images provide detailed information regarding the 3D printing parameters used for all prototypes in this study. The images were captured from the Ultimaker Cura in which was the slicing software used for the study.

Quality	
Layer Height	0.2 mm
Initial Layer Height	0.2 mm
Line Width	0.7 mm
Wall Line Width	0.7 mm
Outer Wall Line Width	0.7 mm
Inner Wall(s) Line Width	0.7 mm
Top/Bottom Line Width	0.7 mm
Infill Line Width	0.7 mm
Initial Layer Line Width	100.0 %
Shell	
Wall Thickness	2.1 mm
Wall Line Count	4
Outer Wall Wipe Distance	0.4 mm
Top Surface Skin Layers	0
Top/Bottom Thickness	1.6 mm
Top Thickness	1.6 mm
Top Layers	2
Bottom Thickness	1.6 mm
Bottom Layers	999999
Top/Bottom Pattern	Zig Zag
Bottom Pattern Initial Layer	Zig Zag
Top/Bottom Line Directions	[0,90]
Outer Wall Inset	0 mm
Optimize Wall Printing Order	<input type="checkbox"/>
Outer Before Inner Walls	<input checked="" type="checkbox"/>
Alternate Extra Wall	<input type="checkbox"/>
Compensate Wall Overlaps	<input checked="" type="checkbox"/>
Compensate Outer Wall Overlaps	<input type="checkbox"/>
Compensate Inner Wall Overlaps	<input checked="" type="checkbox"/>
Fill Gaps Between Walls	Everywhere
Filter Out Tiny Gaps	<input checked="" type="checkbox"/>
Print Thin Walls	<input checked="" type="checkbox"/>
Horizontal Expansion	0 mm
Initial Layer Horizontal Expansion	0 mm
Z Seam Alignment	Random
Ignore Small Z Gaps	<input checked="" type="checkbox"/>
Extra Skin Wall Count	1
Enable Ironing	<input type="checkbox"/>
Infill	
Infill Density	100 %
Infill Line Distance	0.7 mm
Infill Pattern	Lines
Infill Line Directions	[0,90]
Infill X Offset	0 mm
Infill Y Offset	0 mm
Infill Overlap Percentage	0 %
Infill Overlap	0 mm
Skin Overlap Percentage	0 %
Skin Overlap	0.0 mm
Infill Wipe Distance	0.175 mm
Infill Layer Thickness	0.2 mm

(a)

(b)

Figure A - 1: Parameters used to 3D print all prototypes in the research taken from the Ultimaker Cura.

Gradual Infill Steps	0
Infill Before Walls	<input checked="" type="checkbox"/>
Minimum Infill Area	0 mm <sup>2</sup>
Skin Removal Width	2.8 mm
Top Skin Removal Width	2.8 mm
Bottom Skin Removal Width	2.8 mm
Skin Expand Distance	2.8 mm
Top Skin Expand Distance	2.8 mm
Bottom Skin Expand Distance	2.8 mm
Maximum Skin Angle for Expansion	90 °
Minimum Skin Width for Expansion	0.0 mm
<b>Material</b>	▼
Initial Layer Flow	100 %
Enable Retraction	<input checked="" type="checkbox"/>
Retract at Layer Change	<input checked="" type="checkbox"/>
Retraction Extra Prime Amount	0 mm <sup>3</sup>
<i>Retraction Minimum Travel</i>	1.4 mm
Maximum Retraction Count	90
Minimum Extrusion Distance Window	1 mm
Nozzle Switch Retraction Distance	20 mm
Nozzle Switch Retraction Speed	20 mm/s
Nozzle Switch Retract Speed	20 mm/s
Nozzle Switch Prime Speed	20 mm/s
<b>Speed</b>	▼
<i>Print Speed</i>	45 mm/s
<i>Infill Speed</i>	45 mm/s

(c)

<i>Wall Speed</i>	40 mm/s
<i>Outer Wall Speed</i>	45 mm/s
<i>Inner Wall Speed</i>	45 mm/s
<i>Top/Bottom Speed</i>	45 mm/s
<i>Travel Speed</i>	45 mm/s
<i>Initial Layer Speed</i>	45 mm/s
Initial Layer Print Speed	45 mm/s
Initial Layer Travel Speed	150 mm/s
Maximum Z Speed	0 mm/s
<i>Number of Slower Layers</i>	1
<i>Equalize Filament Flow</i>	<input checked="" type="checkbox"/>
Maximum Speed for Flow Equalization	150 mm/s
<i>Enable Acceleration Control</i>	<input checked="" type="checkbox"/>
Print Acceleration	2300 mm/s <sup>2</sup>
Infill Acceleration	2300 mm/s <sup>2</sup>
Wall Acceleration	2300 mm/s <sup>2</sup>
Outer Wall Acceleration	2300 mm/s <sup>2</sup>
Inner Wall Acceleration	2300 mm/s <sup>2</sup>
Top/Bottom Acceleration	2300 mm/s <sup>2</sup>
Travel Acceleration	2300 mm/s <sup>2</sup>
Initial Layer Acceleration	2300 mm/s <sup>2</sup>
Initial Layer Print Acceleration	2300 mm/s <sup>2</sup>
Initial Layer Travel Acceleration	2300.0 mm/s <sup>2</sup>
Skirt/Brim Acceleration	2300 mm/s <sup>2</sup>
Enable Jerk Control	<input type="checkbox"/>

(d)

Figure A - 1. Continued

<b>Travel</b>	
Combing Mode	Off
Retract Before Outer Wall	<input type="checkbox"/>
Layer Start X	0.0 mm
Layer Start Y	0.0 mm
Z Hop When Retracted	<input type="checkbox"/>
<b>Cooling</b>	
Enable Print Cooling	<input type="checkbox"/>
Regular/Maximum Fan Speed Threshold	25 s
Regular Fan Speed at Height	0.2 mm
Regular Fan Speed at Layer	1
Minimum Layer Time	15 s
Minimum Speed	15 mm/s
Lift Head	<input checked="" type="checkbox"/>
<b>Support</b>	
Generate Support	<input type="checkbox"/>
<b>Build Plate Adhesion</b>	
Build Plate Adhesion Type	None
<b>Mesh Fixes</b>	
Union Overlapping Volumes	<input checked="" type="checkbox"/>
Remove All Holes	<input type="checkbox"/>
Extensive Stitching	<input type="checkbox"/>
Keep Disconnected Faces	<input type="checkbox"/>
Merged Meshes Overlap	0.15 mm
Remove Mesh Intersection	<input type="checkbox"/>
Remove Empty First Layers	<input checked="" type="checkbox"/>

(e)

<b>Special Modes</b>	
Print Sequence	All at Once
Mold	<input type="checkbox"/>
Surface Mode	Normal
Spiralize Outer Contour	<input type="checkbox"/>
<b>Experimental</b>	
Tree Support	<input type="checkbox"/>
Slicing Tolerance	Middle
Infill Travel Optimization	<input type="checkbox"/>
Maximum Resolution	0.01 mm
Enable Draft Shield	<input type="checkbox"/>
Make Overhang Printable	<input type="checkbox"/>
Enable Coasting	<input type="checkbox"/>
Alternate Skin Rotation	<input type="checkbox"/>
Spaghetti Infill	<input type="checkbox"/>
Hollow Out Objects	<input type="checkbox"/>
Fuzzy Skin	<input type="checkbox"/>
Flow rate compens... extrusion offset	0 mm
Flow rate compensation factor	100 %
Wire Printing	<input type="checkbox"/>
Use adaptive layers	<input type="checkbox"/>
Enable Bridge Settings	<input type="checkbox"/>
Try Multiple Line Thicknesses	<input type="checkbox"/>

(f)

Figure A - 1. Continued

# Appendix B: Properties of the TC-1614 A/B epoxy

The images below are the properties of the TC-1614 A/B epoxy used on the pressure vessel experiment. The images were obtained from the manufacture’s website (TC-1614 A/B, BJB Enterprises).



## TC-1614 A/B EPOXY PENETRATING SEALING AND COATING RESIN SYSTEM

TC-1614 A/B is an unfilled, low viscosity epoxy resin system. It is designed to seal porous to semi-porous substrates developing remarkable strength. TC-1614 A/B also has exceptional adhesive characteristics and is capable of high temperatures.

- Easy to use and apply
- Penetrates and seals porous surfaces with excellent adhesion
- Works great for sealing 3D Printed parts
- Withstands temperatures up to 350°F (177°C)
- Can be pigmented for color enhancement
- Recommended by several 3D Printer Manufacturers

PHYSICAL PROPERTIES	TEST METHOD	TEST RESULTS
Hardness, Shore D	ASTM D2240	85 ± 2
Density (g/cc)	ASTM D792	1.14
Cubic Inches per Pound	N/A	25.1
Color/Appearance	Visual	Yellow Opaque
Tensile Strength (psi)	ASTM D638	9,500
Tensile Modulus (psi)	ASTM D638	320,000
Elongation (%)	ASTM D638	5
Flexural Strength (psi)	ASTM D790	12,600
Flexural Modulus (psi)	ASTM D790	380,000
Shrinkage (in/in) linear	12"x 1/2" x 1/2"	0.008
Izod Impact, notched (ft-lb/in)	ASTM D256	0.44

Reported physical properties based on elevated temperature cured test specimens.

HANDLING PROPERTIES	Part A	Part B
Mix Ratio by weight	100	20
Mix Ratio by volume	100	23
Specific Gravity @ 77°F (25°C)	1.13	0.98
Color	Colorless	Amber
Viscosity (cps) @ 77°F (25°C) Brookfield	550	250
Mixed Viscosity (cps) @ 77°F (25°C) Brookfield	600	
Work Time, 100g mass @ 77°F (25°C)	2 hours	
Tack Free	10 – 12 hours @ 77°F (25°C) 5 hours @ 120°F (48.9°C)	

Properties above are typical and not for specifications.

\*Application Procedures – see page 3

Quality Management  
System Registered  
to ISO 9001:2008

TC-1614 A/B Page 1 of 3  
For more information call BJB Enterprises, Inc. (714) 734-8450 Fax (714) 734-8929  
www.bjenterprises.com

Date: 07/21/2017

Figure B - 1: Specifications of the epoxy (TC-1614 A/B, BJB Enterprises) used for the pressure vessel experiment [122].

**POST CURING:**

All physical property results are based upon post-curing this system. The following procedure provides the best results:

- 150°F (66°C) for 1.5 to 2 hours
- 250°F (121°C) for 2 hours
- 300°F (149°C) for 1 hour
- 350°F (177°C) for 1 hour

Allow to cool in the oven. This procedure provides further stabilization and eliminates possible thermal shocks for cavity tools that are temporarily clamped together for curing purposes.

**STORAGE:**

Store at ambient temperatures, 65-80°F (18-27°C). Unopened containers will have a shelf life of 12 months from date of shipment when properly stored at recommended temperatures. Purge opened containers with dry nitrogen before re-sealing.

PACKAGING	Part A	Part B	Cubic Inches per Kit
Quart Kits	2 lbs.	7 oz.	61
Gallon Kits	9 lbs.	1.8 lbs.	271
5-Gallon Kits	40 lbs.	8 lbs.	1,205

**SAFETY PRECAUTIONS:**

Use in a well-ventilated area. Avoid contact with skin using protective gloves and protective clothing. Repeated or prolonged contact on the skin may cause an allergic reaction. Eye protection is extremely important. Always use approved safety glasses or goggles when handling this product.

**IF CONTACT OCCURS:**

- Skin:** Immediately wash with soap and water. Remove contaminated clothing and launder before reuse. It is *not* recommended to remove resin from skin with solvents. Solvents only increase contact and dry skin. Seek qualified medical attention if allergic reactions occur.
- Eyes:** Immediately flush with water for at least 15 minutes. Call a physician.
- Ingestion:** If swallowed, call a physician immediately. Remove stomach contents by gastric suction or induce vomiting only as directed by medical personnel. Never give anything by mouth to an unconscious person.

Refer to the Material Safety Data Sheet before using this product.



TC-1614 Part A SDS



TC-1614 Part B SDS

Quality Management  
System Registered  
to ISO 9001:2008

TC-1614 A/B Page 3 of 3

Date: 07/21/2017

For more information call BJB Enterprises, Inc. (714) 734-8450 Fax (714) 734-8929

NON-WARRANTY \*Except for a warranty that materials substantially comply with the data presented in Manufacturer's latest bulletin describing the product (the basis for this substantial compliance is to be determined by the standard quality control tests generally performed by Manufacturer), all materials are sold "AS IS" and without any warranty express or implied as to merchantability, fitness for a particular purpose, patent, trademark or copyright infringement, or as to any other matter. In no event shall Manufacturer's liability for damages exceed Manufacturer's sale price of the particular quantity with respect to which damages are claimed.\*

Figure B - 1. Continued.

## Product Application Procedure for 3D Printed Parts

**Material:** TC-1614 Epoxy

**Purpose of Procedure:** To impregnate rigid, porous 3D Printed Parts with epoxy. Infusing epoxy into the surface is a beneficial procedure to increase strength, improve handling qualities and in some parts, improve aesthetics. Some systems will absorb more material than others.

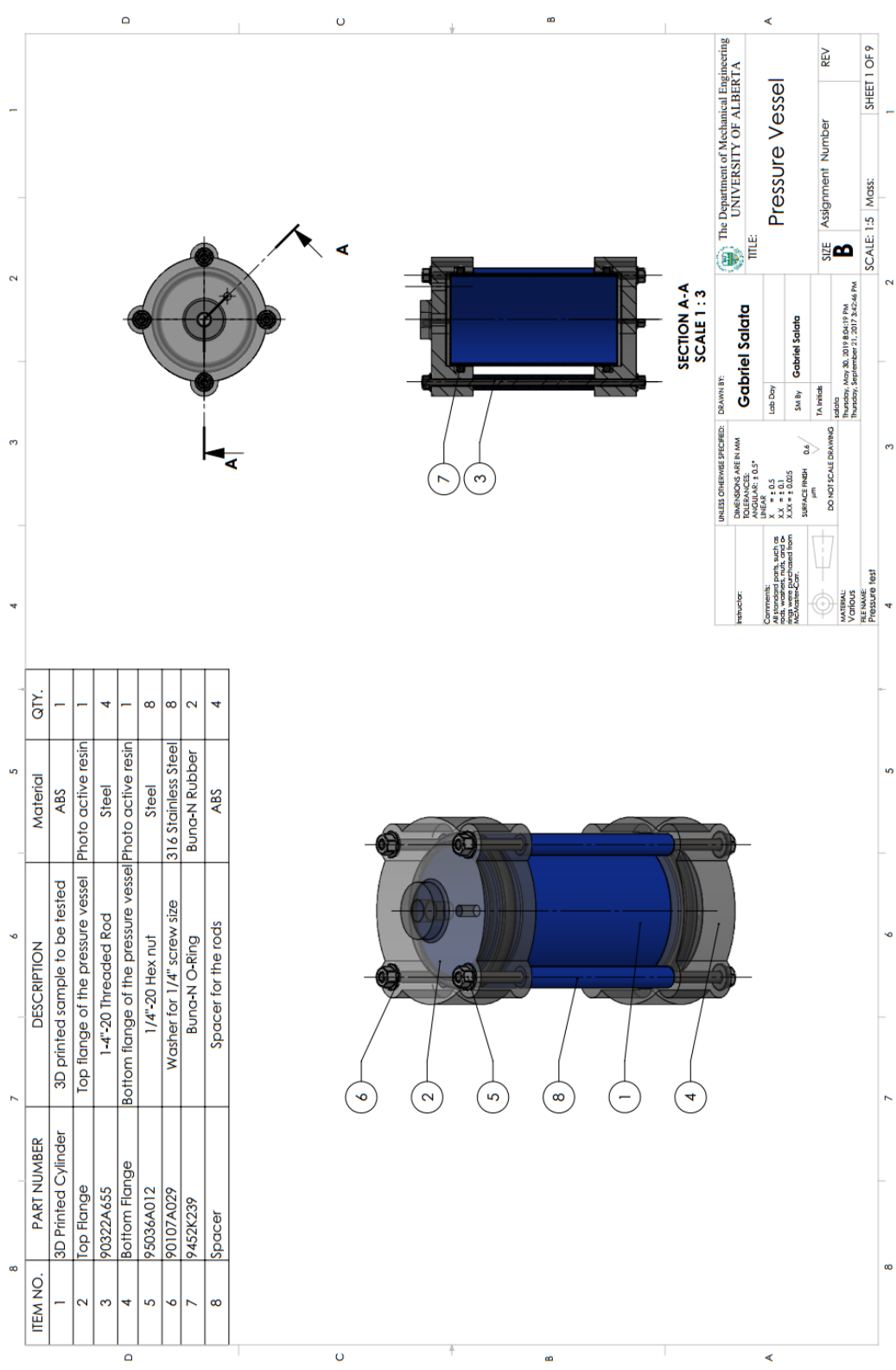
**Procedure:**

- Pre-warm A&B material in separate containers to 90°-100°F maximum (32°-37°C max) in a temperature controlled industrial oven. This will help to lower the viscosity and increase the absorption rate of epoxy into the part (never use a household oven that may be in contact with food).
  - You can also pre-warm the 3D printed part to aid in epoxy infiltration. 100°-120°F (37°-49°C) is a good range but refer to your 3D printed material recommendations for heat resistance in an effort to avoid distortion.
  - Place a small 3D Printed Part into a self-sealing (zipper lock) plastic bag and fill with an appropriate amount of epoxy. A bag that is too large will require more volumetric amounts of epoxy. Squeeze out as much of the extra air in the bag to assure part is fully submerged and coated with epoxy then seal bag.
  - Allow the part to soak in the epoxy for roughly 20-25 minutes. A recommended optional procedure would be to place bag with soaking 3D Printed part into 100°-120°F (37°-49°C) oven in a leak-proof, metal container, and allow to soak for 15-20 minutes. Check part at 5 minute intervals to monitor viscosity levels and for any exothermic reaction. Larger batches of mixed epoxy will have a shorter reaction time.
  - Once part has soaked for allotted time, pull part out of bag and drain excess epoxy off of part.
  - For larger parts, mix enough A&B together so you have sufficient material to brush an even coat over the part. Continue brushing drips and runs to keep part coated for 20-30 minutes. Then drain off excess epoxy and wipe down surface with clean, dry paper towels. Avoid using any solvents since it will affect the curing properties.
- \*Note that mixing a large mass of epoxy can produce an increase in chemical reaction shortening work time and increasing exotherm (heat) as it sits. Do not leave a large, concentrated mass of epoxy in a container unattended. After soaking the part, it may be best to split up a large batch (over 200-300g) by draining the bag into 2-3 separate small containers and allow to harden.**
- Hang part with wire over a cup or bucket to allow continued drainage of excess epoxy. Wipe off any areas of pooled epoxy with a gloved finger or brush. Monitor any sags or drips for the next hour or until epoxy has gelled.
  - You can expedite curing of the epoxy in an oven at 100°-120°F (37°-49°C) and promote better physical properties of the finished material. You can also allow the epoxy to cure at room temperature but an elevated post cure will achieve the best results.

Figure B - 1. Continued.

## **Appendix C: Drawing package**

This section contains the drawing packages for the pressure vessel experiment, tensile, and 3-point bending tests.



ITEM NO.	PART NUMBER	DESCRIPTION	Material	QTY.
1	3D Printed Cylinder	3D printed sample to be tested	ABS	1
2	Top Flange	Top flange of the pressure vessel	Photo active resin	1
3	90322A655	1-4"-20 Threaded Rod	Steel	4
4	Bottom Flange	Bottom flange of the pressure vessel	Photo active resin	1
5	95036A012	1/4"-20 Hex nut	Steel	8
6	90107A029	Washer for 1/4" screw size	316 Stainless Steel	8
7	9452K239	Buna-N O-Ring	Buna-N Rubber	2
8	Spacer	Spacer for the rods	ABS	4

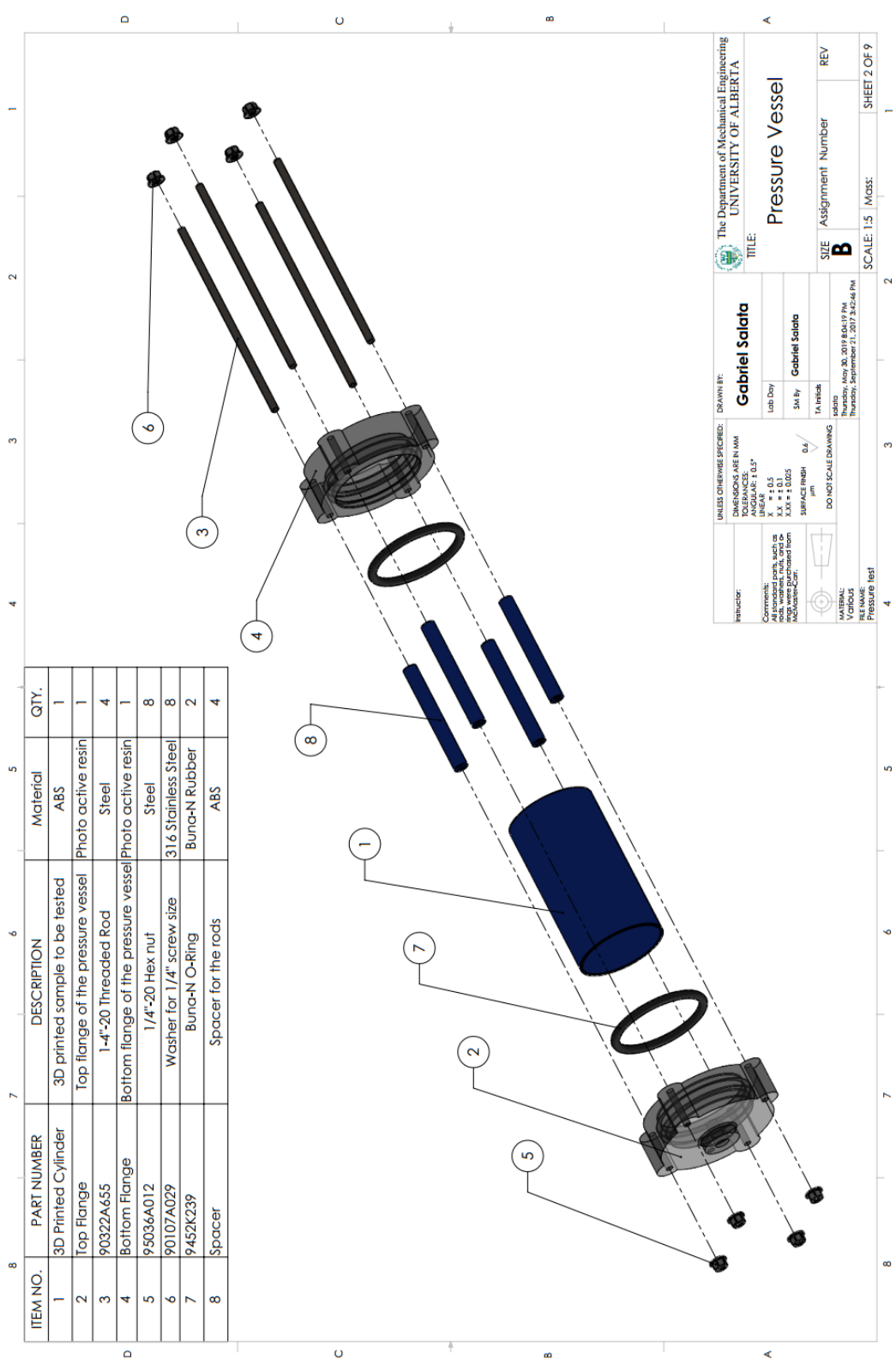
**UNLESS OTHERWISE SPECIFIED:**  
 DIMENSIONS ARE IN MM  
 TOLERANCES:  
 FRACTIONS ± 0.125"  
 DECIMALS ± 0.1  
 X.X ± 0.1  
 X.XX ± 0.025  
 SURFACE FINISH: 0.6 µm  
 DO NOT SCALE DRAWING

**INSTRUCTOR:** Gabriel Salata  
**Lab Day:** Gabriel Salata  
**SA By:** Gabriel Salata  
**TA Initials:** Gabriel Salata

**Comments:**  
 All standard parts, such as fasteners, should be purchased from McMaster-Carr.

**MATERIAL:** Acrylic, 30118-04019 PM  
**DATE:** Thursday, September 21, 2017 2:22:46 PM  
**REV NAME:** Pressure Vessel

**SCALE:** 1:5 | **Mass:** SHEET 1 OF 9



ITEM NO.	PART NUMBER	DESCRIPTION	Material	QTY.
1	3D Printed Cylinder	3D printed sample to be tested	ABS	1
2	Top Flange	Top flange of the pressure vessel	Photo active resin	1
3	90322A655	1/4"-20 Threaded Rod	Steel	4
4	Bottom Flange	Bottom flange of the pressure vessel	Photo active resin	1
5	95036A012	1/4"-20 Hex nut	Steel	8
6	90107A029	Washer for 1/4" screw size	316 Stainless Steel	8
7	9452K239	Buna-N O-Ring	Buna-N Rubber	2
8	Spacer	Spacer for the rods	ABS	4

UNLESS OTHERWISE SPECIFIED: DRAWN BY: **Gabriel Salata**

THE DEPARTMENT OF MECHANICAL ENGINEERING  
UNIVERSITY OF ALBERTA

TITLE: **Pressure Vessel**

REVISIONS: **1**

DATE: **May 30, 2019 8:41:19 PM**

SCALE: **1:5**

SIZE: **B**

ASSIGNMENT NUMBER: **REV**

DATE: **Thursday, September 21, 2017 3:42:46 PM**

SHEET 2 OF 9

REVISIONS: **1**

DATE: **May 30, 2019 8:41:19 PM**

SCALE: **1:5**

SIZE: **B**

ASSIGNMENT NUMBER: **REV**

DATE: **Thursday, September 21, 2017 3:42:46 PM**

SHEET 2 OF 9

REVISIONS: **1**

DATE: **May 30, 2019 8:41:19 PM**

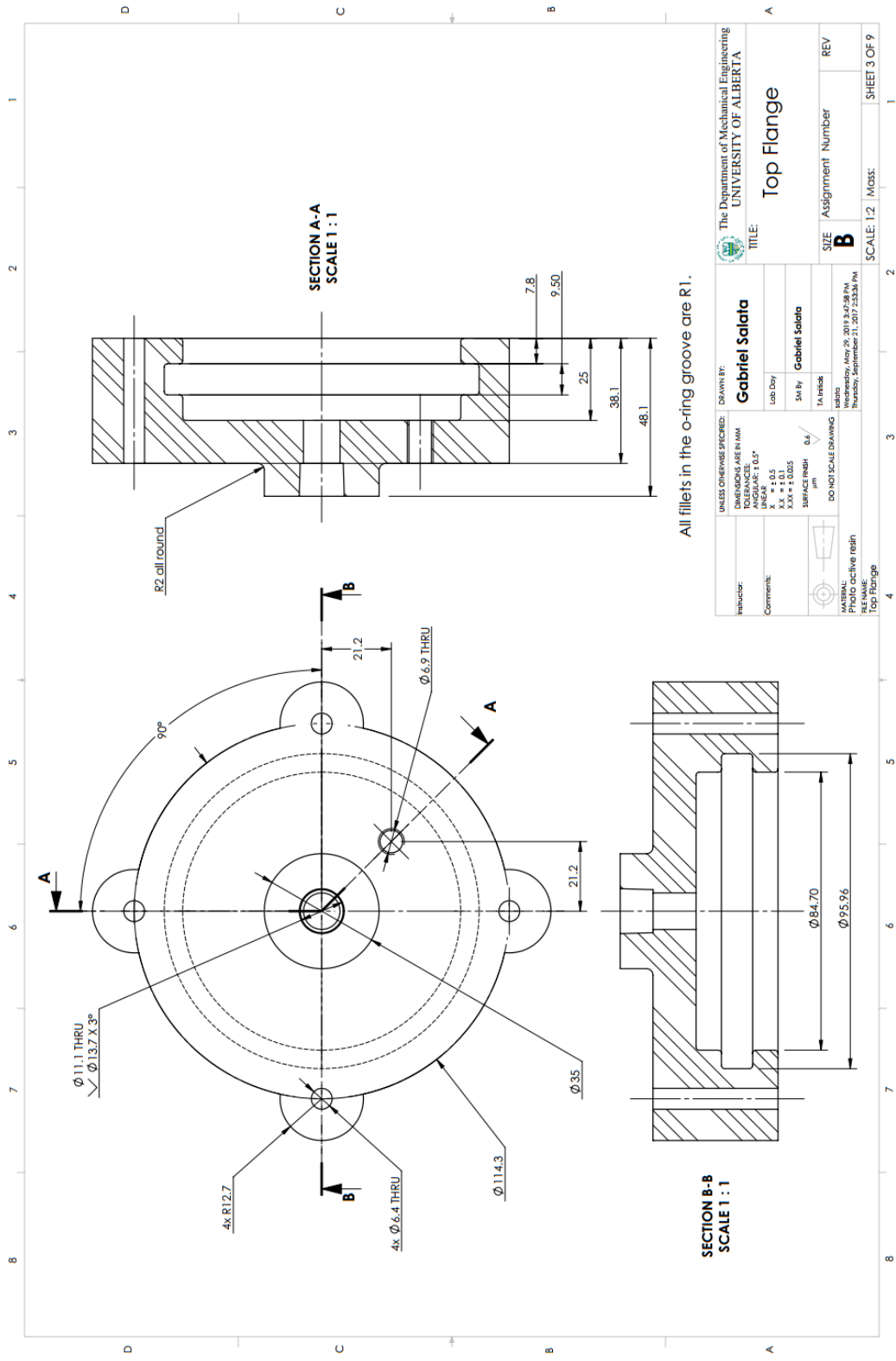
SCALE: **1:5**

SIZE: **B**

ASSIGNMENT NUMBER: **REV**

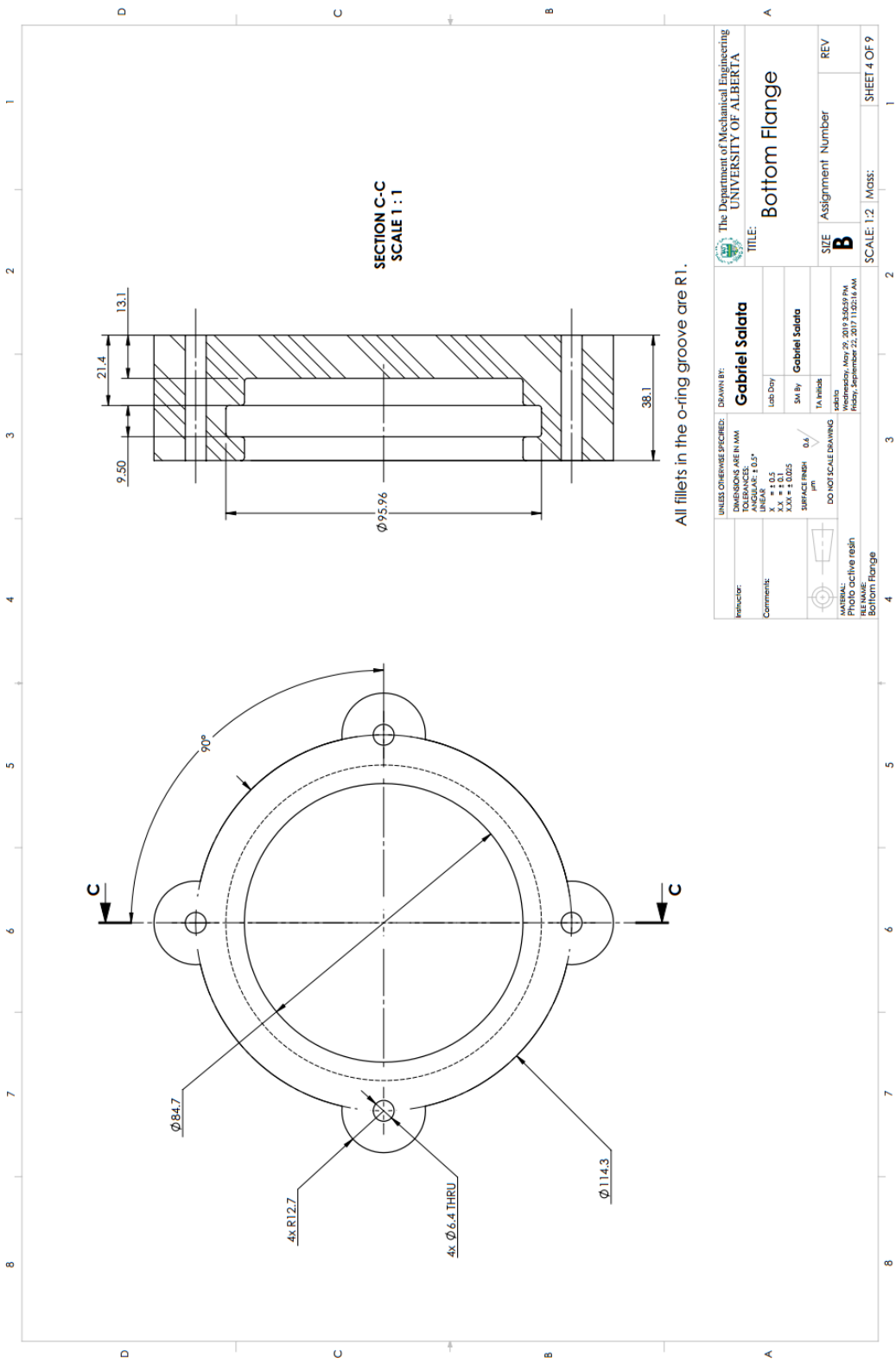
DATE: **Thursday, September 21, 2017 3:42:46 PM**

SHEET 2 OF 9



All fillets in the o-ring groove are R1.

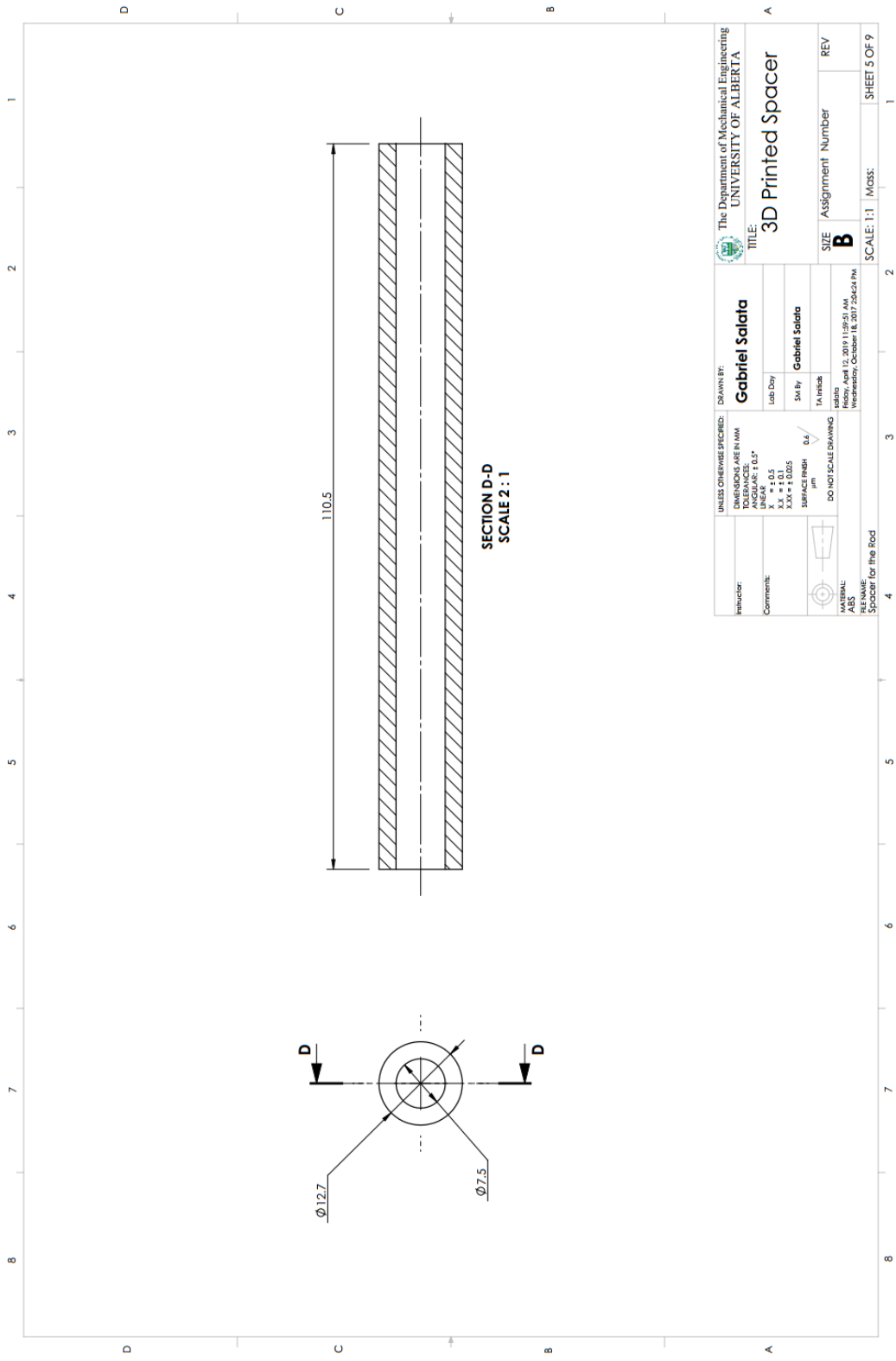
UNLESS OTHERWISE SPECIFIED:		DRAWN BY:	
DIMENSIONS ARE IN MM		Gabriel Salata	
TOLERANCES ARE IN MM		Lab Day	
DECIMALS TO 0.1		SAI By	
LINEAR ±0.1		Gabriel Salata	
ANGULAR ±0.5		TA In/Out	
SURFACE FINISH 0.8		Date	
DO NOT SCALE DRAWING		Wednesday, May 29, 2019 3:42:08 PM	
MATERIAL: Epoxy resin		Thursday, September 21, 2017 2:53:26 PM	
REF NAME: Top Flange		Top Flange	



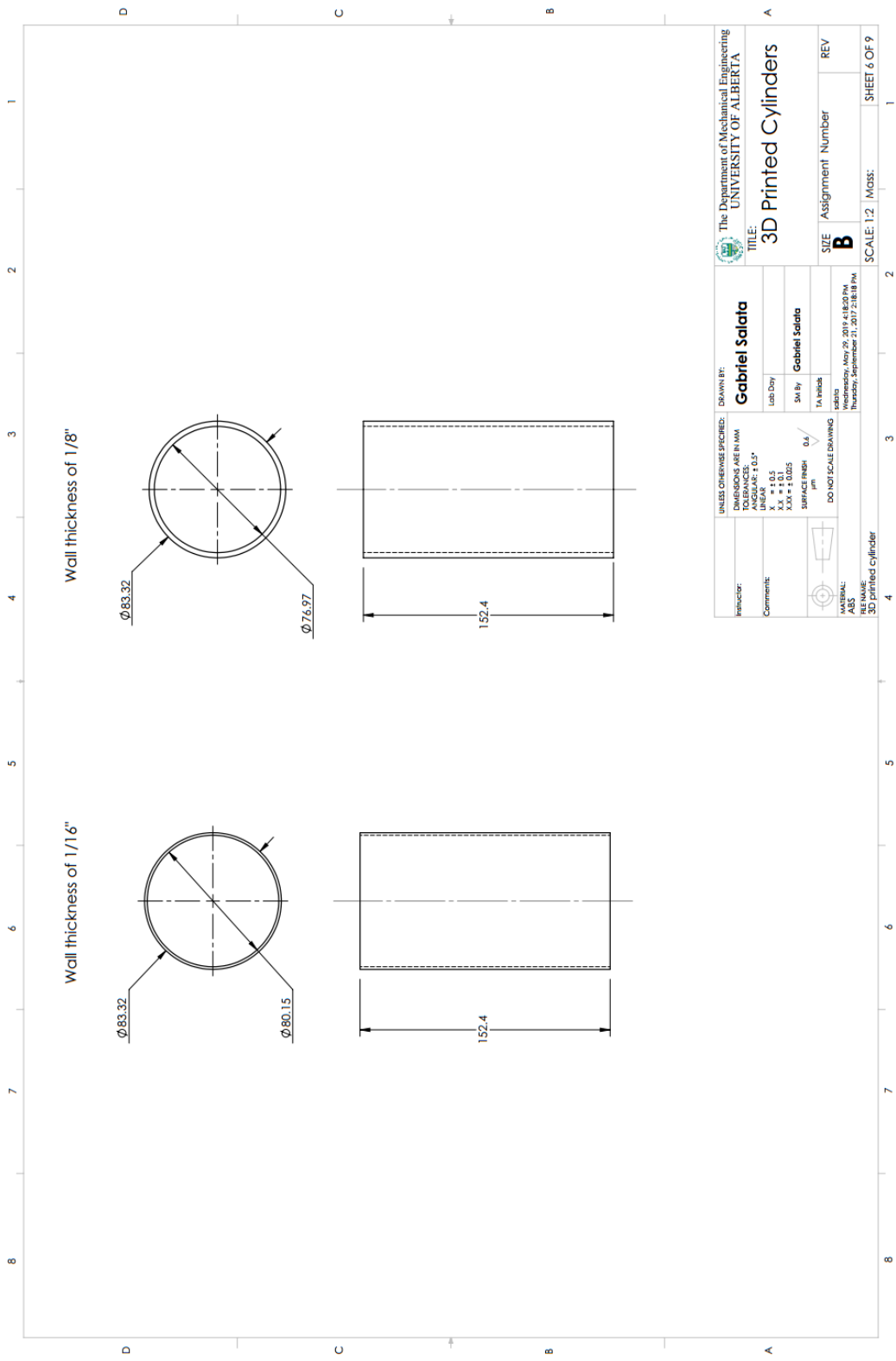
SECTION C-C  
SCALE 1:1

All fillets in the o-ring groove are R1.

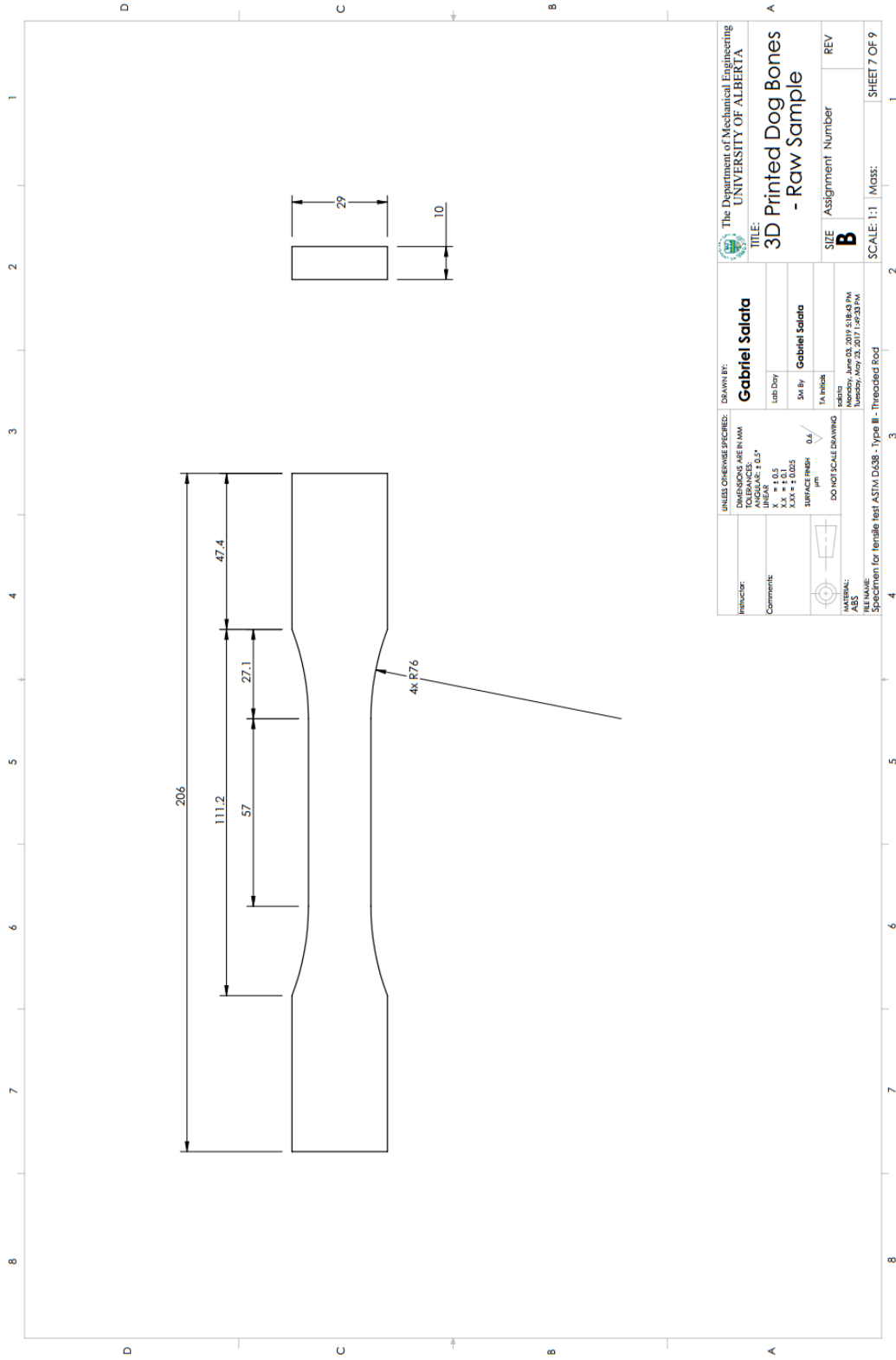
UNLESS OTHERWISE SPECIFIED: DIMENSIONS ARE IN MM TOLERANCES UNLESS OTHERWISE SPECIFIED: LINEAR ± 0.1 XX ± 0.1 XXX ± 0.025 SURFACE FINISH 0.6 µm DO NOT SCALE DRAWING		DRAWN BY: <b>Gabriel Salata</b>		The Department of Mechanical Engineering UNIVERSITY OF ALBERTA	
Instructor:		Lab Day:		TITLE: <b>Bottom Flange</b>	
Comments:		SA By: Gabriel Salata		SIZE: Assignment Number	
		TA Initials:		REV	
MATERIAL: non-reflective resin		DATE: Wednesday, May 29, 2019 3:00:59 PM		SCALE: 1:2	
PLOT DATE: Friday, September 22, 2017 11:02:16 AM		FILE NAME: Bottom Flange		SHEET 4 OF 9	



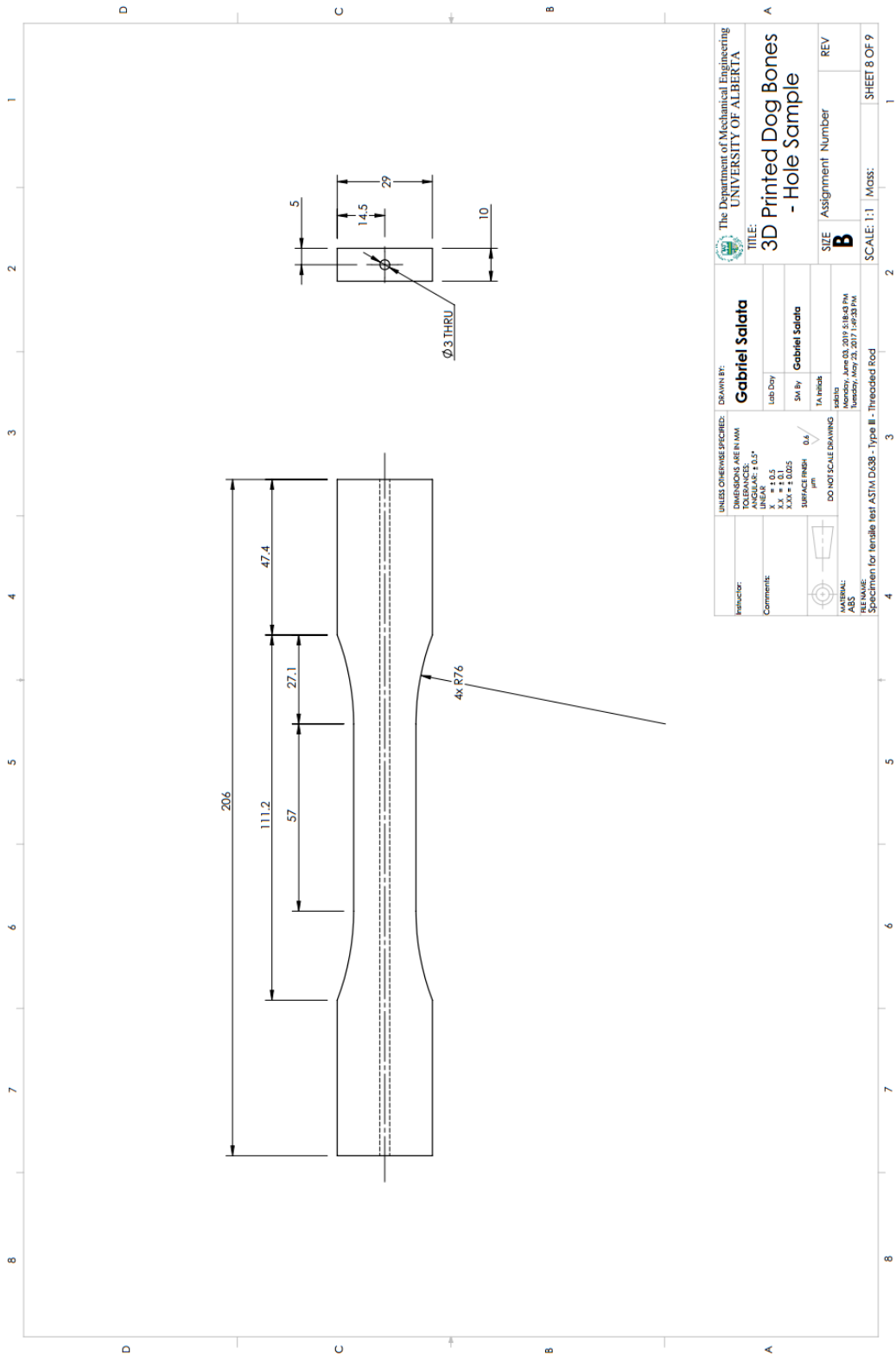
UNLESS OTHERWISE SPECIFIED:		The Department of Mechanical Engineering <b>UNIVERSITY OF ALBERTA</b>	<b>TITLE:</b> 3D Printed Spacer	
<b>INDUCED BY:</b> Gabriel Salata	<b>DRAWN BY:</b> Gabriel Salata	<b>DATE:</b> Friday, April 12, 2019 11:59:53 AM	<b>SIZE:</b> B	<b>ASSIGNMENT NUMBER:</b> REV
<b>COMMENTS:</b> DIMENSIONS ARE IN MM TOLERANCES: FRACTIONS ± 0.15" DECIMALS ± 0.1 ANGLES ± 0.5 SURFACE FINISH: XX ± 1.005 μm	<b>DATE:</b> Wednesday, October 18, 2017 2:04:24 PM	<b>SCALE:</b> 1:1	<b>DO NOT SCALE DRAWING</b>	<b>MASS:</b> SHEET 5 OF 9
<b>FILE NAME:</b> Spacer for the Rod	<b>DATE:</b> Friday, April 12, 2019 11:59:53 AM	<b>SCALE:</b> 1:1	<b>DO NOT SCALE DRAWING</b>	<b>MASS:</b> SHEET 5 OF 9



The Department of Mechanical Engineering UNIVERSITY OF ALBERTA		<b>TITLE:</b> 3D Printed Cylinders	
<b>DRAWN BY:</b> Gabriel Salata	<b>Lab Day:</b> SA By: Gabriel Salata TA In-charge: Gabriel Salata	<b>SIZE:</b> B	<b>Assignment Number:</b> REV
<b>INSTRUCTOR:</b> <b>Comments:</b>	<b>UNLESS OTHERWISE SPECIFIED:</b> DIMENSIONS ARE IN MM TOLERANCES: LINEAR = ± 0.15 ANGULAR = ± 0.5 SURFACE FINISH: 0.8 μm DO NOT SCALE DRAWING	<b>DATE:</b> Wednesday, May 29, 2019 4:18:00 PM Thursday, September 21, 2017 2:18:18 PM	<b>SCALE:</b> 1:2   <b>Mass:</b>
<b>FILE NAME:</b> 3D printed cylinder			<b>SHEET 6 OF 9</b>



The Department of Mechanical Engineering UNIVERSITY OF ALBERTA	
<b>TITLE:</b> 3D Printed Dog Bones - Raw Sample	
<b>SIZE:</b> B	Assignment Number REV
<b>SCALE:</b> 1:1 Mass: SHEET 7 OF 9	
<b>DRAWN BY:</b> Gabriel Salata	<b>Lab Day:</b> Gabriel Salata
<b>DATE:</b> Monday, June 03, 2017 5:16:43 PM	<b>DATE:</b> Monday, May 22, 2017 7:42:31 PM
<b>UNLESS OTHERWISE SPECIFIED:</b> DIMENSIONS ARE IN MM DECIMALS ARE TO 0.1 ANGLES TO 0.5° LINEAR SURFACE FINISH: 0.8 XX ± 0.1 XXX ± 0.025 SURFACE FINISH: 0.8 μm	<b>DO NOT SCALE DRAWING</b> 
<b>REFLECTOR:</b> Gabriel Salata	<b>FILE NAME:</b> Specimen for tensile test ASTM D638 - Type III - Threaded Rod



UNLESS OTHERWISE SPECIFIED:		DRAWN BY:	
DIMENSIONS ARE IN MM		<b>Gabriel Salata</b>	
TOLERANCES		DATE:	
LINEAR	$\pm 0.15^{\circ}$	Last Day	
ANGULAR	$\pm 0.5$	BY:	
XX	$\pm 0.3$	Gabriel Salata	
XXX	$\pm 0.0025$	DATE:	
SURFACE FINISH		TA INCH:	
0.4		skato	
DO NOT SCALE DRAWING		SCALE:	
		1:1	
		MASS:	
TITLE:		SHEET 8 OF 9	
<b>3D Printed Dog Bones - Hole Sample</b>		ASSIGNMENT NUMBER:	
SIZE:		REV:	
<b>B</b>			
DATE:			
Monday, June 03, 2019 5:38:43 PM			
Tuesday, May 23, 2017 1:42:33 PM			
FILE NAME:			
Specimen for female test ASTM D638 - Type II - Threaded Rod			



The Department of Mechanical Engineering <b>UNIVERSITY OF ALBERTA</b>		<b>TITLE:</b> <b>Three-point Bending samples</b>	
<b>DRAWN BY:</b> <b>Gabriel Salata</b>		<b>SIZE:</b> Assignment Number <b>B</b>	
<b>INSTRUCTOR:</b> _____	<b>Lab Day:</b> _____	<b>DATE:</b> _____	<b>REV</b>
<b>COMMENT:</b> _____	<b>SAFETY:</b> _____	<b>DATE:</b> _____	<b>REV</b>
<b>UNLESS OTHERWISE SPECIFIED:</b> DIMENSIONS ARE IN MM TOLERANCES ARE: FRACTIONS ± 0.1* DECIMALS ± 0.1 ANGLES ± 0.1 SURFACE FINISH 0.6 μm DO NOT SCALE DRAWING		<b>SCALE:</b> 1:1 <b>Mass:</b> SHEET 9 OF 9	
<b>DATE:</b> _____		<b>DATE:</b> _____	
<b>FILE NAME:</b> Specimen for bending test ASTM D790		<b>DATE:</b> _____	

## Appendix D: Codes written for processing data

The codes written for processing the data obtained during the experiments are provided in Appendix D. It will be divided into two subsections where the first one provides codes for data processed in Chapter 3, and the second one provides the codes used on Chapter 4.

Before providing the codes used to process the data, this following code was used to convert .log files into .xlsx files.

```
function TxtCnvert
% Function made to create data .xlsx files from .txt files
% The .xlsx files are created in the same folder as the .txt files.
% This program is able to function with non-text files being present in the
% folder with the text files.

% Clear current workspace.
clear

% When the user clicks the "Load Image Folder," a window pops up to allow
% them to select a folder where their images are held. The location of this
% folder is saved.

% If the user presses cancel, than an error message pops up stating "Load
% Cancelled."
flocation = uigetdir('C:\','Select Pictures Location');
    if flocation == 0
        msgbox(sprintf('Load Cancelled'),'Error','Error');
        return

    % If a folder is chosen, the location is saved as a string.
    elseif flocation ~= 0

        % Gets names of files in the folder.
        FileListing = dir(flocation);
        FileListingCell = struct2cell(FileListing);

        % Determines number of files in the selected folder, and saves
        % the names in a single-column cell array. NOTE: when MATLAB
        % opens a folder, two non-existing files are always listed
        % first, so the actual file names begin in the third column of
        % FileListingCell.
        [r,c] = size(FileListingCell);
        FileNames = FileListingCell(1,3:c).';
```

```

% Initializing variables for a loop to delete file and folders.
i = 1;
j = 1;
DeleteArray = [0];
FilesCounterArray = zeros(1, (c-2));

% A while loop to check if folders and non-image files exist in
% the users chosen folder. If a folder or non-image file is
% found, it's position index is saved in the DeleteArray.

% For Folders: no extension will exist, so the remain variable
% will be empty.
% For non-text files: The extension of the file is checked
% against the txt extension.
while i < (c-1)
    FileToCheck = FileNames(i);
    FileToCheck = num2str(cell2mat(FileToCheck));
    RevFileToCheck = fliplr(FileToCheck);
    [token, remain] = strtok(RevFileToCheck, '.');
    properToken = fliplr(token);
    properRemain = fliplr(remain);
    b = isempty(properToken);
    d = lower(properToken);
    if b == 1
        DeleteArray(j) = i;
        j = j + 1;
    elseif (strncmp(d, 'log', 5) == 0)
        DeleteArray(j) = i;
        j = j + 1;
    end
    i = i + 1;
end

% if loop for deleting unwanted files and folders if they exist in
% the main folder. The DeleteArray variable is is flipped so the
% unwanted folders/files are deleted from the bottom to the top
% (otherwise the files are shifted up each time one is deleted).
% The original count of files, c, is modified accordingly.
k = 1;
if DeleteArray(1,1) > 0
    revSubFoldersDelete = fliplr(DeleteArray);
    [r3, c3] = size(revSubFoldersDelete);
    c = c - c3;
    for k = 1:c3
        FileNames(revSubFoldersDelete(k)) = [];
        FilesCounterArray(revSubFoldersDelete(k)) = [];
        k = k + 1;
    end
end
end

```

```

    % Checks if user's chosen folder is empty. Returns error message
    % box if no files detected
    if c < 3
        msgbox(sprintf('No Files Detected in Selected Folder.\n'));
        return
    end
end

% Take .txt out of the FileNames so that .xlsx can be added later when
% saving the excel files.
FileNames2 = strrep(FileNames, '.log', '');

% While loop that utilizes the actxserver function to run excel, open text
% files, and save the excel files. These actions are left invisible to the
% user.
i = 1;
while i < (c - 1)
    % Generates .txt file name to open
    string = FileNames(i);
    string = num2str(cell2mat(string));
    FileName = [flocation '\\' string];

    % Excel automation - prompts excel to run
    e = actxserver('Excel.Application');

    % Opens text file in excel with desired format:
    % .OpenText(FileName, Origin, StartRow, DataType, TextQualifier,
    % ConsecutiveDelimiter, Tab, Semicolon, Comma, Space, Other,
    % OtherChar, FieldInfo)
    % To change, use website for reference:
    % https://msdn.microsoft.com/en-us/library/office/ff837097.aspx
    invoke(e.Workbooks, 'OpenText', FileName, 437, 1, 1, 1, 1, 1, 0, 1);

    % Make the first sheet active & change the name to 'Sheet1'
    eSheets = e.ActiveWorkBook.Sheets;
    eSheet1 = eSheets.get('Item', 1);
    eSheet1.Activate;
    eSheet1.Name = 'Sheet1';

    % Generates .xlsx file name to save
    string2 = FileNames2(i);
    string2 = num2str(cell2mat(string2));
    FileName = [flocation '\\' string2];
    FullFileName = [FileName '.xlsx'];

    % Saves excel file in folder and ends excel session.
    % Note: 51 refers to file format the file is saved in. The file
    % format must be correct, or the file will save as a corrupted
    % file. Excel 16 used originally, and file format number may need to
    % be changed with different Excel versions.
    % To change, use website for reference:

```

```

% https://msdn.microsoft.com/en-us/library/office/ff837097.aspx
invoke(e.ActiveWorkBook, 'SaveAs', FullFileName, 51);
Close(e.Workbooks);
Quit(e);
delete(e);
i = i + 1;
end
end

```

The following codes were used to process the data related to Chapter 3.

- Plot Pressure vs Time: this code was used to the Pressure vs Time graph to all samples used on the pressure test.

```

clear all
close all
clc
% Set default plot properties
set(0, 'defaultfigurecolor', [1 1 1])
set(0, 'defaultAxesFontName', 'Times New Roman');
set(0, 'defaultTextFontName', 'Times New Roman');
set(0, 'defaultAxesFontSize', 11);
set(0, 'defaultTextFontSize', 11);

% Set Figure Size
Width=17; %Centimeters
Height=6; %Centimeters
get(0, 'ScreenSize');
set(0, 'Units', 'centimeter');
a=get(0, 'ScreenSize');
set(groot, 'defaultFigureUnits', 'centimeters');
set(groot, 'defaultFigurePosition', [5,5,Width,Height]);
data_files = dir('*.xlsx');

for i=1:length(data_files)
    start_pt = 8;
    data_time= xlsread(data_files(i).name);
    time = data_time(start_pt:end,1);
    data_pressure= xlsread(data_files(i).name);
    P = data_pressure(start_pt:end,2);
    P = (P*10);
    plot(time ,P)
    set(gca, 'FontSize', 11)
    xlim([0 300])
    ylim([0 110])
    hold on
end
%Set plot and saving parameters
%Code used to all samples just changing the saving name according to sample
xlabel('Time, sec', 'FontSize', 11, 'FontName', 'Times New Roman');
ylabel('Pressure, psi', 'FontSize', 11, 'FontName', 'Times New Roman');
legend('10psi', '20psi', '30psi', '40psi', '50psi', '60psi', '70psi', '80psi', '90psi', '100psi', 'Location', 'eastoutside')
savefig('Raw_1 8')

```

```
saveas(gcf, 'Raw_1_8', 'meta')
```

- Code used to plot Figure 22.

```
clear all
close all
clc
% Set default plot properties
set(0, 'defaultfigurecolor', [1 1 1])
set(0, 'defaultAxesFontName', 'Times New Roman');
set(0, 'defaultTextFontName', 'Times New Roman');
set(0, 'defaultAxesFontSize', 11);
set(0, 'defaultTextFontSize', 11);

% Set Figure Size
Width=17; %Centimeters
Height=6; %Centimeters
get(0, 'ScreenSize');
set(0, 'Units', 'centimeter');
a=get(0, 'ScreenSize');
set(groot, 'defaultFigureUnits', 'centimeters');
set(groot, 'defaultFigurePosition', [5,5,Width,Height]);
data_files = dir('*.xlsx');

for i=1:length(data_files)
    start_pt = 8;
    data_time= xlsread(data_files(i).name);
    time = data_time(start_pt:end,1);
    data_pressure= xlsread(data_files(i).name);
    P = data_pressure(start_pt:end,2);
    P = (P*10);
    plot(time ,P)
    set(gca, 'FontSize', 11, 'XGrid', 'off', 'YGrid', 'on', 'YMinorGrid', 'on')
    xlim([0 300])
    ylim([95 102])
    hold on
end
xlabel('Time, sec', 'FontSize', 11, 'FontName', 'Times New Roman');
ylabel('Pressure, psi', 'FontSize', 11, 'FontName', 'Times New Roman');
legend('Spray Painted Sample', 'Raw Sample', 'Epoxy Coated Sample', 'location', 'eastoutside')
savefig('Combined_90_100_Plot')
saveas(gcf, 'Combined_90_100', 'meta')
```

- Code used to plot Figure 23

```

clear all
close all
clc
% Set default plot properties
set(0,'defaultfigurecolor',[1 1 1])
set(0,'defaultAxesFontName','Times New Roman');
set(0,'defaultTextFontName','Times New Roman');
set(0,'defaultAxesFontSize',11);
set(0,'defaultTextFontSize',11);

% Set Figure Size
Width=17; %Centimeters
Height=6; %Centimeters
get(0,'ScreenSize');
set(0,'Units','centimeter');
a=get(0,'ScreenSize');
set(groot,'defaultFigureUnits','centimeters');
set(groot,'defaultFigurePosition',[5,5,Width,Height]);
data_files = dir('*.xlsx');
P2 = zeros(length(data_files),1);

for i=1:length(data_files)
    start_pt = 8;
    data_time= xlsread(data_files(i).name);
    time = data_time(start_pt:end,1);
    data_pressure= xlsread(data_files(i).name);
    P = data_pressure(start_pt:end,2);
    P = (P*10);
    P2(i) = data_pressure(start_pt,2);
    P2 = (P2(i)*10)
    plot(time ,(P-P2))
    set(gca,'FontSize',11,'XGrid','off','YGrid','on','YMinorGrid','on')
    xlim([0 300])
    ylim([-3 1])
    hold on
end

xlabel('Time, sec','FontSize',11,'FontName','Times New Roman');
ylabel('Pressure drop, psi','FontSize',11,'FontName','Times New Roman');
legend('10psi','20psi','30psi','40psi','50psi','60psi','70psi','80psi','90psi','100psi',
'Location','eastoutside')
savefig('Raw_1 8')
saveas(gcf,'Raw_1 8','meta')

```

- Code used to plot the Pressure after 5 min vs Set point pressure graph.

```

clear all
close all
clc

% Set default plot properties
set(0,'defaultfigurecolor',[1 1 1])
set(0,'defaultAxesFontName','Times New Roman');
set(0,'defaultTextFontName','Times New Roman');
set(0,'defaultAxesFontSize',11);
set(0,'defaultTextFontSize',11);

% Set Figure Size
Width=17; %Centimeters
Height=6; %Centimeters
get(0,'ScreenSize');
set(0,'Units','centimeter');
a=get(0,'ScreenSize');
set(groot,'defaultFigureUnits','centimeters');
set(groot,'defaultFigurePosition',[5,5,Width,Height]);
data_files = dir('*.xlsx');

for Column=1:3
    Array=1
    for File=Column:3:length(data_files)

        start_pt = 8;
        data_time= xlsread(data_files(File).name);
        time = data_time(607,1);
        data_pressure= xlsread(data_files(File).name);
        P(Array,Column)= data_pressure(607,2)*10;
        Array=Array+1
    end
end

end
t=(10:10:100)
bar(t,P)
set(gca,'FontSize',11)
ylim([0 110])
xlim([0 110])
set(gca,'YGrid','on','YMinorGrid','on','XGrid','off')

xlabel('Set point pressure, psi','FontSize',11,'FontName','Times New Roman');
ylabel('Pressure after 5 min, psi','FontSize',11,'FontName','Times New Roman');
legend('Raw','Spray Painted','Epoxy Coated','location','eastoutside')
savefig('Combined')
saveas(gcf,'Combined','meta')

```

The following codes were used to process the data related to Chapter 4, starting with the codes to process the data related to the tensile tests.

- Code used to plot Stress vs Strain curves of tensile tests.

```

clear all
close all
clc
% Set default plot properties
set(0,'defaultfigurecolor',[1 1 1])
set(0,'defaultAxesFontName','Times New Roman');
set(0,'defaultTextFontName','Times New Roman');
set(0,'defaultAxesFontSize',11);
set(0,'defaultTextFontSize',11);
% Set Figure Size
Width=17; %Centimeters
Height=6; %Centimeters
get(0,'ScreenSize');
set(0,'Units','centimeter');
a=get(0,'ScreenSize');
set(groot,'defaultFigureUnits','centimeters');
set(groot,'defaultFigurePosition',[5,5,Width,Height]);
data_files = dir('*.xlsx');

    fig=figure();
    TurnlAxes = axes();
    grid on
    grid minor
    set(TurnlAxes,'FontSize',11)
    xlim(TurnlAxes,[0 50])
    ylim(TurnlAxes,[0 550])

for i=1:length(data_files)
    start_pt = 6;
    data_stroke= xlsread(data_files(i).name);
    stroke = data_stroke(start_pt:end,3);
    data_load= xlsread(data_files(i).name);
    load = data_load(start_pt:end,2);
    load = ((load*1000)/2.84); %2.84 is equal to the crosssectional area of the metal
rod
    plot(stroke ,load)
    set(gca,'FontSize',11)
    xlim([0 0.05])
    ylim([0 2000])
    grid on
    grid minor
    hold on
end
xlabel('Strain, mm/mm','FontSize',11,'FontName','Times New Roman');
ylabel('Stress, MPa','FontSize',11,'FontName','Times New Roman');
legend('Metal rod-sample01','Metal rod-sample02','Metal rod-sample03','Metal rod-
sample04','Metal rod-sample05','Location','eastoutside')
saveas(gcf,'Tensile_Metal_rod_Stress_Strain','meta')
saveas(gcf,'Tensile_Metal_rod_Stress_Strain.png')

```

- Code used to generate plots comparing the elastic modulus/tensile strength/flexural modulus/flexural strength amongst all the samples tested (i.e. Figure 34).

```

clear all
close all
clc
% Set default plot properties
set(0,'defaultfigurecolor',[1 1 1])
set(0,'defaultAxesFontName','Times New Roman');
set(0,'defaultTextFontName','Times New Roman');
set(0,'defaultAxesFontSize',11);
set(0,'defaultTextFontSize',11);

% Set Figure Size
Width=17; %Centimeters
Height=6; %Centimeters
get(0,'ScreenSize');
set(0,'Units','centimeter');
a=get(0,'ScreenSize');
set(groot,'defaultFigureUnits','centimeters');
set(groot,'defaultFigurePosition',[5,5,Width,Height]);
A = categorical({'Raw';'Hole';'1turn';'3turn';'5turn'});
B = reordercats(A,{'Raw';'Hole';'1turn';'3turn';'5turn'});
data = [1011.3 1068.3 1569.3 1592.7 1585.1]';
errhigh = [45.1 22.3 54.2 32.6 76.6];
errlow = [45.1 22.3 54.2 32.6 76.6];

bar(B,data,'barwidth',0.3)
set(gca,'YGrid','on','XGrid','off')
grid minor
hold on

er = errorbar(B,data,errlow,errhigh);
er.Color = [0 0 0];
er.LineStyle = 'none';

hold on

ylabel('Elastic Modulus, MPa','FontSize',11,'FontName','Times New Roman');
savefig('Elastic Modulus')
saveas(gcf,'Elastic Modulus','meta')
saveas(gcf,'Elastic Modulus.png')

```

- Code used to plot a Stress vs Strain comparing the results of the raw and hole samples (i.e. Figure 36).

```

clear all
close all
clc
% Set default plot properties
set(0,'defaultfigurecolor',[1 1 1])
set(0,'defaultAxesFontName','Times New Roman');
set(0,'defaultTextFontName','Times New Roman');
set(0,'defaultAxesFontSize',11);
set(0,'defaultTextFontSize',11);

% Set Figure Size
Width=17; %Centimeters
Height=6; %Centimeters
get(0,'ScreenSize');
set(0,'Units','centimeter');
a=get(0,'ScreenSize');
set(groot,'defaultFigureUnits','centimeters');
set(groot,'defaultFigurePosition',[5,5,Width,Height]);
data_files = dir('*.xlsx');

for i=1:length(data_files)
    start_pt = 6;
    data_stroke= xlsread(data_files(i).name);
    NumTurns = double(data_files(i).name(3));
    stroke = data_stroke(start_pt:end,3);
    data_load= xlsread(data_files(i).name);
    load = data_load(start_pt:end,2);
    load1 = ((load*1000)/182.93);
    load2 = ((load*1000)/190);

    if NumTurns == 72
        h_1=plot(stroke ,load1,'r');
        set(gca,'FontSize',11)
        hold on
    elseif NumTurns == 82
        h_2= plot(stroke ,load2,'k');
        set(gca,'FontSize',11)
        hold on
    end
end
xlim([0 0.05])
ylim([0 60])
grid on
grid minor
hold on
xlabel('Strain, mm/mm','FontSize',11,'FontName','Times New Roman');
ylabel('Stress, MPa','FontSize',11,'FontName','Times New Roman');
legend([h_1(1), h_2(1)], 'Hole-samples', 'Raw-
samples','Location','eastoutside','FontName','Times New Roman')
savefig('Tensile_Raw vs Hole_Stress_Strain')
saveas(gcf,'Tensile_Raw vs Hole_Stress_Strain','meta')
saveas(gcf,'Tensile_Raw vs Hole_Stress_Strain.png')

```

- Code used to plot a Stress vs Strain comparing the results of the raw and 5 turn samples (i.e. Figure 37).

```

clear all
close all
clc
% Set default plot properties
set(0,'defaultfigurecolor',[1 1 1])
set(0,'defaultAxesFontName','Times New Roman');
set(0,'defaultTextFontName','Times New Roman');
set(0,'defaultAxesFontSize',11);
set(0,'defaultTextFontSize',11);

% Set Figure Size
Width=17; %Centimeters
Height=6; %Centimeters
get(0,'ScreenSize');
set(0,'Units','centimeter');
a=get(0,'ScreenSize');
set(groot,'defaultFigureUnits','centimeters');
set(groot,'defaultFigurePosition',[5,5,Width,Height]);
data_files = dir('*.xlsx');

for i=1:length(data_files)
    start_pt = 6;
    data_stroke= xlsread(data_files(i).name);
    NumTurns = double(data_files(i).name(3));
    NumTurns2 = str2double(data_files(i).name(3));
    stroke = data_stroke(start_pt:end,3);
    data_load= xlsread(data_files(i).name);
    load = data_load(start_pt:end,2);
    load1 = ((load*1000)/185.47);
    load2 = ((load*1000)/190);

    if NumTurns2 == 5
        h_1=plot(stroke ,load1,'r');
        set(gca,'FontSize',11)
        hold on
    elseif NumTurns == 82
        h_2= plot(stroke ,load2,'k');
        set(gca,'FontSize',11)
        hold on
    end
end
xlim([0 0.05])
ylim([0 60])
grid on
grid minor
hold on
xlabel('Strain, mm/mm','FontSize',11,'FontName','Times New Roman');
ylabel('Stress, MPa','FontSize',11,'FontName','Times New Roman');
legend([h_1(1), h_2(1)], '5turn-samples','Raw-
samples','Location','eastoutside','FontName','Times New Roman')
savefig('Tensile_1turn_Stress_Strain')
saveas(gcf,'Tensile_Raw vs 5turn_Strain','meta')
saveas(gcf,'Tensile_1turn_Stress_Strain.png')

```

- Code used to plot a Stress vs Strain comparing the results of the reinforced samples (i.e. Figure 38).

```

clear all
close all
clc
% Set default plot properties
set(0,'defaultfigurecolor',[1 1 1])
set(0,'defaultAxesFontName','Times New Roman');
set(0,'defaultTextFontName','Times New Roman');
set(0,'defaultAxesFontSize',11);
set(0,'defaultTextFontSize',11);

% Set Figure Size
Width=17; %Centimeters
Height=6; %Centimeters
get(0,'ScreenSize');
set(0,'Units','centimeter');
a=get(0,'ScreenSize');
set(groot,'defaultFigureUnits','centimeters');
set(groot,'defaultFigurePosition',[5,5,Width,Height]);
data_files = dir('*.xlsx');

for i=1:length(data_files)
    start_pt = 6;
    data_stroke= xlsread(data_files(i).name);
    NumTurns = str2double(data_files(i).name(3));
    stroke = data_stroke(start_pt:end,3);
    data_load= xlsread(data_files(i).name);
    load = data_load(start_pt:end,2);
    load = (load*1000)/185.47);

    if NumTurns == 3
        h_1=plot(stroke ,load,'r')
    set(gca,'FontSize',11)
        hold on
    elseif NumTurns == 5
        h_2= plot(stroke ,load,'k')
    set(gca,'FontSize',11)
        hold on
    end
    end
    xlim([0 0.05])
    ylim([0 60])
    grid on
    grid minor
    hold on
xlabel('Strain, mm/mm','FontSize',11,'FontName','Times New Roman');
ylabel('Stress, MPa','FontSize',11,'FontName','Times New Roman');
legend([h_1(1), h_2(1)], '3turn-samples', '5turn-
samples','Location','eastoutside','FontName','Times New Roman')
savefig('Tensile_1turn_Stress_Strain')
saveas(gcf,'Tensile_3turn vs 5 turn_Stress_Strain','meta')
saveas(gcf,'Tensile_3turn vs 5 turn_Stress_Strain.png')

```

- Code used to plot a Stress vs Strain comparing the results of the raw, 1 turn, and 5 turn samples (i.e. Figure 39).

```

clear all
close all
clc
% Set default plot properties
set(0,'defaultfigurecolor',[1 1 1])
set(0,'defaultAxesFontName','Times New Roman');
set(0,'defaultTextFontName','Times New Roman');
set(0,'defaultAxesFontSize',11);
set(0,'defaultTextFontSize',11);
% Set Figure Size
Width=17; %Centimeters
Height=6; %Centimeters
get(0,'ScreenSize');
set(0,'Units','centimeter');
a=get(0,'ScreenSize');
set(groot,'defaultFigureUnits','centimeters');
set(groot,'defaultFigurePosition',[5,5,Width,Height]);
data_files = dir('*.xlsx');
for i=1:length(data_files)
    start_pt = 6;
    data_stroke= xlsread(data_files(i).name);
    NumTurns = double(data_files(i).name(3));
    NumTurns2 = str2double(data_files(i).name(3));
    stroke = data_stroke(start_pt:end,3);
    data_load= xlsread(data_files(i).name);
    load = data_load(start_pt:end,2);
    load1 = ((load*1000)/185.47);
    load2 = ((load*1000)/190);

    if NumTurns2 == 1
        h_1=plot(stroke ,load1,'r');
        set(gca,'FontSize',11)
        hold on
    elseif NumTurns2 == 5
        h_2= plot(stroke ,load1,'k');
        set(gca,'FontSize',11)
        hold on
    elseif NumTurns == 82
        h_3= plot(stroke ,load2,'b');
        set(gca,'FontSize',11)
        hold on
    end
end
xlim([0 0.05])
ylim([0 60])
grid on
grid minor
hold on

xlabel('Strain, mm/mm','FontSize',11,'FontName','Times New Roman');
ylabel('Stress, MPa','FontSize',11,'FontName','Times New Roman');
legend([h_1(1), h_2(1),h_3(1)], '1turn-samples', '5turn-samples', 'Raw-
samples','Location','eastoutside','FontName','Times New Roman')
savefig('Tensile_Raw vs 1 turn vs 5 turn_Stress_Strain')
saveas(gcf,'Tensile_Raw vs 1 turn vs 5 turn_Stress_Strain','meta')
saveas(gcf,'Tensile_Raw vs 1 turn vs 5 turn_Stress_Strain.png')

```

- Code used to plot a Stress vs Strain comparing the results of the raw/and hole samples of the two different printing orientation (i.e. Figure 48).

```

clear all
close all
clc
% Set default plot properties
set(0,'defaultfigurecolor',[1 1 1])
set(0,'defaultAxesFontName','Times New Roman');
set(0,'defaultTextFontName','Times New Roman');
set(0,'defaultAxesFontSize',11);
set(0,'defaultTextFontSize',11);
% Set Figure Size
Width=17; %Centimeters
Height=6; %Centimeters
get(0,'ScreenSize');
set(0,'Units','centimeter');
a=get(0,'ScreenSize');
set(groot,'defaultFigureUnits','centimeters');
set(groot,'defaultFigurePosition',[5,5,Width,Height]);
data_files = dir('*.xlsx');
for i=1:length(data_files)
    start_pt = 6;
    data_stroke= xlsread(data_files(i).name);
    NumTurns = double(data_files(i).name(1));
    stroke = data_stroke(start_pt:end,3);
    data_load= xlsread(data_files(i).name);
    load = data_load(start_pt:end,2);
    load = ((load*1000)/190);
    if NumTurns == 76
        h_1=plot(stroke ,load,'r');
        set(gca,'FontSize',11)
        hold on
    elseif NumTurns == 90
        h_2= plot(stroke ,load,'k');
        set(gca,'FontSize',11)
        hold on
    elseif NumTurns == 90
        h_3= plot(stroke ,load,'k');
        set(gca,'FontSize',11)
        hold on
    elseif NumTurns == 90
        h_4= plot(stroke ,load,'k');
        set(gca,'FontSize',11)
        hold on
    end
end
xlim([0 0.05])
ylim([0 60])
grid on
grid minor
hold on
xlabel('Strain, mm/mm','FontSize',11,'FontName','Times New Roman');
ylabel('Stress, MPa','FontSize',11,'FontName','Times New Roman');
legend([h_1(1), h_2(1)], 'Raw-Longitudinal samples', 'Raw-Z direction
samples','Location','eastoutside','FontName','Times New Roman')
savefig('Tensile_Raw vs Hole_Stress_Strain')
saveas(gcf,'Tensile_Raw vs Hole_Stress_Strain','meta')
saveas(gcf,'Tensile_Raw vs Hole_Stress_Strain.png')

```

- Code used to plot a Stress vs Strain comparing the results of the reinforced samples of the two different printing orientation (i.e. Figure 49).

```

clear all
close all
clc
% Set default plot properties
set(0,'defaultfigurecolor',[1 1 1])
set(0,'defaultAxesFontName','Times New Roman');
set(0,'defaultTextFontName','Times New Roman');
set(0,'defaultAxesFontSize',11);
set(0,'defaultTextFontSize',11);

% Set Figure Size
Width=17; %Centimeters
Height=6; %Centimeters
get(0,'ScreenSize');
set(0,'Units','centimeter');
a=get(0,'ScreenSize');
set(groot,'defaultFigureUnits','centimeters');
set(groot,'defaultFigurePosition',[5,5,Width,Height]);
data_files = dir('*.xlsx');

for i=1:length(data_files)
    start_pt = 6;
    data_stroke= xlsread(data_files(i).name);
    NumTurns = double(data_files(i).name(1));
    stroke = data_stroke(start_pt:end,3);
    data_load= xlsread(data_files(i).name);
    load = data_load(start_pt:end,2);
    load = ((load*1000)/185.47);

    if NumTurns == 76
        h_1=plot(stroke ,load,'r');
        set(gca,'FontSize',11)
        hold on
    elseif NumTurns == 90
        h_2= plot(stroke ,load,'k') ;
        set(gca,'FontSize',11)
        hold on
    end
end
end
xlim([0 0.05])
ylim([0 60])
grid on
grid minor
hold on
xlabel('Strain, mm/mm','FontSize',11,'FontName','Times New Roman');
ylabel('Stress, MPa','FontSize',11,'FontName','Times New Roman');
legend([h_1(1), h_2(1)], '5 turn-Longitudinal samples', '5 turn-Z direction
samples','Location','eastoutside','FontName','Times New Roman')
savefig('Tensile_1turn_Stress_Strain')
saveas(gcf,'Tensile_5turn Comparison_Stress_Strain','meta')
saveas(gcf,'Tensile_5turn Comparison_Stress_Strain.png')

```

- Code used to plot a Stress vs Strain comparing the results of the raw and reinforced samples of the two different printing orientation (i.e. Figure 50).

```

clear all
close all
clc
% Set default plot properties
set(0,'defaultfigurecolor',[1 1 1])
set(0,'defaultAxesFontName','Times New Roman');
set(0,'defaultTextFontName','Times New Roman');
set(0,'defaultAxesFontSize',11);
set(0,'defaultTextFontSize',11);
% Set Figure Size
Width=17; %Centimeters
Height=6; %Centimeters
get(0,'ScreenSize');
set(0,'Units','centimeter');
a=get(0,'ScreenSize');
set(groot,'defaultFigureUnits','centimeters');
set(groot,'defaultFigurePosition',[5,5,Width,Height]);
data_files = dir('*.xlsx');
for i=1:length(data_files)
    start_pt = 6;
    data_stroke= xlsread(data_files(i).name);
    NumTurns2 = str2double(data_files(i).name(1));
    stroke = data_stroke(start_pt:end,3);
    data_load= xlsread(data_files(i).name);
    load = data_load(start_pt:end,2);
    load1 = ((load*1000)/185.47);
    load2 = ((load*1000)/190);
    if NumTurns2 == 1
        h_1=plot(stroke ,load1,'r');
        set(gca,'FontSize',11)
        hold on
    elseif NumTurns2 == 2
        h_2= plot(stroke ,load2,'r');
        set(gca,'FontSize',11)
        hold on
    elseif NumTurns2 == 3
        h_3= plot(stroke ,load1,'k');
        set(gca,'FontSize',11)
        hold on
    elseif NumTurns2 == 4
        h_4= plot(stroke ,load2,'k');
        set(gca,'FontSize',11)
        hold on
    end
end
xlim([0 0.05])
ylim([0 60])
grid on
grid minor
hold on
xlabel('Strain, mm/mm','FontSize',11,'FontName','Times New Roman');
ylabel('Stress, MPa','FontSize',11,'FontName','Times New Roman');
legend([h_1(1), h_3(1)], 'Longitudinal samples','Z direction
samples','Location','eastoutside','FontName','Times New Roman')
saveas(gcf,'Tensile_Raw vs 5turn Strain','meta')
saveas(gcf,'Tensile_1turn Stress Strain.png')

```

- Code used to plot an overall comparison between elastic modulus/tensile strength for all samples of the two different printing orientation (i.e. Figure 51).

```

clear all
close all
clc
% Set default plot properties
set(0,'defaultfigurecolor',[1 1 1])
set(0,'defaultAxesFontName','Times New Roman');
set(0,'defaultTextFontName','Times New Roman');
set(0,'defaultAxesFontSize',11);
set(0,'defaultTextFontSize',11);

% Set Figure Size
Width=17; %Centimeters
Height=6; %Centimeters
get(0,'ScreenSize');
set(0,'Units','centimeter');
a=get(0,'ScreenSize');
set(groot,'defaultFigureUnits','centimeters');
set(groot,'defaultFigurePosition',[5,5,Width,Height]);

data1 = [1111.11 1092.78 1510.44 1624.44 1616.00]';

errhigh1 = [38.67 10.64 54.46 25.90 38.61]';

errlow1 = [38.67 10.64 54.46 25.90 38.61]';

data2 = [1011.33 1068.33 1574.67 1592.67 1593.89]';

errhigh2 = [45.10 22.30 58.77 32.60 82.22]';

errlow2 = [45.10 22.30 58.77 32.60 82.22]';

data = [data1,data2];

errhigh = [errhigh1,errhigh2];

errlow = [errlow1,errlow2];

bar(data,'barwidth',1)
set(gca,'YGrid','on','XGrid','off')
grid minor
hold on

ngroups = size(data,1);
nbars = size(data,2);

```

```

groupwidth = min(1, nbars/(nbars + 1.5));

for i = 1:nbars
    x = (1:ngroups) - groupwidth/2 + (2*i-1) * groupwidth/(2*nbars);
    er = errorbar(x,data(:,i),errlow(:,i),errhigh(:,i),...
        'XDataMode','manual',...
        'Color',[0 0 0],...
        'LineStyle','none');
end

hold on

ylabel('Elastic Modulus, MPa','FontSize',11,'FontName','Times New Roman');
legend('Z direction samples','Longitudinal samples','Location','eastoutside')
savefig('Flexural Modulus')
saveas(gcf,'Flexural Modulus','meta')
saveas(gcf,'Flexural Modulus.png')

```

The following codes were used to process the data from the 3-point bending tests.

- Code used to plot Axial load vs Stroke curves of 3-point bending tests.

```
clear all
close all
clc
% Set default plot properties
set(0,'defaultfigurecolor',[1 1 1])
set(0,'defaultAxesFontName','Times New Roman');
set(0,'defaultTextFontName','Times New Roman');
set(0,'defaultAxesFontSize',11);
set(0,'defaultTextFontSize',11);

% Set Figure Size
Width=17; %Centimeters
Height=6; %Centimeters
get(0,'ScreenSize');
set(0,'Units','centimeter');
a=get(0,'ScreenSize');
set(groot,'defaultFigureUnits','centimeters');
set(groot,'defaultFigurePosition',[5,5,Width,Height]);
data_files = dir('*.xlsx');

for i=1:length(data_files)
    start_pt = 6;
    data_stroke= xlsread(data_files(i).name);
    stroke = data_stroke(start_pt:end,1);
    data_load= xlsread(data_files(i).name);
    load = data_load(start_pt:end,2);
    load = (load*(-1000));
    stroke = (stroke*(-1));
    plot(stroke ,load)
    set(gca,'FontSize',11)
    xlim([0 50])
    ylim([0 550])
    grid on
    grid minor
    hold on
end
xlabel('Stroke, mm','FontSize',11,'FontName','Times New Roman');
ylabel('Axial load, N','FontSize',11,'FontName','Times New Roman');
legend('Raw-sample01','Raw-sample02','Raw-sample03','Raw-sample04','Raw-
sample05','Location','eastoutside')
savefig('Bending_Raw')
saveas(gcf,'Bending_Raw','meta')
saveas(gcf,'Bending_Raw.png')
```

- Code used to plot the comparison of flexural modulus/flexural strength amongst all samples.

```

clear all
close all
clc
% Set default plot properties
set(0,'defaultfigurecolor',[1 1 1])
set(0,'defaultAxesFontName','Times New Roman');
set(0,'defaultTextFontName','Times New Roman');
set(0,'defaultAxesFontSize',11);
set(0,'defaultTextFontSize',11);

% Set Figure Size
Width=17; %Centimeters
Height=6; %Centimeters
get(0,'ScreenSize');
set(0,'Units','centimeter');
a=get(0,'ScreenSize');
set(groot,'defaultFigureUnits','centimeters');
set(groot,'defaultFigurePosition',[5,5,Width,Height]);
A = categorical({'Raw';'Hole';'3turn';'5turn'});
B = reordercats(A,{'Raw';'Hole';'3turn';'5turn'})
data = [1726.76 1769.37 1858.50 1823.74]';
errhigh = [71.58 73.83 85.6 100.96];
errlow = [71.58 73.83 85.6 100.96];

bar(B,data,'barwidth',0.3)
set(gca,'YGrid','on','XGrid','off')
grid minor
hold on

er = errorbar(B,data,errlow,errhigh);
er.Color = [0 0 0];
er.LineStyle = 'none';

hold on

ylabel('Flexural Modulus, MPa','FontSize',11,'FontName','Times New Roman');
legend('Longitudinal samples','Z direction samples','Location','eastoutside')
saveas(gcf,'test','meta')

```

- Code used to plot Axial load vs Stroke comparing the results obtained for each printing orientation on the 3-point bending tests (i.e. Figure 56).

```

clear all
close all
clc
% Set default plot properties
set(0,'defaultfigurecolor',[1 1 1])
set(0,'defaultAxesFontName','Times New Roman');
set(0,'defaultTextFontName','Times New Roman');
set(0,'defaultAxesFontSize',11);
set(0,'defaultTextFontSize',11);

% Set Figure Size
Width=17; %Centimeters
Height=6; %Centimeters
get(0,'ScreenSize');
set(0,'Units','centimeter');
a=get(0,'ScreenSize');
set(groot,'defaultFigureUnits','centimeters');
set(groot,'defaultFigurePosition',[5,5,Width,Height]);
data_files = dir('*.xlsx');

for i=1:length(data_files)
    start_pt = 6;
    data_stroke= xlsread(data_files(i).name);
    NumTurns = double(data_files(i).name(5));
    NumTurns2 = str2double(data_files(i).name(5));
    stroke = data_stroke(start_pt:end,1);
    data_load= xlsread(data_files(i).name);
    load = data_load(start_pt:end,2);
    load = (load*(-1000));
    stroke = (stroke*(-1));

    if NumTurns2 == 5
        h_1=plot(stroke ,load,'k');
        set(gca,'FontSize',11)
        hold on
    elseif NumTurns == 82
        h_2= plot(stroke ,load,'r') ;
        set(gca,'FontSize',11)
        hold on
    end
end
xlim([0 50])
ylim([0 550])
grid on
grid minor
hold on
xlabel('Stroke, mm','FontSize',11,'FontName','Times New Roman');
ylabel('Axial load, N','FontSize',11,'FontName','Times New Roman');
legend([h_1(1), h_2(1)], '5 turn-samples', 'Raw-
samples','Location','eastoutside','FontName','Times New Roman')
savefig('Tensile_1turn_Stress_Strain')
saveas(gcf,'Tensile_1turn_Stress_Strain','meta')
saveas(gcf,'Tensile_1turn_Stress_Strain.png')

```

- Code used to plot the comparison of flexural modulus/flexural strength amongst all samples of the two different printing orientation (i.e. Figure 64).

```

clear all
close all
clc
% Set default plot properties
set(0,'defaultfigurecolor',[1 1 1])
set(0,'defaultAxesFontName','Times New Roman');
set(0,'defaultTextFontName','Times New Roman');
set(0,'defaultAxesFontSize',11);
set(0,'defaultTextFontSize',11);

% Set Figure Size
Width=17; %Centimeters
Height=6; %Centimeters
get(0,'ScreenSize');
set(0,'Units','centimeter');
a=get(0,'ScreenSize');
set(groot,'defaultFigureUnits','centimeters');
set(groot,'defaultFigurePosition',[5,5,Width,Height]);
data1 = [1726.76 1769.37 1858.50 1823.74]';

errhigh1 = [71.58 73.83 85.60 100.96]';

errlow1 = [71.58 73.83 85.60 100.96]';

data2 = [2010.11 1899.02 1652.53 1919.93]';

errhigh2 = [41.08 85.96 46.02 51.21]';

errlow2 = [41.08 85.96 46.02 51.21]';

data = [data1,data2];

errhigh = [errhigh1,errhigh2];

errlow = [errlow1,errlow2];

bar(data,'barwidth',1)
set(gca,'YGrid','on','XGrid','off')
grid minor
hold on

ngroups = size(data,1);
nbars = size(data,2);

```

```

groupwidth = min(1, nbars/(nbars + 1.5));

for i = 1:nbars
    x = (1:ngroups) - groupwidth/2 + (2*i-1) * groupwidth/(2*nbars);
    er = errorbar(x,data(:,i),errlow(:,i),errhigh(:,i),...
        'XDataMode','manual',...
        'Color',[0 0 0],...
        'LineStyle','none');
end

hold on

ylabel('Flexural Modulus, MPa','FontSize',11,'FontName','Times New Roman');
legend('Longitudinal samples','Z direction samples','Location','eastoutside')
savefig('Flexural Modulus')
saveas(gcf,'Flexural Modulus','meta')
saveas(gcf,'Flexural Modulus.png')

```